COMPUTING FLOW AND PRESSURE TRANSIENTS IN HETEROGENEOUS MEDIA USING BOUNDARY ELEMENT METHODS

A DISSERTATION
SUBMITTED TO THE DEPARTMENT OF PETROLEUM ENGINEERING
AND THE COMMITTEE ON GRADUATE STUDIES
OF STANFORD UNIVERSITY
IN PARTIAL FULFILLMENT OF THE REQUIREMENTS
FOR THE DEGREE OF
DOCTOR OF PHILOSOPHY

Rosalind Ann Archer
March 2000

I certify that I have read this thesis and that in my opinion it is fully adequate, in scope and in quality, as a dissertation for the degree of Doctor of Philosophy.

Dr. Roland N. Horne
(Principal Advisor)

I certify that I have read this thesis and that in my opinion it is fully adequate, in scope and in quality, as a dissertation for the degree of Doctor of Philosophy.

Dr. Thomas A. Hewett

I certify that I have read this thesis and that in my opinion it is fully adequate, in scope and in quality, as a dissertation for the degree of Doctor of Philosophy.

Dr. Lou Durlofsky

Approved for the University Committee on Graduate Studies:

Acknowledgements

I would like to acknowledge input and support from many people. First I must thank the faculty, staff, and students of the Department of Petroleum Engineering for making my time at Stanford such a great experience. I would especially like to thank my advisor, Professor Roland Horne, for his constant advice and guidance. I would also like to thank the members of the committee for their review of this work. I would like to express my gratitude for financial support from SUPRID which made this work possible.

I must thank Professors Akpofure E. Taigbenu (National University of Science and Technology, Bulawayo, Zimbabwe) and Okey O. Onyejekwe (University of Durban-Westville, South Africa) for their interest in my work. Without their input my study of the Green Element Method would have been much more difficult.

My thanks also go to Professor Mike O'Sullivan, Dr. Roger Nokes and Liz Godfrey from the University of Auckland. Without their encouragement I may never have even applied to Stanford.

I would like to thank everyone involved with the Stanford Aerobics organization. Participation in that group helped give me the energy to make this work possible. I would also like to thank Nikki and Darcy who are both fellow instructors were room-mates of mine.

My family deserve special thanks for supporting my education every step of the way. Finally I must thank my husband Colin for all the love, strength and confidence he has given me on this journey.

This dissertation is dedicated to my husband,
Colin Doyle

Abstract

This work studied the modeling of well tests, tracer tests and multiphase flow in heterogeneous media using boundary element based methods. The motivation for this work was to provide accurate forward models of these processes to be used with parameter estimation/data integration schemes. Boundary element methods are attractive because of their rigorous Green's function basis. The classical boundary element method is however limited to single-phase flow in homogeneous media. This work explored how to recast the differential equations of practical interest to petroleum reservoir engineers in a form suitable for solution with a boundary element scheme.

For flows in heterogeneous media the integral forms of the flow equations contain domain integrals which can not be treated with the classical boundary element method. To handle these terms two hybrid boundary element methods were considered, the Dual Reciprocity Boundary Element Method (DRBEM) and the Green Element Method (GEM). The theory of both methods was considered, however most of the applications presented used GEM because of its sparse matrix structure and amenability to nonlinear problems.

A numerical method that combines GEM with singularity programming was proposed for the modeling of well tests in heterogeneous reservoirs. The method showed excellent accuracy when reproducing the pressure and pressure derivative curves. These results were compared to finite difference simulations which suffer from significant numerical artifacts including artificial wellbore storage effects and difficulty reproducing the boundary effects.

Tracer flows governed by the convection-diffusion equation were considered using both DRBEM and GEM. In numerical experiments at a range of moderate to large Peclét numbers GEM suffered much less from spurious oscillations in the solution than DRBEM. The application of GEM to transport in heterogeneous media was demonstrated.

An IMPES (Implicit Pressure Explicit Saturation) scheme for multiphase flow based on GEM was developed and applied. It showed promising results for a Buckley-Leverett flow example. Unfortunately the method is nonconservative so mass balance

errors occured when it was applied to problems in heterogeneous media.

A parameter estimation scheme was developed for the estimation of reservoir permeability distributions from pressure data. This scheme was applied to match pressure data from multiple wells.

Contents

List of Tables

List of Figures

Chapter 1

Introduction

1.1 Statement of the Problem

When creating a reservoir description engineers have multiple types of data available to them. Landa [32] presented a framework for integrating pressure, water cut and 4-D seismic data. Landa's parameter estimation scheme is an iterative scheme using a Gauss-Newton algorithm. The process relies on a suitable forward simulation scheme being available to model each data type and to generate sensitivity coefficients. Accurate forward models are required to avoid artifacts from the simulations affecting the ultimate reservoir description.

This work focuses mainly on the development of accurate forward simulation schemes as opposed to parameter estimation. However the motivation behind the development of the simulation schemes is to provide accurate reservoir models to be used in parameter estimation. The specific data types considered are well tests, tracer flow and multiphase flow.

The simulation methods developed are based on hybrid forms of the boundary element method, specifically the Dual Reciprocity Boundary Element (DRBEM) and the Green Element Method (GEM). The boundary element method was chosen for study because of its rigorous basis on Green's functions. The classical boundary element method can not be used because it is only applicable to single phase flow in

homogeneous media. This work explores how to cast the differential equations governing well tests, tracer flow and multiphase flow in heterogeneous media, in a suitable form for solution with DRBEM and GEM. Singularity programming is incorporated in the simulation methods to ensure accurate modeling of the singularity that occurs commonly in the pressure distribution at the well. With their basis in the underlying Green's functions classical boundary element methods are highly accurate. This work explores whether DRBEM, GEM and singularity programming can be applied to problems of practical interest to petroleum engineers with similar accuracy.

1.2 Literature Review

Green's functions are the basis for the boundary element method. The usefulness of Green's functions in solving diffusion problems has been demonstrated by Carslaw and Jaegar [6]. Boundary element methods extend the use of Green's functions to problems with arbitrary geometries and boundary conditions. The boundary element method was first published in 1963 by Jaswon [26] and Symm [63] who applied it to the two-dimensional Laplace equation. Rizzo [53] extended the boundary element method to elastostatics. The first three-dimensional formulations were presented by Cruse [10].

1.2.1 Boundary Element Applications to Flow in Porous Media

Boundary element methods were first applied to flow in porous media by Ligget and Liu [34], [35], [36], who considered flow in aquifers that were homogeneous, or at least sectionally homogeneous. Lafe and Cheng [31] considered heterogeneous media using a pertubation based method. Cheng [8] also presented a boundary element formulation applicable to heterogeneous media. This formulation relied on deriving a Green's function that is related to the permeability distribution. The applicability of Cheng's method is limited because it can only be applied when the Laplacian of the square root of the permeability is zero. Cheng and Ouazar [9] presented a

comprehensive review of boundary element applications in groundwater flow.

Gringarten and Ramey [22] demonstrated the power of Green's functions for the solution of well testing problems. The success of this approach makes it natural to pursue boundary element solutions for more general well testing problems.

Numbere and Tiab [39] generated steady-state streamlines using the boundary element method. They considered arbitrarily shaped homogeneous and sectionally homogenous two-dimensional reservoirs. They found the technique superior to the image well techniques used by earlier workers in the area [37].

Masukawa and Horne [38] applied boundary element methods and singularity programming to immiscible displacement problems. This work aimed to assess to the influence of pattern geometry and mobility ratio on displacement performance. The front tracking techniques Masukawa and Horne developed were able to handle nonunit mobility ratio problems. No reservoir heterogeneity was included in the work.

Kikani and Horne [27], [28] applied the boundary element method to single-phase flow in arbitrarily shaped homogeneous reservoirs. A convolution technique was developed for the evaluation of some of the integrals involved in the method. The work demonstrated the usefulness of the boundary element method for streamline generation in steady-state cases. Their work also presented highly accurate pressure transients for well testing problems. Multiwell and multirate cases were considered.

The reduction of the dimensionality of the problem that occurs when using traditional boundary element methods was exploited by Koh and Tiab [29]. Their work considered single-phase three-dimensional flow to horizontal wells in a homogenous reservoir. Both the boundaries of the reservoir and the surface of the wellbore were gridded. Since the boundary element method required only a two-dimensional grid the complex geometry of the horizontal wellbore could be honored readily.

Sato [57] and Sato and Horne [58],[59] addressed single-phase flow in heterogeneous reservoirs, by expressing the pressure as a perturbation series. In highly heterogeneous media the convergence of such a series can be slow so Padé approximants were used to accelerate convergence. Sato and Horne used singularity programming to remove the well singularities from the boundary element problem.

Performance predictions for water drive gas reservoirs were computed by Layne et

al. [33]. The model was composed of two homogeneous zones, one for gas and one for water. A classical boundary element formulation was used. This only required the boundary to be gridded so arbitrary reservoir boundary geometries could be modeled easily.

The effect of thin objects such as fractures or barriers on reservoir performance was considered by Sato and Abbaszadeh [60], whose work used the complex variable boundary element method to study tracer breakthrough and well productivity. Both uniformly and stochastically distributed objects were considered. The work showed that representing fracture systems as equivalent anisotropic media could lead to an erroneous prediction of the pressure distribution at the well.

Zhang and Zeng [78] applied the boundary element method to compute pressure transients in irregularly shaped double porosity reservoirs. The transient aspect of the problem was handled by performing the calculations in Laplace space and inverting the result using the Stehfest [62] algorithm. The method used the fundamental solution to the modified Helmholtz operator. The boundary element scheme used was only applicable to single-phase problems in homogeneous media. It was assumed that flow to the well came only from the fracture system and that the flow between the matrix and fractures was at pseudosteady-state.

Roy and Grilli [55] modeled groundwater flow in formations whose log-transmissivity can be represented by a Gaussian random field. The transmissivity field could be conditional or unconditional. Unlike any of the other work discussed so far the transmissivity field Roy and Grilli considered was stochastic. The log-transmissivity was expanded in a "Fourier-type" series with random coefficients known as the Karhunen-Loève expansion. Roy and Grilli combined this expansion with a small parameter perturbation to transform the stochastic problem into a series of deterministic differential equations. These equations were then solved using DRBEM. The solutions to these equations provide the mean pressure field and the random fluctuation about that mean. Both quantities are of interest when considering solute transport. Roy and Grilli compared their results to the ensemble averages of results simulated over many realizations of the transmissivity field. They found agreement to within 15%, but at ten to 100 times less computational effort.

Numbere and Erkal [40] developed a model for tracer flow in heterogeneous porous media. A key contribution of this work was to address the use of scale-dependent dispersion coefficients. Gelhar [19] observed that assuming that the dispersion coefficient is a constant is not valid at interwell scales because of the many scales of heterogeneity involved. Measured field dispersion coefficients are found to depend linearly on the scale of measurement. To integrate the multiple scales in the problem Numbere and Erkal [40] considered the stochastic form of the governing form of the convection-dispersion equation. In this approach the velocity is broken into an ensemble average velocity and a fluctuation about the average. This requires an assumption that the variance of the velocity is small. Numbere and Erkal made further progress by assuming that the pressure gradient is also constant. This appears to be a very limiting assumption. Numbere and Erkal derived the following equation for the case of unidirectional flow:

$$\frac{\partial C}{\partial t} = D \cdot \left(\frac{\partial^2 C}{\partial x^2} + \frac{\partial^2 C}{\partial y^2} \right) - \bar{v} \frac{\partial C}{\partial x} \tag{1.1}$$

The dispersion coefficient D is a function of $\bar{v}$ (the ensemble average velocity), time and a fractal exponent β. Numbere and Erkal solved Equation (1.1) using DRBEM. The only results presented are for a problem with a known analytical solution and an average Peclét number of 0.01. No discussion of the gridding, time-stepping or stability was included in this work.

Another recent application of boundary element methods in petroleum reservoir engineering problems was by Pecher and Stanislav [51]. This work was limited to single-phase flow in two dimensions and used a traditional boundary element formulation. Heterogeneity was handled by breaking the reservoir into a series of homogeneous zones. The time domain was handled by solving the flow equations in Laplace space. The performance of linear, quadratic and cubic isoparametric elements was considered.

1.2.2 Dual Reciprocity Boundary Element Method

DRBEM is under discussion because it is an extension of the classical boundary element method, that allows the equations governing flow in heterogeneous media to be solved. Wrobel et al. [76] presented the first DRBEM formulation and applied it to transient heat conduction problems.

El Harrouni et al. [13] applied DRBEM to flow in one- and two-dimensional heterogeneous media. To extract a Laplace operator from Darcy's law they worked in terms of a transformed pressure variable. The solutions to the two steady-state examples presented were highly accurate. However in the second example the term accounting for heterogeneity in the transformed differential equation is zero due to a particular analytical representation of the permeability field. El Harrouni et al. [12], [14], [15], [16], [17] also considered parameter estimation in aquifers using a combination of DRBEM, genetic algorithms and Kalman filtering.

Eldho [18] presented one- and two-dimensional DRBEM solutions to the convection-diffusion equation in homogeneous porous media. In one example an analytical solution was available. The agreement between this and the numerical solution was very good. Amoah et al. [1] also applied DRBEM to the convection-diffusion problem, and found its accuracy compared well to finite element and method of characteristics calculations. Wrobel and DeFiguiredo [77] demonstrated the use of DRBEM in problems with nonconstant velocity fields. These published examples of the applications of DRBEM to tracer transport all considered very modest Peclét numbers (less than ten) so further work was warranted to see how well DRBEM performs at higher Peclét numbers (which are common in petroleum reservoir engineering problems).

Most work published using DRBEM has used radial basis functions. However these are only one possible choice. Partridge [48] discusses other choices. Singh and Kalra [61] presented an extensive discussion of time integration and DRBEM.

1.2.3 Green Element Method

The Green Element Method was first presented in 1990 by Taigbenu [64], who described GEM as an element-by-element implementation of boundary element theory.

This approach results in a sparse coefficient matrix assembled in the same manner as the finite element method. Taigbenu [64] considered the Laplace, diffusion, nonlinear Boussinesq and convection-diffusion equations. Of the examples presented the only two-dimensional example is a solution to the Laplace equation. Taigbenu [65] explored the use of quadratic interpolation functions with GEM, and showed that quadratic elements offer increased accuracy. Taigbenu's [66] theoretical discussion of GEM states that GEM requires 15% to 45% less computational time than conventional boundary element methods. Further consideration of the diffusion equation was made by Onyejekwe [42]. In the case of the diffusion equation in one or two dimensions all the integrals required can be evaluated analytically so no numerical quadrature is required, unlike classical boundary element methods.

Taigbenu and Onyejekwe [67] applied GEM to one- and two-dimensional groundwater flow in the unsaturated zone. This is a nonlinear problem involving the flow of water and air. The Picard iteration scheme was used to solve the resulting equations.

The one-dimensional convection-diffusion equation was considered in detail by Taigbenu and Onyejekwe [68]. This work paid careful attention to the different time-stepping schemes available. Stable, accurate solutions to a convection-difffusion problem were presented up to Peclét numbers of 50. These cases are convection-dominated however the problems posed by reservoir engineering applications require a method to have good numerical properties at much higher Peclét numbers.

Onyejekwe [43], [44] demonstrated the ability of GEM to solve nonlinear problems. This work considered mass transfer in a one-dimensional chemical reactor including nonlinear kinetics. This process is governed by the convection-diffusion with an additional term representing reaction kinetics. The GEM scheme gave a prediction of the outlet concentration accurate to within 1%.

Flow in heterogeneous porous media was explored by Onyejekwe [45]. GEM was applied to a transformed form of Darcy's law in a manner similar to the current work. Onyejekwe analyzed several schemes for the interpolation of material properties within the elements.

Onyejekwe [46] presented one- and two-dimensional solutions to flow in the unsaturated zone using three variations of GEM which use different interpolation schemes to handle the nonlinear terms.

A formal proof of the order of accuracy of GEM is not available. Through numerical experiments this work explores how the domain discretization involved in the method detracts from the high accuracy that is associated with the classical boundary element method.

1.2.4 Other Methods

Bokota [4] presented a boundary element solution scheme for the convection-diffusion equation using a traditional boundary element method. This solution was only applicable to problems in homogeneous media with constant fluid velocity. Domain integrals were required in the right hand side of the matrix equation. The fundamental solution for the two-dimensional convection-diffusion problem involves a Bessel function, which means some of the integrals involved in the matrix equation must be performed in time-consuming numerical fashion.

Another recent approach to formulating BEM so that a sparse matrix equation is generated was discussed by Koro [30]. This work used Haar wavelets as shape functions in the classical boundary element method. By varying the resolution level of the wavelets Koro showed how an h-adpative BEM can be developed based on a local error estimator. h-adaptive methods refine the grid automatically according to local error estimates. Currently this method has only been applied to the steady-state Laplace equation.

Chen [7] demonstrated how compactly supported approximating (basis) functions can be used in conjunction with DRBEM. Radial basis functions were used e.g.:

$$f = \begin{cases} (1-r)^n & 0 \leq r \leq 1 \\ 0 & r > 1 \end{cases} \tag{1.2}$$

This approach leads to a sparse matrix system. Chen applied radial basis functions to the steady-state Poisson equation in two and three dimensions.

1.3 Outline of Approach

This work outlined the theory of DRBEM and GEM for flow in hetereogeneous reservoirs (Chapter 2). A general technique for simulating well tests in heterogeneous reservoirs using hybrid boundary element methods and singularity programming was developed. The results from this method were then compared to analytical solutions and finite difference simulations (Chapter 3). Numerical experiments were performed to assess the performance of DRBEM and GEM for tracer transport problems at high Peclét number. Realistic reservoir tracer flows were considered (Chapter 4). An IMPES scheme for multiphase flow was developed and tested on a Buckley-Leverett problem and a five-spot waterflooding problem (Chapter 5). Finally the well test simulation scheme is coupled with a Gauss-Newton parameter estimation scheme to perform parameter estimation (Chapter 6).

Chapter 2

Mathematical Preliminaries

This work studied the application of the Dual Reciprocity Boundary Element Method and the Green Element Method to reservoir engineering problems. These methods are both based on the Boundary Element Method. This chapter begins with a section describing a derivation of the Boundary Element Method so it can be compared with DRBEM and GEM which are presented in subsequent sections. Only the pressure diffusion equation is considered in this chapter. The diffusion equation is the basis for the other differential equations which will be discussed later.

2.1 Boundary Element Method

2.1.1 Development of the Integral Equation

Consider solving the steady-state Laplace equation in two dimensions:

$$\nabla^2 p = 0 \tag{2.1}$$

For the problem to be properly posed either the pressure, p, or the normal derivative of the pressure, q, must be specified at every point on the boundary. To proceed with the BEM the appropriate free-space Green's function must be available. The Green's function, G, satisfies:

$$\nabla^2 G = \delta(r - r_i) \tag{2.2}$$

where δ is the Dirac delta function. Therefore

$$G = \frac{1}{2\pi} ln \left(\frac{1}{r - r_i} \right) \tag{2.3}$$

where r is a point in the domain, Ω, and r_i is a point on the boundary, Γ.
Green's second identity can be applied to change the differential equation of interest, Equation (2.1), into an integral equation:

$$\int\int_{\Omega} (p\nabla^2 G - G\nabla^2 p) d\Omega = \int_{\Gamma} \left(p\frac{\partial G}{\partial n} - G\frac{\partial p}{\partial n} \right) d\Gamma \tag{2.4}$$

To address the singularity as $(r - r_i) \rightarrow 0$ consider surrounding the point r_i by a small circle of radius ϵ. In the limit as $\epsilon \rightarrow 0$ Equation (2.4) becomes:

$$\int\int_{\Omega - \Omega_\epsilon} (p\nabla^2 G - G\nabla^2 p) d\Omega = \int_{\Gamma + \Gamma_\epsilon} \left(p\frac{\partial G}{\partial n} - G\frac{\partial p}{\partial n} \right) d\Gamma \tag{2.5}$$

Since $\nabla^2 p = 0$ and $\nabla^2 G = 0$ everywhere within $\Omega - \Omega_\epsilon$ Equation (2.5) becomes:

$$\int_{\Gamma} (p\frac{\partial G}{\partial n} - G\frac{\partial p}{\partial n}) d\Gamma + \int_{\Gamma_\epsilon} \left(p\frac{\partial G}{\partial n} - G\frac{\partial p}{\partial n} \right) d\Gamma = 0 \tag{2.6}$$

The integral over Γ_ϵ can be evaluated by noting that:

$$\frac{\partial G}{\partial n} = \frac{\partial G}{\partial r}\frac{\partial r}{\partial n} = \frac{1}{2\pi r} \tag{2.7}$$

Defining θ as the angle measured anticlockwise from the x-axis at point r_i and substituting Equation (2.7) into Equation (2.6) gives:

$$\begin{aligned} \int_{\Gamma_\epsilon} \left(p\frac{\partial G}{\partial n} - G\frac{\partial P}{\partial n} \right) d\Gamma &= \frac{1}{2\pi} \int_0^{\theta_i} \left[p\left(\frac{1}{\epsilon}\right) - ln\left(\frac{1}{\epsilon}\right) \frac{\partial p}{\partial n} \right] \epsilon d\theta \\ &= \frac{1}{2\pi} \int_0^{\theta_i} \left[p + (\epsilon ln \epsilon) \frac{\partial p}{\partial n} \right] d\theta \\ &= \frac{\theta_i}{2\pi} p(r_i) \end{aligned} \tag{2.8}$$

At internal points $\theta_i = 2\pi$ and at smooth boundaries $\theta_i = \pi$. Equation (2.6) is usually written in terms of kernel functions K_1 and K_2:

$$\frac{\theta_i}{2\pi} p(r_i) + \int_{\Gamma} K_1(r, r_i) p(r) d\Gamma = \int_{\Gamma} K_2(r, r_i) \frac{\partial p(r)}{\partial n} d\Gamma \tag{2.9}$$

where

$$K_1 = \frac{\partial G(r, r_i)}{\partial n} = \frac{1}{2\pi r} \tag{2.10}$$

$$K_2 = G(r, r_i) = \frac{1}{2\pi} ln \left(\frac{1}{r - r_i} \right) \tag{2.11}$$

At this stage no approximations have been introduced. The use of Green's second identity has transformed the differential form of Laplace's equation into the integral form in Equation (2.9). This equation only involves boundary integrals. To proceed further the distribution of pressure and flux on the boundary must be interpolated in terms of nodal values of pressure and flux.

2.1.2 Shape Functions

To implement the boundary element method the boundary must be discretized into elements. To evaluate the integrals required, the interpolation scheme used to represent the nodal pressure and flux values in a functional form must be selected. The interpolation is performed using Lagrange shape functions. The three most common choices are constant, linear and quadratic. This work used linear elements in most cases. More specialised shape functions are considered in Chapter 5.

Lagrange shape functions are defined in terms of local coordinates, ξ and η that vary from 0 to 1 along an edge of an element. If a quantity z is being interpolated the Lagrange linear shape functions for a one-dimensional element are:

$$u(\xi) = N_1(\xi) z_1 + N_2 z_2(\xi) \tag{2.12}$$

where

$$N_1 = 1 - \xi \tag{2.13}$$

$$N_2 = \xi \tag{2.14}$$

In the two-dimensional case:

$$u(\xi, \eta) = N_1(\xi, \eta) z_1 + N_2(\xi, \eta) z_2 + N_3(\xi, \eta) z_3 + N_4(\xi, \eta) z_4 \tag{2.15}$$

where

$$N_1 = (1 - \xi)(1 - \eta) \tag{2.16}$$

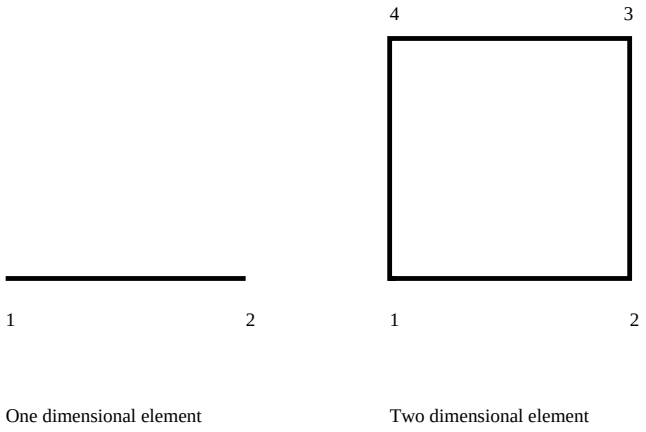

Figure 2.1: Node numbering for one- and two-dimensional elements

$$N_2 = \xi(1-\eta) \tag{2.17}$$

$$N_3 = \xi\eta \tag{2.18}$$

$$N_4 = (1-\xi)\eta \tag{2.19}$$

The node numbering is as shown in Figure 2.1.

2.1.3 Boundary Discretization and Solution Procedure

The integral equation (2.9) can be discretized by breaking the boundary integrals into the sum of the integrals over the elements defining the boundary:

$$\frac{\theta_i}{2\pi}p(r_i) + \sum_{e=1}^{M}\int_{\Gamma^e} K_1(r,r_i)p(r)d\Gamma = \sum_{e=1}^{M}\int_{\Gamma^e} K_2(r,r_i)\frac{\partial p(r)}{\partial n}d\Gamma \tag{2.20}$$

The shape functions being used to interpolate the nodal pressure values are now substituted into Equation (2.20). For example if linear shape functions are used in a two-dimensional problem, i.e. with one-dimensional boundaries, Equation (2.20) becomes:

$$\begin{aligned}\frac{\theta_i}{2\pi}p(r_i) + \sum_{e=1}^{M}\int_{\Gamma^e} K_1(r,r_i)(N_1p_1^e + N_2p_2^e)d\Gamma \\ = \sum_{e=1}^{M}\int_{\Gamma^e} K_2(r,r_i)(N_1q_1^e + N_2q_2^e)d\Gamma\end{aligned} \tag{2.21}$$

where p_1^e, p_2^e, q_1^e and q_2^e denote the nodal values of pressure and pressure derivative at each end of the element.

Equation (2.21) is used to generate one equation per boundary node by placing the source node of the Green's function, r_i, at each boundary node in turn. To assemble these equations into a matrix equation the kernel integrals must be evaluated. These are of the form:

$$\int_{\Gamma_j} K_1(r, r_i) f(\xi) d\Gamma \tag{2.22}$$

and

$$\int_{\Gamma_j} K_2(r, r_i) f(\xi) d\Gamma \tag{2.23}$$

where $f(\xi)$ is a shape function which has the form of a polynomial in ξ. These integrals can not usually be performed analytically and are evaluated with Gaussian quadrature. If the source node i occurs in element j the integrals are singular and can not be evaluated accurately with standard Gaussian quadrature. In one dimension logarithmic quadrature can be applied [3].

When all the kernel integrals have been evaluated Equation (2.21) can be assembled into a matrix equation of the form:

$$Ap = Bq \tag{2.24}$$

It should be noted that the matrices A and B are fully populated because the kernels K_1 and K_2 couple the pressure and its normal derivative at the source point, r_i, to the values at all other locations on the boundary. The matrices have dimensions N by N, where N is the number of nodes on the boundary. Since either p or q is known at every boundary node this equation can be reduced to an equation of the form:

$$Ax = y \tag{2.25}$$

where the vector x contains the unknown p and q values. Once the unknowns on the boundary have been determined the pressure at any point inside the domain can then be determined. This is done by referring to Equation (2.21) and placing the source, r_i, of the Green's function at the point of interest. Since all the nodal values of p and q are known Equation (2.21) can be solved for $p(r_i)$. The accuracy of the solution at

internal points is actually higher than the accuracy of the solution on the boundary because there is no interior discretization or approximation [3].

2.2 Treatment of Heterogeneity

To use the classical boundary element method described in Section 2.1 the differential equation being considered must include a ∇^2 operator. The single phase flow equation:

$$\nabla \cdot (k \nabla p) = \phi \mu c_t \frac{\partial p}{\partial t} \tag{2.26}$$

is therefore not in a form suitable for solution by a boundary element method. This work used two approaches to write the flow equation in a form suitable for solution using DRBEM or GEM. The first was a change of variables as used by El Harrouni et al. [13]. The second was an expansion of the flow equation into a $\nabla^2 p$ term and a further term accounting for reservoir heterogeneity.

El Harrouni et al.'s approach

El Harrouni et al. [13] began from the steady-state single phase flow equation. To extract a Laplacian operator from this equation they introduced a new variable, u:

$$u = \sqrt{k} p \tag{2.27}$$

After this transformation the flow equation can be written as:

$$\nabla^2 u = k' u + \frac{\phi \mu c_t}{k} \frac{\partial u}{\partial t} \tag{2.28}$$

where

$$k' = \frac{\nabla^2 \sqrt{k}}{\sqrt{k}} \tag{2.29}$$

Equation (2.28) is in a form suitable for a boundary element based solution. The right hand side of the equation requires special treatment because application of Green's second identity can not be used to convert this into a boundary integral in the integral form of the equation. Both DRBEM and GEM offer means to handle this term.

The change of variable causes the way that the boundary conditions are expressed to change. Dirichlet boundary conditions change from:

$$p = \bar{p} \tag{2.30}$$

to

$$u = \sqrt{k}\bar{p} \tag{2.31}$$

Neumann boundary conditions change from:

$$\frac{\partial p}{\partial n} = \bar{q}_n \tag{2.32}$$

to

$$\frac{\partial u}{\partial n} = \frac{1}{2k}\frac{\partial k}{\partial n}u + \sqrt{k}\bar{q}_n \tag{2.33}$$

Robin boundary conditions change from:

$$\frac{\partial p}{\partial n} = \gamma h + \eta \tag{2.34}$$

to

$$\frac{\partial u}{\partial n} = \left(\gamma + \frac{1}{2k}\frac{\partial k}{\partial n}\right)u + \sqrt{k}\eta \tag{2.35}$$

The Neumann boundary conditions becomes a Robin boundary condition in the new variable. This requires an iterative solution.

Under this change of variable the treatment of anisotropy is difficult.

Taigbenu and Onyejekwe's Approach

The second approach was presented by Taigbenu and Onyejekwe [67]. The single phase steady-state flow equation is written as:

$$\nabla^2 p = -\nabla lnk \cdot \nabla p + \frac{\phi\mu c_t}{k}\frac{\partial p}{\partial t} \tag{2.36}$$

This form of the flow equation can be used when the permeability field is anisotropic. Unlike El Harrouni et al.'s [13] approach no modifications to the boundary conditions are required. Like El Harrouni et al.'s approach hybrid boundary element methods such as DRBEM and GEM are required to handle the right hand side of the flow equation.

2.3 Dual Reciprocity Boundary Element Method

The Boundary Element Method is well suited to solving problems of the form:

$$\nabla^2 p = 0 \tag{2.37}$$

The Dual Reciprocity Boundary Element Method (DRBEM) extends the applicability of the Boundary Element Method to a wider class of problems by treating p as the sum of a homogeneous solution and a particular solution $\hat{p}$. The features of the method will be demonstrated by presenting its application to steady-state and transient diffusion problems in homogenous and heterogeneous media.

2.3.1 Steady-State Pressure Diffusion

Consider a steady state pressure diffusion problem governed by:

$$\nabla^2 p = b(x, y) \tag{2.38}$$

The particular solution satisfies:

$$\nabla^2 \hat{p} = b(x, y) \tag{2.39}$$

Note that the particular solution does not neccesarily satisfy the boundary conditions imposed on the problem in Equation (2.38). DRBEM expands the right hand side of Equation (2.39) as the sum of a series of specified approximating functions, f_j.

$$b = \sum_{j=1}^{N+L} \alpha_j f_j \tag{2.40}$$

where α_j are initially unknown weights and f_j are the approximating functions. N is the number of nodes on the boundary and L is the number of internal nodes. The accuracy of DRBEM improves if internal nodes are used. The use of internal nodes does not require any associated internal gridding however.

The approximating functions are user-defined functions. The only condition that these functions must satisfy is that they are the Laplacian of another function $\hat{p}_j$.

$$\nabla^2 \hat{p}_j = f_j \tag{2.41}$$

Partridge et al. [49] suggested three possible choices for the approximating functions - elements of the Pascal triangle, trigonometric series and terms from the series:

$$f = 1 + r + r^2 + ... + r^m \tag{2.42}$$

The approximating function most often chosen is $f = 1 + r$. Substituting Equations (2.39), (2.40) and (2.41) into (2.38) produces the equation that is the starting point for DRBEM:

$$\nabla^2 p = \sum_{j=1}^{N+L} \alpha_j \nabla^2 \hat{p}_j \tag{2.43}$$

Multiplying both sides of Equation (2.43) by G and integrating over the domain gives:

$$\iint_\Omega G \nabla^2 p \, d\Omega = \sum_{j=1}^{M+L} \alpha_j \iint_\Omega G \nabla^2 \hat{p}_j \, d\Omega \tag{2.44}$$

As in the derivation of the boundary element method Green's second identity can be applied to reduce these domain integrals to surface integrals:

$$\begin{aligned} \frac{\theta_i}{2\pi} p(r) + \int_\Gamma K_1(r, r_i) p(r) d\Gamma - \sum_{j=1}^{M+L} \alpha_j \int_\Gamma K_1(r, r_i) \hat{p}_j d\Gamma = \\ \int_\Gamma K_2(r, r_i) \frac{\partial p(r)}{\partial n} d\Gamma - \sum_{j=1}^{M+L} \alpha_j \int_\Gamma K_2(r, r_i) \frac{\partial p(r)}{\partial n} d\Gamma \end{aligned} \tag{2.45}$$

In matrix form this can written as:

$$Ap - Bq = \sum_{j=1}^{N+L} \alpha_j (A\hat{p}_j - B\hat{q}_j) \tag{2.46}$$

To proceed further the weights α must be computed. This can be done by writing the expansion of the right hand side b in matrix form:

$$b = F\alpha \tag{2.47}$$

where F is an $(N+L)$ by $(N+L)$ square matrix whose jth column is f_j evaluated at each node. The vector α can be found by solving Equation (2.47). The matrix equation (2.46) can now be written as:

$$Ap - Bq = d \tag{2.48}$$

where

$$d = (A\hat{P} - B\hat{Q})\alpha \tag{2.49}$$

As in the boundary element method this equation may be reduced to the form, $Ax = y$. After the unknowns have been solved for on the boundary and at any internal nodes, the pressure can be found at any point in the domain in a manner similar to the classical boundary element method. The source point of the Green's function, r_i, is placed at the point of interest. Equation (2.45) can then be solved for the pressure at that point. Like the classical boundary element method DRBEM produces a dense matrix equation.

2.3.2 Transient Pressure Diffusion

DRBEM can be applied to transient problems in a manner similar to the treatment of steady-state problems given in Section 2.3.1. Consider solving:

$$\nabla^2 p = \gamma \frac{\partial p}{\partial t} \tag{2.50}$$

where

$$\gamma = \frac{\phi \mu c_t}{k} \tag{2.51}$$

In this case the medium is assumed to be homogeneous. Applying DRBEM as before gives:

$$Ap - Bq = \gamma(A\hat{P} - B\hat{Q})\alpha \tag{2.52}$$

In the transient case the time derivative term is expanded as a weighted sum of approximating functions as in the steady-state case. However in the transient case the weights are time dependent:

$$\frac{\partial p}{\partial t} = \sum_{j=1}^{N+L} f_j \, \alpha_j(t) \tag{2.53}$$

Equation (2.53) can be written in matrix form, in a manner similar to Equation (2.47):

$$\dot{p} = F\alpha \tag{2.54}$$

where $\dot{p}$ is a vector containing the values of $\frac{\partial p}{\partial t}$ at each node.
Substituting Equation (2.54) into (2.52) gives:

$$Ap - Bq = \gamma(A\hat{P} - B\hat{Q})F^{-1}\dot{p} \tag{2.55}$$

To allow the equation to be written more compactly a matrix C is defined as:

$$C = -\gamma(A\hat{P} - B\hat{Q})F^{-1} \tag{2.56}$$

Substituting Equation (2.56) into (2.55) gives:

$$Ap + C\dot{p} = Bq \tag{2.57}$$

Partridge et al. [49] employ a two-level time integration scheme for the variation of p and q:

$$p = (1 - \theta_p)p^m + \theta_p p^{m+1} \tag{2.58}$$

$$q = (1 - \theta_q)q^m + \theta_q q^{m+1} \tag{2.59}$$

$$\dot{p} = \frac{1}{\Delta t}(p^{m+1} - p^m) \tag{2.60}$$

where the indices m and $m + 1$ correspond to timesteps. $\theta = 1$ corresponds to a fully implicit formulation. Substituting Equation (2.58), (2.59) and (2.60) into (2.57) yields:

$$\left(\frac{1}{\Delta t}C + \theta_p A\right)p^{m+1} - \theta_q B q^{m+1} = \left(\frac{1}{\Delta t}C - (1 - \theta_p)A\right)p^m + (1 - \theta_q)Bq^m \tag{2.61}$$

Partridge et al. [49] observed good accuracy using $\theta_p = 0.5$ and $\theta_q = 1.0$. This corresponds to:

$$\left(\frac{2}{\Delta t}C + A\right)p^{m+1} - 2Bq^{m+1} = \left(\frac{2}{\Delta t}C - A\right)p^m \tag{2.62}$$

2.3.3 Pressure Diffusion in Heterogeneous Media

The only modeling of flow in heterogeneous media performed used DRBEM incorporated El Harrouni et al.'s [13] change of variable (Equation 2.27) to handle heterogeneity. Recall that the differential equation that governs this is:

$$\nabla^2 u = k'u + \frac{\phi\mu c_t}{k}\frac{\partial u}{\partial t} \tag{2.63}$$

DRBEM is applied to this equation in the same manner as the previous two examples to give:

$$Au - Bq = \gamma(A\hat{U} - B\hat{Q})\alpha \tag{2.64}$$

Note that in this example q refers to the normal derivative of the transformed pressure, u, not the actual pressure, p. The key to DRBEM is defining the vector weights, α. In this case α is defined by the matrix equation:

$$k'u + \gamma\dot{u} = F\alpha \tag{2.65}$$

where

$$\gamma = \frac{\phi\mu c_t}{k} \tag{2.66}$$

Substituting Equation (2.65) into (2.64) gives:

$$Au - Bq = (A\hat{U} - B\hat{Q})F^{-1}(k'u + \gamma\dot{u}) \tag{2.67}$$

This can be simplified by defining a matrix C as;

$$C = (A\hat{U} - B\hat{Q})F^{-1} \tag{2.68}$$

Substituting Equation (2.68) into (2.67) gives:

$$Au + Ck'u + C\gamma\dot{u} = Bq \tag{2.69}$$

The two level time integration scheme shown in Equations (2.58), (2.59) and (2.60) can be applied to Equation (2.69) to give:

$$\left(\frac{1}{\Delta t}C\gamma + \theta_u A - \theta_u Ck'\right)u^{m+1} - \theta_q Bq^{m+1}$$
$$= \left(\frac{1}{\Delta t}C\gamma - (1-\theta_u)A + (1-\theta_u)Ck'\right)u^m + (1-\theta_q)Bq^m \tag{2.70}$$

2.4 Green Element Method

The Green Element Method is an element-by-element implementation of boundary element theory that can handle terms that result in domain integrals. The terms that result from the treatment of heterogeneity are an example of such terms. GEM requires the entire domain to be discretized and produces a large sparse matrix equation. In this work GEM was applied to one- and two-dimensional problems. The theory has also been developed by Taigbenu [70] for three-dimensional problems, though no results from this formulation have been published.

2.4.1 One-Dimensional Problems

The fundamentals of GEM can be demonstrated by considering the transient diffusion equation in a homogeneous medium on $x[0, L]$:

$$\frac{\partial^2 p}{\partial x^2} = \gamma \frac{\partial p}{\partial t} \tag{2.71}$$

Like any boundary element based method GEM begins by finding the relevant free space Green's function for the problem:

$$\frac{\partial^2 G}{\partial x^2} = \delta(x_i - x) \tag{2.72}$$

The solution to Equation (2.72) is:

$$G(x_i, x) = \frac{1}{2}(|x_i - x| + le) \tag{2.73}$$

where le is an arbitrary constant taken to be the length of the element.
In one dimension Green's second identity is:

$$\int_0^L \left(p\frac{\partial^2 G}{\partial x^2} - G\frac{\partial^2 p}{\partial x^2} \right) dx = p\, \frac{\partial G}{\partial x}\bigg|_0^L - G\, \frac{\partial p}{\partial x}\bigg|_0^L \tag{2.74}$$

Equation (2.71) can be cast as an integral equation substituting Equation (2.73) and (2.71) into Green's second identity (2.74). The resulting integral equation is:

$$\int_0^L \left(p\delta(x - x_i) - G\gamma\frac{\partial p}{\partial t} \right) dx = p\, \frac{\partial G}{\partial x}\bigg|_0^L - G\, \frac{\partial p}{\partial x}\bigg|_0^L \tag{2.75}$$

The final integral equation is derived from Equation (2.75) by noting that the area under a Dirac delta function is one:

$$-\lambda_i p(x_i) + \left[p\frac{\partial G}{\partial x} - G\frac{\partial p}{\partial x} \right]_0^L + \int_0^L G\gamma \frac{\partial p}{\partial t} dx = 0 \tag{2.76}$$

where $\lambda_i = 1$ at points within the domain and $\lambda_i = 0.5$ at the end nodes.
GEM proceeds by discretizing the domain into elements. Equation (2.76) is evaluated as a summation over these elements:

$$\sum_{e=1}^{M} \left(-\lambda_i p(x_i) + \left[p\frac{\partial G}{\partial x} - G\frac{\partial p}{\partial x} \right]_{x_2}^{x_1} + \int_{x_1}^{x_2} G\gamma \frac{\partial p}{\partial t} dx \right) = 0 \tag{2.77}$$

where M is the total number of elements.
Note that until this point no approximations have been made. Further progress can be made by introducing Lagrange shape functions, N, to approximate p and $\frac{\partial p}{\partial x}$ over the element in terms of the nodal values at the end of each element. In this case linear shape functions will be used:

$$p = N_1 p_1 + N_2 p_2 \tag{2.78}$$

Denoting $\frac{\partial p}{\partial x}$ as q:

$$q = N_1 q_1 + N_2 q_2 \tag{2.79}$$

Equation (2.77) also requires the spatial derivative of the Green's function which is:

$$\frac{\partial G(x, x_i)}{\partial x} = \frac{1}{2} \left[H(x - x_i) - H(x_i - x) \right] \tag{2.80}$$

where H is the Heaviside step function

$$H(x_i - x) = \begin{cases} 1, x > x_i \\ 0, x < x_i \end{cases} \tag{2.81}$$

Substituting Equations (2.78), (2.79) and (2.80) into (2.77) gives:

$$\sum_{e=1}^{M} -2\lambda_i p(x_i) + [H(x_2 - x_i) - H(x_i - x_2)] p_2$$

$$-[H(x_1 - x_i) - H(x_i - x_1)] p_1 - (|x_2 - x_i| + 1) q_2$$

$$+(|x_1 - x_i| + 1)q_1 + \int_{x_1}^{x_2} G\left(N_1\gamma\frac{\partial p_1}{\partial t} + N_2\gamma\frac{\partial p_2}{\partial t}\right)dx = 0 \tag{2.82}$$

Equation(2.82) can be expanded into two equations by placing the source node x_i at either of the nodes at the end of an element, x_1 or x_2.

When $x_i = x_1$ Equation (2.82) becomes:

$$\sum_{e=1}^{M}(-p_1 + p_2 + q_1 - (1 + le)q_2) + \int_{x_1}^{x_2} G\left(N_1\frac{\partial p_1}{\partial t} + N_2\frac{\partial p_2}{\partial t}\right)dx = 0 \tag{2.83}$$

When $x_i = x_2$:

$$\sum_{e=1}^{M}(p_1 - p_2 + (1 + le)q_1 - q_2) + \int_{x_1}^{x_2} G\left(N_1\frac{\partial p_1}{\partial t} + N_2\frac{\partial p_2}{\partial t}\right)dx = 0 \tag{2.84}$$

Equations (2.83) and (2.84) can be combined and written in matrix form as:

$$\sum_{e=1}^{M} R_{ij}p_j + L_{ij}q_j + T_{ij}\frac{\partial p_j}{\partial t} \tag{2.85}$$

where

$$R = \begin{bmatrix} -1 & 1 \\ 1 & -1 \end{bmatrix} \tag{2.86}$$

$$L = \begin{bmatrix} 1 & -(1 + le) \\ 1 + le & -1 \end{bmatrix} \tag{2.87}$$

$$T_{ij} = \int_0^{le} G(x_i, x)N_j dx \tag{2.88}$$

$$T = \begin{bmatrix} \frac{le(3+le)}{6} & \frac{le(3+2le)}{6} \\ \frac{le(3+2le)}{6} & \frac{le(3+le)}{6} \end{bmatrix} \tag{2.89}$$

Time is handled using finite differences:

$$\alpha\sum_{e=1}^{M}(R_{ij}p_j + L_{ij}q_j) + (1 - \alpha)\sum_{e=1}^{M}(R_{ij}p_j + L_{ij}q_j) + T_{ij}\frac{1}{\Delta t}(p_j^{m+1} - p_j^m) = 0 \tag{2.90}$$

The value of α can be chosen to give a fully implicit, Crank-Nicolson, explicit scheme etc.

2.4.2 Two-Dimensional Problems

Steady-State Pressure Diffusion

The differences between the standard boundary element method and GEM will be made clearer by considering the application of GEM to steady-state pressure diffusion in a two-dimensional heterogenous medium. The governing differential equation is:

$$\nabla^2 p = -\nabla lnk \cdot \nabla p \tag{2.91}$$

When Equation (2.91) is multiplied by G and integrated over the domain the following integral equation is formed:

$$\theta_i p(r_i) + \int_\Gamma K_1(r, r_i) p(r) d\Gamma - \int_\Gamma K_2(r, r_i) \frac{\partial p(r)}{\partial n} d\Gamma = \iint_\Omega G \left(-\nabla lnk \cdot \nabla p\right) d\Omega \tag{2.92}$$

where θ_i is the nodal angle at r_i.

Note that the left hand side of this equation is the same as the left hand side of Equation (2.9) derived as part of BEM. The Green's function used for the two-dimensional case is:

$$G = ln(r - r_i) \tag{2.93}$$

GEM theory now departs from standard BEM theory. BEM performs the boundary integrals on the left hand side as a sum of integrals over one-dimensional elements which discretize the boundary. Instead GEM computes the boundary integrals as a sum of integrals over the boundaries of the two-dimensional elements that discretize the domain. The two approaches are equivalent because integrals along the "internal" parts of the boundary cancel. This is shown in Figure 2.2. The arrows indicate the direction of integration around the boundaries of elements 1 and 2. Because the directions are opposite the contributions of the integrals over the segment AB cancel each other when the integrals over the boundary of elements 1 and 2 are summed. The discretized form of the integral equation is:

$$\begin{aligned} \theta_i p(r_i) + \sum_{e=1}^{M} \int_{\Gamma^e} K_1(r, r_i) p(r) d\Gamma - \sum_{e=1}^{M} \int_{\Gamma^e} K_2(r, r_i) \frac{\partial p(r)}{\partial n} d\Gamma \\ = \sum_{e=1}^{M} \iint_{\Omega^e} G \left(-\nabla lnk \cdot \nabla p\right) d\Omega \end{aligned} \tag{2.94}$$

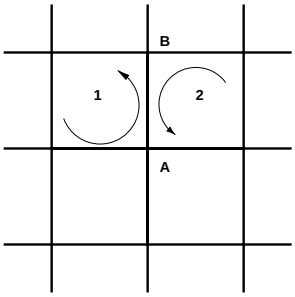

Figure 2.2: Segment of a discretized domain showing integration over integral segements of the boundary

To evaluate these integrals the pressure and its normal derivative at any point within an element are expressed in terms of the values at the four nodes of the element and linear shape functions:

$$p(x,y) = \sum_{j=1}^{4} p_j N_j \tag{2.95}$$

$$q(x,y) = \sum_{j=1}^{4} p_j N_j \tag{2.96}$$

The permeability is also interpolated using shape functions:

$$lnk(x,y) = \sum_{j=1}^{4} lnk_j N_j \tag{2.97}$$

Introduction of the elemental matrices R, L and V and the use of summation notation allow the integral equation to be written more compactly as:

$$\sum_{e=1}^{M} \left(R_{ij}^{e} p_j + L_{ij}^{e} q_j - V_{ijl}^{e} lnk_j p_l \right) = 0 \tag{2.98}$$

where

$$R_{ij}^{e} = \int_{\Gamma_e} \frac{\partial G(r, r_i)}{\partial n} N_j d\Gamma - \delta_{ij}\theta_i \tag{2.99}$$

$$L_{ij}^{e} = -\int_{\Gamma_e} G(r, r_i) N_j d\Gamma \tag{2.100}$$

$$V^e_{ijl} = \iint_{\Omega_e} G(r, r_i) \left[\frac{\partial N_j}{\partial x} \frac{\partial N_l}{\partial x} + \frac{\partial N_j}{\partial y} \frac{\partial N_l}{\partial y} \right] d\Omega \tag{2.101}$$

The elements of R, L and V can be evaluated analytically for triangular and rectangular elements. The expressions for each term of the element matrices are given in Appendix A.

Treatment of Pressure Derivative at Internal Nodes

Equation (2.98) represents one equation per node. The equations however have two unknowns at every internal node, p and two components of q. The internal pressure derivative terms are eliminated from Equation (2.98) by expressing them in terms of the nodal pressure values and derivatives of the shape functions:

$$\frac{\partial p}{\partial x} = \sum_{j=1}^{4} \frac{\partial N_j}{\partial x} p_j \tag{2.102}$$

$$\frac{\partial p}{\partial y} = \sum_{j=1}^{4} \frac{\partial N_j}{\partial y} p_j \tag{2.103}$$

This is the simplest treatment of the derivatives available. This treatment does not ensure continuity of the derivatives across the element boundaries. This problem is discussed extensively in Section 5.3.

Transient Pressure Diffusion

The steady-state GEM formulation can be extended to solve the transient pressure diffusion equation in a heterogeneous medium:

$$\nabla^2 p = -\nabla lnk \cdot \nabla p + \gamma \frac{\partial p}{\partial t} \tag{2.104}$$

The fundamental procedure is the same as the steady-state case. When the differential equation has been multiplied by G and integrated over the doman the following integral equation is formed:

$$\begin{aligned} \frac{\theta_i}{2\pi} p(r_i) + \int_\Gamma K_1(r, r_i) p(r_i)\, d\Gamma - \int_\Gamma K_2(r, r_i) \frac{\partial p(r_i)}{\partial n}\, d\Gamma \\ = -\iint_\Omega G \nabla lnk \cdot \nabla p \; d\Omega + \iint_\Omega G\gamma \frac{\partial p}{\partial t} \; d\Omega \end{aligned} \tag{2.105}$$

As in the steady-state case this equation can be written in discretized form as:

$$\theta_i p(r_i) + \sum_{e=1}^{M} \int_{\Gamma^e} K_1(r, r_i) p(r_i)\, d\Gamma - \sum_{e=1}^{M} \int_{\Gamma^e} K_2(r, r_i) \frac{\partial p(r_i)}{\partial n}\, d\Gamma \qquad (2.106)$$
$$= -\sum_{e=1}^{M} \iint_{\Omega_e} G \nabla lnk \cdot \nabla p \; d\Omega + \sum_{e=1}^{M} \iint_{\Omega^e} G\gamma \frac{\partial p}{\partial t}\, d\Omega$$

Introducing shape functions as before this equation be written more compactly as:

$$\sum_{e=1}^{M} \left(R_{ij} p_j + L_{ij} q_j - V_{ijl} lnk_j p_l + U_{ijl} \gamma_j \frac{\partial p_l}{\partial t} \right) = 0 \qquad (2.107)$$

where R_{ij}, L_{ij} and V_{ijl} are defined by Equations (2.99), (2.100) and (2.101) and U_{ijl} is defined by:

$$U_{ijl} = \iint_{\Omega^e} G(r, r_i) N_j N_l \, d\Omega \qquad (2.108)$$

To proceed further the time derivative is expanded as:

$$\frac{\partial p}{\partial t} = \frac{p^{m+1} - p^m}{\Delta t} \qquad (2.109)$$

A two level time integration scheme is applied to Equation (2.107) to give:

$$\theta \sum_{e=1}^{M} \left(R_{ij} p_j^{m+1} + L_{ij} q_j^{m+1} - V_{ijl} lnk_j p_l^{m+1} \right) + \frac{U_{ijl}\gamma_j}{\Delta t} p_l^{m+1}$$
$$+(1-\theta) \sum_{e=1}^{M} \left(R_{ij} p_j^{m} + L_{ij} q_j^{m} - V_{ijl} lnk_j p_l^{m} \right) - \frac{U_{ijl}\gamma_l}{\Delta t} p_l^{m} = 0 \qquad (2.110)$$

2.5 Summary

This section has introduced the classical form of BEM. Application of BEM is only possible when the differential equation of interest contains a ∇^2 operator. Two approaches to transforming the equation governing single phase flow in heterogeneous media were considered to allow this equation to be solved using BEM. El Harrouni et al. [13] proposed a method that required a change of variable. The changes required to the boundary conditions, especially the fact that Neumann boundary conditions become Robin boundary conditions, make this approach less attractive than the approach proposed by Taigbenu and Onyejekwe [67]. Two boundary element hybrids,

DRBEM and GEM, which are capable of solving the flow equation in a heterogeneous medium were introduced. The main difference between the methods is the way they handle the terms that arise from right hand side of the integral equations. These terms need special treatment because, unlike a ∇^2 term, the application of Green's second identity does not convert the domain integral into a boundary integral. DRBEM expands the right hand side as the sum of a series of approximating functions. These functions are chosen so that they are Laplacians of particular solutions to the diffusion equation. This property means that that the series can be converted to a boundary integral. The matrix equation that results is dense and has a dimension equal to the number of nodes (both internal and external) in the problem.

GEM takes a philosophically different approach to the right hand side terms. Instead of taking measures to convert the terms from domain integrals to boundary integrals they are left as domain integrals. To do so the domain must be discretized and the boundary integrals on the left hand side must be treated as a sum of integrals over the boundaries of all the two-dimensional elements that form the domain. The chief advantage in doing so is the form of the resulting matrix equation which is large and sparse instead of dense. In two dimensions the matrix has nine bands as opposed to the five bands that would arise from a standard finite difference formulation.

The following chapters discuss both DRBEM and GEM. DRBEM is considered because it is a central technique for solving BEM problems that include domain integrals. The dense matrix structure is a major disadvantage for practical reservoir engineering problems however, so most of the examples presented only consider GEM. Numerical results comparing DRBEM and GEM, and assessing the accuracy of GEM are presented in Appendix C. These results show GEM is more accurate than DRBEM for the example considered, and that the one-dimensional GEM formulation is more accurate than the two-dimensional GEM formulation.

Chapter 3

Pressure Transient Analysis

The first reservoir engineering problem considered using the Green Element Method (GEM) is the modeling of single-phase well tests in heterogeneous porous media. Singularity programming is incorporated with GEM to do so. The first step in this analysis is the derivation of the differential equation governing the nonsingular component of the flow. This equation is then developed into an integral equation and discretized. The results are compared to analytical solutions and finite difference simulations. These results show that finite difference simulations of well tests are hampered by numerical artifacts not present in the GEM approach.

3.1 Theory

3.1.1 Application of Singularity Programming

Masukawa and Horne [38] and Sato [57] applied singularity programming in conjunction with boundary element methods to compute pressure transients. Unlike the current study Sato's solution was performed in Laplace space. Singularity programming decomposes the solution into singular and nonsingular components:

$$p_D = p_D^{ns} + p_D^s \tag{3.1}$$

The singular solution used in this work is based on the pressure response of a well flowing at a given rate in an infinite homogeneous reservoir with uniform permeability,

k_0 (Dake, [11]):

$$p^s = p_i - \frac{q\mu}{4\pi k_0 h} Ei\left(\frac{\phi\mu c_t r^2}{4k_0 t}\right) \tag{3.2}$$

Out of regard for numerical stability dimensionless variables were used in the implementation of the singularity programming. The choice of dimensionless variables in this work follows that of Sato [57]:

$$p_D = \frac{p_i - p}{p_i} \tag{3.3}$$

$$x_D = \frac{x}{\sqrt{A}} \tag{3.4}$$

$$y_D = \frac{y}{\sqrt{A}} \tag{3.5}$$

$$q_D = -\frac{q\mu}{4\pi k_0 h p_i} \tag{3.6}$$

$$t_D = \frac{k_0 t}{\phi\mu c_t A} \tag{3.7}$$

Using this choice of variables the singular solution is:

$$p^s_D = -q_D Ei\left(\frac{r^2_D}{4t_D}\right) \tag{3.8}$$

where $Ei(x)$ is the exponential integral:

$$Ei(x) = \int_x^\infty \frac{e^s}{s}\, ds \tag{3.9}$$

To apply singularity programming in a heterogeneous reservoir careful consideration must be made of the nonsingular solution. The GEM solution scheme will be used to solve for the nonsingular solution. To ascertain what differential equation must be solved for the nonsingular solution consider the equations that govern the pressure and the singular part of the pressure. The pressure satisfies:

$$\nabla^2 p_D = \frac{k_0}{k}\frac{\partial p_D}{\partial t_D} - \nabla lnk \cdot \nabla p_D \tag{3.10}$$

The singular part of the pressure solution given in Equation (3.2) satisfies:

$$\nabla^2 p^s_D = \frac{\partial p^s_D}{\partial t_D} \tag{3.11}$$

Subtracting Equation (3.11) from (3.10) gives:

$$\nabla^2 p_D - \nabla^2 p_D^s = \frac{k_o}{k}\frac{\partial p_D}{\partial t_D} - \frac{\partial p_D^s}{\partial t_D} - \nabla lnk \cdot \nabla p_D \tag{3.12}$$

Noting that $p_D = p_D^{ns} + p_D^s$ Equation (3.12) can be simplifed to:

$$\nabla^2 p_D^{ns} = \frac{k_0}{k}\frac{\partial p_D^{ns}}{\partial t_D} + \left(\frac{k_o}{k} - 1\right)\frac{\partial p_D^s}{\partial t_D} - \nabla lnk \cdot \nabla(p_D^{ns} + p_D^s) \tag{3.13}$$

The right hand side of Equation (3.13) includes both the singular and nonsingular solutions. This does not present a problem however since the singular solution is known and can be incorporated easily into the boundary element solution.

Useful Derivatives

Equation (3.13) requires the derivatives of the singular solution with respect to time and space. These expressions are:

$$\frac{\partial p_D^s}{\partial t_D} = exp\left(\frac{-r_D^2}{t_D}\right)\frac{q_D}{t_D} \tag{3.14}$$

$$\frac{\partial p_D^s}{\partial x_D} = -2\, exp\left(\frac{-r_D^2}{t_D}\right)\frac{q_D x_D}{r_D^2} \tag{3.15}$$

$$\frac{\partial p_D^s}{\partial y_D} = -2\, exp\left(\frac{-r_D^2}{t_D}\right)\frac{q_D y_D}{r_D^2} \tag{3.16}$$

3.1.2 Derivation of the Green Element Scheme

To transform Equation (3.13) into an integral equation suitable for solution with GEM the right hand side terms, which do not depend on time or space derivatives of p_D^{ns}, are collected together:

$$\nabla^2 p_D^{ns} = \frac{k_0}{k}\frac{\partial p_D^{ns}}{\partial t_D} - \nabla lnk \cdot \nabla(p_D^{ns}) + f \tag{3.17}$$

where

$$f = \left(\frac{k_o}{k} - 1\right)\frac{\partial p_D^s}{\partial t_D} - \nabla lnk \cdot \nabla(p_D^s) \tag{3.18}$$

Equation (3.17) can be cast as an integral equation in the usual manner by multiplying it by G and integrating over the domain:

$$\frac{\theta_i}{2\pi}p_D^{ns}(r_i) + \int_\Gamma K_1(r,r_i)p_D^{ns}(r)d\Gamma - \int_\Gamma K_2(r,r_i)\frac{\partial p_D^{ns}(r)}{\partial n}d\Gamma$$
$$= \iint_\Omega G\left(\frac{k_0}{k}\frac{\partial p_D^{ns}}{\partial t_D} - \nabla lnk \cdot \nabla p_D^{ns} + f\right)d\Omega \tag{3.19}$$

The integrals in Equation (3.19) are then written as summations over the elements:

$$\frac{\theta_i}{2\pi}p_D^{ns}(r_i) + \sum_{e=1}^{M}\int_{\Gamma^e} K_1(r,r_i)p_D^{ns}(r)d\Gamma - \sum_{e=1}^{M}\int_{\Gamma^e} K_2(r,r_i)\frac{\partial p_D^{ns}(r)}{\partial n}d\Gamma$$
$$= \sum_{e=1}^{M}\iint_{\Omega^e} G\left(\frac{k_0}{k}\frac{\partial p_D^{ns}}{\partial t_D} - \nabla lnk \cdot \nabla p_D^{ns} + f\right)d\Omega \tag{3.20}$$

Equation (3.20) can be written in a more compact form in terms of the element matrices R, L, U, V and T:

$$\sum_{e=1}^{M}\left(R_{ij}p_j + L_{ij}q_j - U_{ijl}\frac{k_0}{k_j}\frac{\partial p}{\partial t_D} - V_{ijl}lnk_j p_l + T_{ij}f_j\right) = 0 \tag{3.21}$$

Note that in Equation (3.21) the subscript and superscript have been dropped from p_D^{ns} for clarity.

The element matrices R,L,V and U have been defined previously in Equations (2.99), (2.100), (2.101) and (2.108). The definition of the matrix T is:

$$T_{ij} = \iint_{\Omega^e} G(r,r_i)N_j \; d\Omega \tag{3.22}$$

The expressions for all the terms in the element matrices are given in Appendix A. Equation(3.21) was solved using a fully implicit treatment i.e:

$$\sum_{e=1}^{M}\left(R_{ij}p_j^{m+1} + L_{ij}q_j^{m+1} - U_{ijl}\frac{k_0}{k_j}\frac{p_l^{m+1}-p_l^m}{\Delta t} - V_{ijl}lnk_j p_l^{m+1} + T_{ij}f_j^{m+1}\right) = 0 \tag{3.23}$$

3.1.3 Well Test Simulation without Singularity Programming

To assess the effectiveness of singularity programming in conjunction with GEM in the simulation of well tests, a GEM scheme was derived without singularity programming.

This scheme treated the well as a source/sink term. The well block pressure was converted into a bottom hole pressure using the Peaceman [50] well index in the same manner as common finite difference simulators. The well index is defined by:

$$q_w = WI\frac{1}{\mu}(p_{block} - p_w) \tag{3.24}$$

where

$$WI = \frac{2\pi kh}{ln(\frac{r_o}{r_w}) + S} \tag{3.25}$$

$$\frac{r_o}{a} = exp\left(-\frac{\pi}{2}\right) \tag{3.26}$$

where a is the side length of the square cell containing the well.

The differential equation governing the problem was presented by Sato [57]. Without loss of generality the current analysis is restricted to homogeneous media:

$$\nabla^2 p = \frac{\phi\mu c_t}{k}\frac{\partial p}{\partial t} + \sum_{l=1}^{Nw}\frac{\mu}{k}q'_l \tag{3.27}$$

where q' is a sink (for a production well) with a strength given in units of fluid volume per reservoir volume per unit time.

Equation (3.27) is then nondimensionalised using the dimensionless variables defined in Section 3.1.1:

$$\nabla^2 p_D = \frac{\partial p_D}{\partial t_D} + \sum_{l=1}^{Nw} q'_{D_l}\delta(x_D - x_{D_l})\delta(y_D - y_{D_l}) \tag{3.28}$$

The Dirac delta terms in Equation (3.28) specify the well locations precisely. The Green Element Method is now applied to Equation (3.28). After multiplying by G and integrating over the domain, Ω, the integral form of Equation (3.28) is:

$$\frac{\theta_i}{2\pi}p_D^{ns}(r_i) + \int_\Gamma K_1(r, r_i)p_D^{ns}(r)d\Gamma - \int_\Gamma K_2(r, r_i)\frac{\partial p_D^{ns}(r)}{\partial n}d\Gamma$$

$$\iint_\Omega G\left(\frac{\partial p_D^{ns}}{\partial t_D} + \sum_{l=1}^{Nw} q'_{D_l}\delta(x_D - x_{D_l})\delta(y_D - y_{D_l})\right)d\Omega \tag{3.29}$$

When the domain is discretized and shape functions are introduced, the integrals in Equation (3.29) can be expressed as summations of integrals over the elements, as

in the previous GEM formulations:

$$\frac{\theta_i}{2\pi}p_D^{ns}(r_i) + \sum_{e=1}^{M}\int_{\Gamma^e} K_1(r,r_i)p_D^{ns}(r)d\Gamma - \sum_{e=1}^{M}\int_{\Gamma^e} K_2(r,r_i)\frac{\partial p_D^{ns}(r)}{\partial n}d\Gamma$$

$$= \sum_{e=1}^{M}\iint_{\Omega^e} G\left(\frac{\partial p_D^{ns}}{\partial t_D} + \sum_{l=1}^{Nw} q'_{D_l}\delta(x_D - x_{D_l})\delta(y_D - y_{D_l})\right)d\Omega \tag{3.30}$$

Introducing the element matrices R, L and T, defined by Equations (2.99), (2.100) and (3.22) Equation (3.29) can be written more compactly as:

$$\sum_{e=1}^{M}\left(R_{ij}p_{D_j} + L_{ij}q_{D_j} - T_{ij}\frac{\partial p_D}{\partial t_D} - Q_i\right) = 0 \tag{3.31}$$

where Q_i accounts for the integral of the sink term. In previous GEM derivations all the right hand side terms were integrated in terms of shape functions. The special nature of the Dirac delta functions in the sink term means the sink term can be integrated analytically without introducing any shape functions.

If node i is in the wellblock then:

$$Q_i = q'_{D_l} ln\left(\sqrt{(x_{D_l} - x_i)^2 + (y_{D_l} - y_i)^2}\right) \tag{3.32}$$

otherwise

$$Q_i = 0 \tag{3.33}$$

Equation (3.31) was solved using a fully implicit treatment.

3.2 Results

3.2.1 Examples 1 and 2: Comparison to Analytical Solutions

Example 1: Well Test in a Closed Reservoir

To test the combination of singularity programming and GEM a pressure transient was computed and compared to a transient generated analytically. The reservoir properties are given in Table 3.1.

The grid used for the GEM solution of the nonsingular component of the problem was a 10 by 10 mesh. The well was located in the center of the reservoir. Constant

Table 3.1: Examples 1 and 2 - Reservoir properties

k	150 md
ϕ	0.3
μ	1 cp
p_i	2000 psi
q_w	50 STB/d
c_t	10e-06 psi^{-1}
r_w	0.3 ft
h	50 ft
Length	3000 ft
Width	2500 ft

pressure boundaries were imposed on all sides. The resulting drawdowns are compared to the analytical solution in Figure 3.1. The agreement between the GEM and analytical solutions is excellent.

Example 2: Interference Test

An interference test was simulated using GEM in a square reservoir, 3000ft by 3000ft. The remaining properties are the same as in Example 1. The mesh used was 20 elements by 20 elements for this case. The observation well was placed three elements to the east and three elements to the south of the production well. This corresponds to a radius of 636.4ft from the producer. For comparison, the pressure transient at the observation well was also generated analytically using the method of images.

Figure 3.2 shows the pressure transient generated when constant pressure boundaries were applied on all sides of the reservoir. Figure 3.3 shows the transient generated when the reservoir has closed boundaries. The agreement between the GEM solution and the analytical solution in both cases is very close. The small steps in each curve for the constant pressure case occur because the data was only reported to two decimal places.

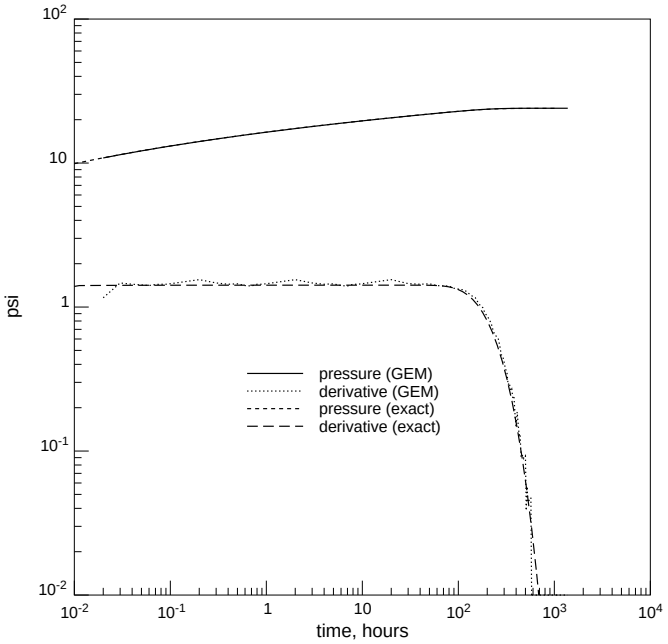

Figure 3.1: Example 1 - GEM + singularity programming

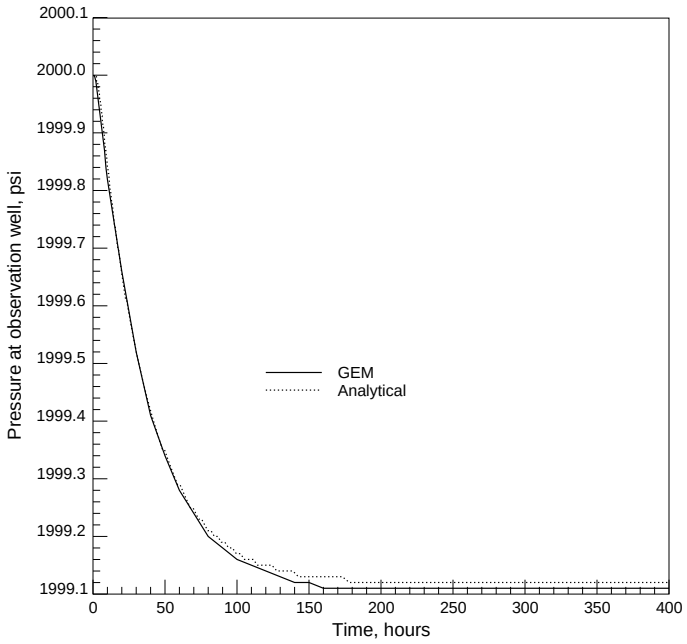

Figure 3.2: Example 2 - Interference testing, constant pressure boundaries

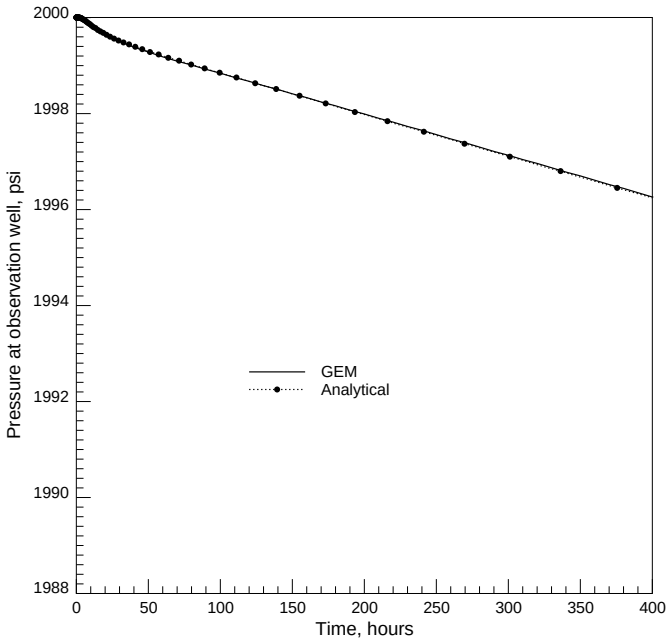

Figure 3.3: Example 2 - Interference testing, closed boundaries

3.2.2 Examples 3 and 4: Comparison to Finite Difference Solutions

Example 3: Reservoir with Closed Boundaries

The value of using singularity programming in combination with the Green Element Method can be demonstrated by comparing well tests simulated using this technique to well tests simulated using the finite difference simulator Eclipse. The first example is a well test in a closed square reservoir. The well is located at the center of the reservoir. The simulator uses a standard Peaceman [50] well index. The reservoir properties are given in Table 3.2.

The GEM solution used a mesh of 21 by 21 nodes and the Eclipse simulation used a grid of 21 by 21 cells. No local grid refinement was used in the Eclipse simulation. The reservoir is homogeneous, so an analytical solution could be generated for this problem. The Eclipse simulation is compared to this analytical solution in Figure 3.4. The GEM simulation is shown in Figure 3.5.

The well test response calculated using Eclipse appears to shows some wellbore

Table 3.2: Examples 3 and 4 - Reservoir properties

k	150 md
ϕ	0.3
μ	1 cp
p_i	2000 psi
q_w	50 STB/d
c_t	10e-06 psi^{-1}
r_w	0.3 ft
h	50 ft
Length	3000 ft
Width	3000 ft

storage effects, however these are artifacts of the finite difference computation approach. In the late part of the well test the data simulated using Eclipse did not sense the closed boundary until much later than it should have.

The poor performance of the finite difference method in reproducing the pressure derivative curve was investigated further by running more finite difference simulations. To assess the role of gridding the simulation was repeated with both uniform and nonuniform grids. The grid parameters used are shown in Table 3.3. For the nonuniform cases the geometric factor is the ratio between adjacent grid cell sizes i.e. in the last case the cell containing the well is 5ft by 5ft and the adjacent cells are 6.5ft by 6.5ft. The grid used for the first nonuniform case is shown in Figure 3.6.

The time stepping scheme was the same for all the models, both GEM and finite difference. The finite difference solution was calculated and reported in the following manner:

- 10 steps of 0.0001 days
- 10 steps of 0.001 days
- 10 steps of 0.01 days
- 20 steps of 0.1 days
- all subsequent time steps one day

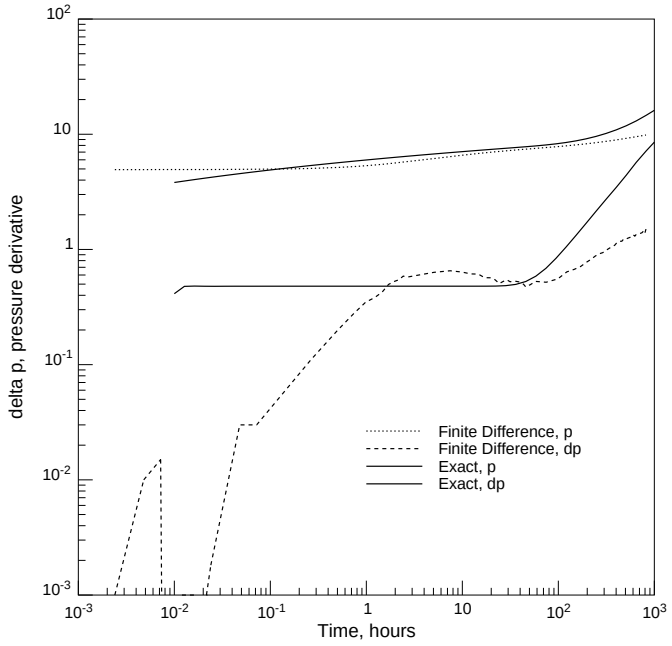

Figure 3.4: Example 3 - Finite difference simulation of well test in closed reservoir

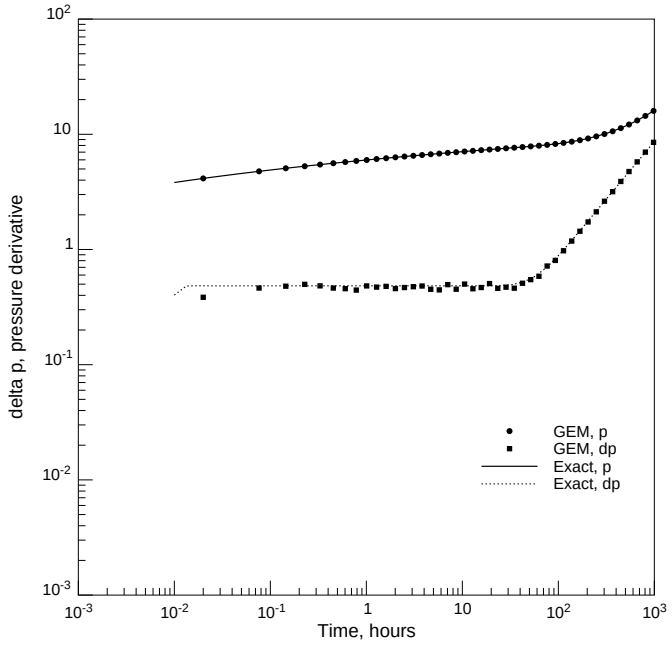

Figure 3.5: Example 3 - GEM simulation of well test in a closed reservoir

Table 3.3: Example 3 - Gridding study

Number of cells	$dx = dy$, ft	Gridding style	Geometric Factor
11 by 11	272.72	Uniform	N/A
21 by 21	142.85	Uniform	N/A
41 by 41	73.17	Uniform	N/A
101 by 101	29.70	Uniform	N/A
37 by 37	10 to 223.83	Nonuniform	1.2
45 by 45	5 to 189.68	Nonuniform	1.2
35 by 35	5 to 215.73	Nonuniform	1.3

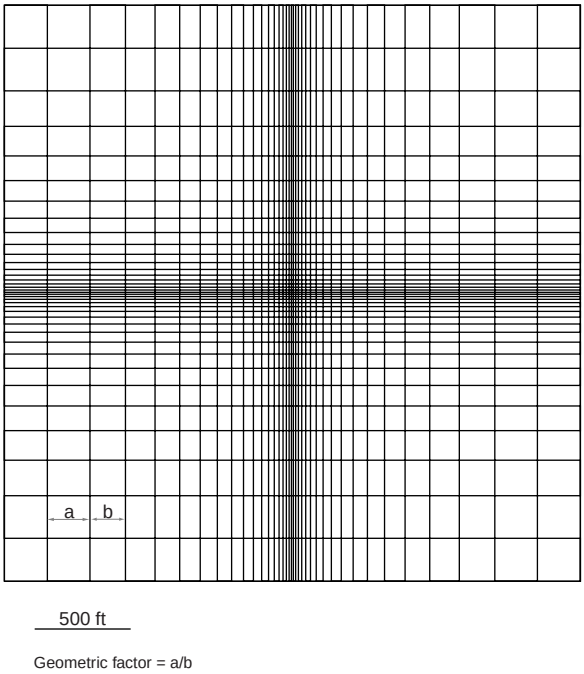

Figure 3.6: Example 3 - Nonuniform grid

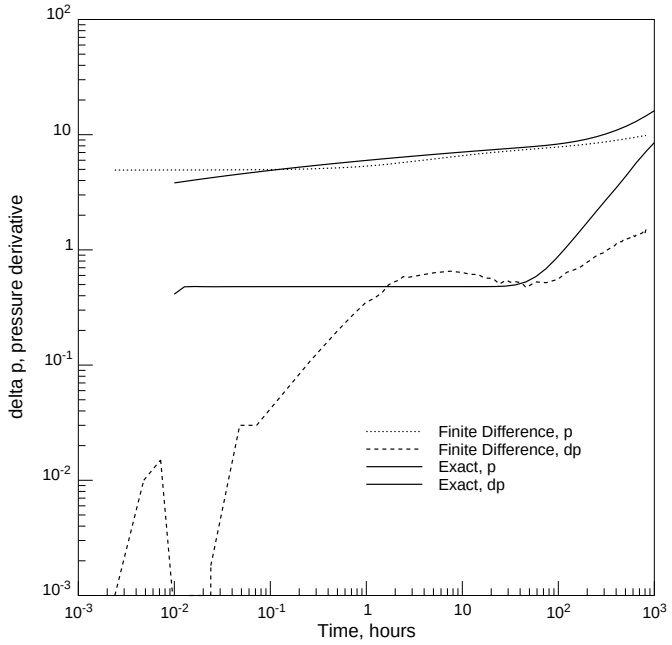

Figure 3.7: Example 3 - Pressure derivative for uniform 11 by 11 grid case

The finite difference simulator was able to compute the solution at intermediate times also if its time step control algorithm required it.

The pressure and pressure derivative curves computed using the uniform and nonuniform grids are shown in Figures 3.7 to 3.12. The derivative curves for all the uniformly gridded cases show that the effect of the boundary on the derivative curve is resolved better as the grid is refined. However even when the grid is refined to 101 by 101 cells the boundary location is still sensed incorrectly. All the uniformly gridded cases exhibit a period of infinite-acting radial flow before sensing the closed reservoir boundary. The nonuniformly gridded cases performed worse than the uniformly gridded cases in their reproduction of the pressure derivative. The infinite-acting radial flow period did not appear. Instead of remaining level during the time corresponding to infinite-acting radial flow the derivative maintains a steady downward slope.

The effects of the errors in the pressure derivative curve in this suite of finite difference simulations were quantified by treating each one as data in a well test analysis. The interpretation was performed using a standard regression procedure. The estimates for skin and permeability from the regression are highly correlated so

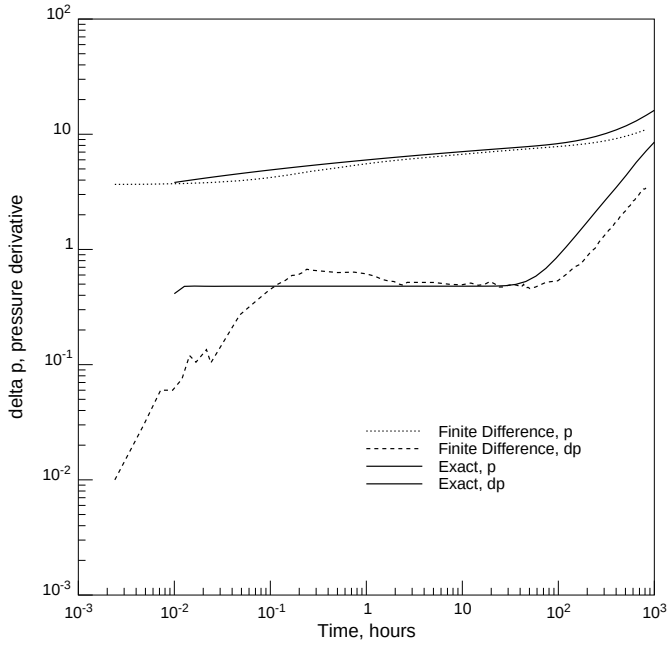

Figure 3.8: Example 3 - Pressure derivative for uniform 41 by 41 grid case

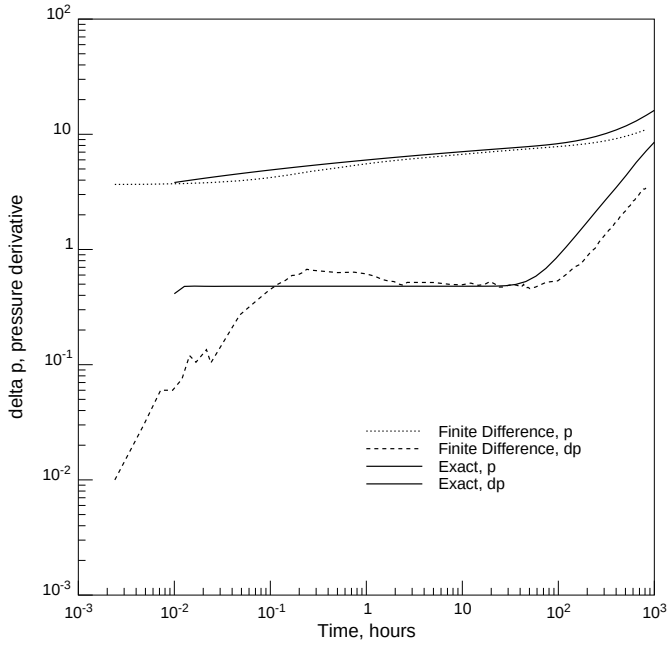

Figure 3.9: Example 3 - Pressure derivative for uniform 101 by 101 grid case

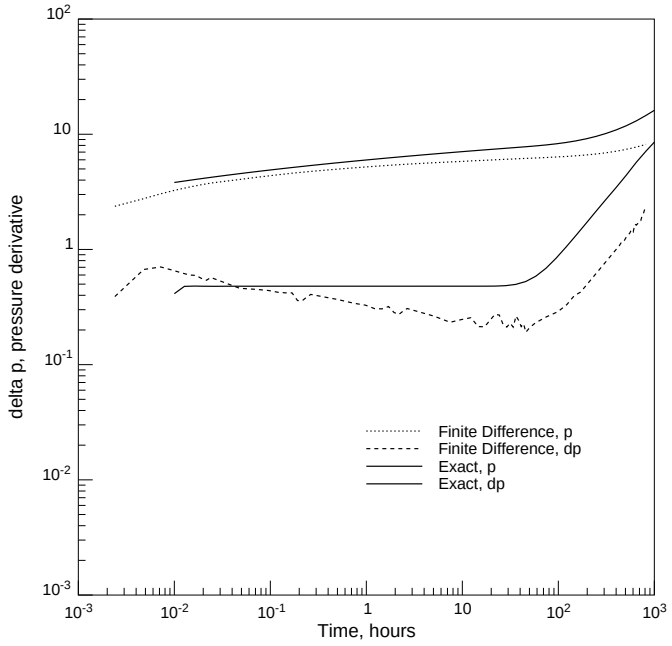

Figure 3.10: Example 3 - Pressure derivative for nonuniform grid case 1

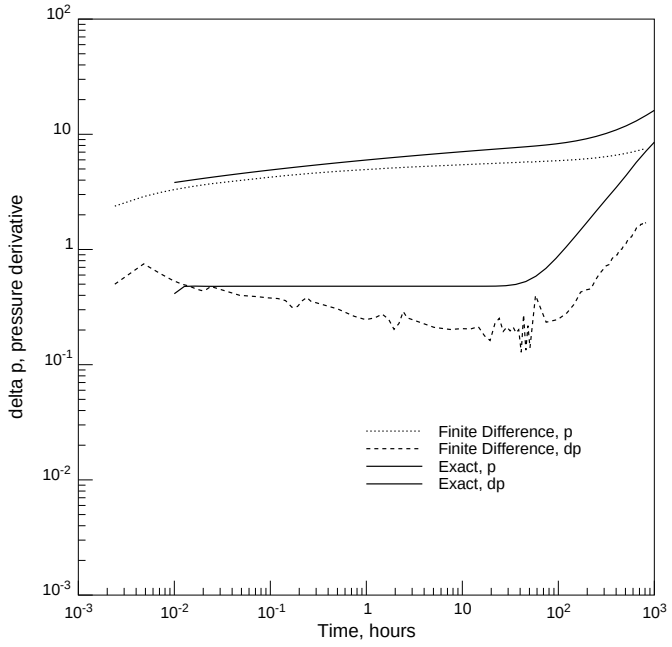

Figure 3.11: Example 3 - Pressure derivative for nonuniform grid case 2

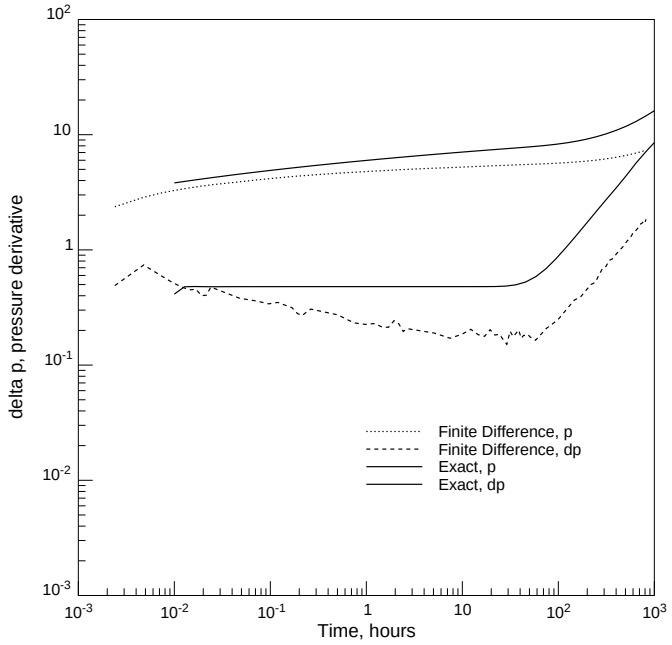

Figure 3.12: Example 3 - Pressure derivative for nonuniform grid case 3

the skin was set to zero in each case to ensure the treatment of the permeability was consistent. The initial pressure was also fixed at its true value of 2000psi. The wellbore storage coefficient was set to zero. Regression was used to determine the reservoir permeability and the location of the boundaries. The results are shown in Table 3.4. Recall that the true permeability is 150md and the true boundary location is 1500ft. The uniformly gridded cases all predict permeability values of 154-161md, which is due to the regression trying to fit the early time derivative data which appear to show wellbore storage. If the fit is performed manually ignoring this data the true permeability of 150md is predicted.

Example 4: Reservoir with Constant Pressure Boundaries

A well test was simulated in a reservoir with the properties given in Table 3.2. The well was located in the center of the reservoir and constant pressure boundary conditions were applied on all sides. Eclipse was used to simulate the well test The constant presure boundary was simulated by putting injection wells in every cell along the boundary. The resulting well test response is shown in Figure 3.13. The effect of the

Table 3.4: Example 3 - Well test interpretation of finite difference simulations

Case	Gridding Style	Permeability Estimate, md	Boundary Estimate, ft
11 by 11	Uniform	154	2750
21 by 21	Uniform	158	2380
41 by 41	Uniform	160	2047
101 by 101	Uniform	161	2024
37 by 37	Nonuniform	185	3430
45 by 45	Nonuniform	196	4010
35 by 35	Nonuniform	203	4000

constant pressure boundary was not well matched on the derivative curve. The same well test was simulated using GEM combined with singularity programming. The transient is shown in Figure 3.14. This simulation captures the effect of the constant pressure boundary accurately also.

3.2.3 Example 5: Interference Test

The interference test simulated using GEM in Example 2 was repeated using a finite difference simulator. The pressure response is shown in Figure 3.15. The same interference test was simulated in Section 3.2.1 (see Figure 3.3) and compared to an analytical solution. GEM produced an accurate match to the pressure response. The finite difference simulator did not accurately match the pressure response.

3.2.4 Examples 6 and 7: Well Test Simulation without Singularity Programming

Two wells tests were modeled to study the performance of the GEM simulation scheme without singularity programming. The set of reservoir properties given in Table 3.5 were common to both models. The boundary conditions applied were constant pressure boundary conditions.

To assess how the strength of the singularity affects the computed results two

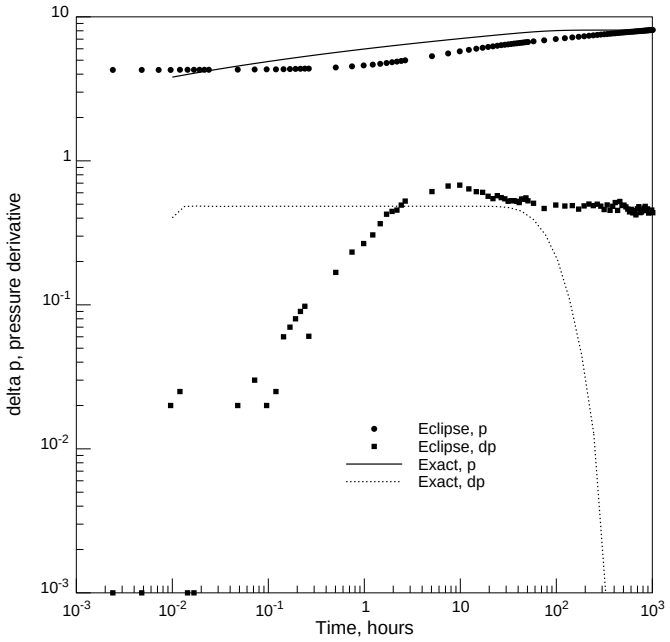

Figure 3.13: Example 4 - Finite difference simulation of well test in a reservoir with constant pressure boundaries

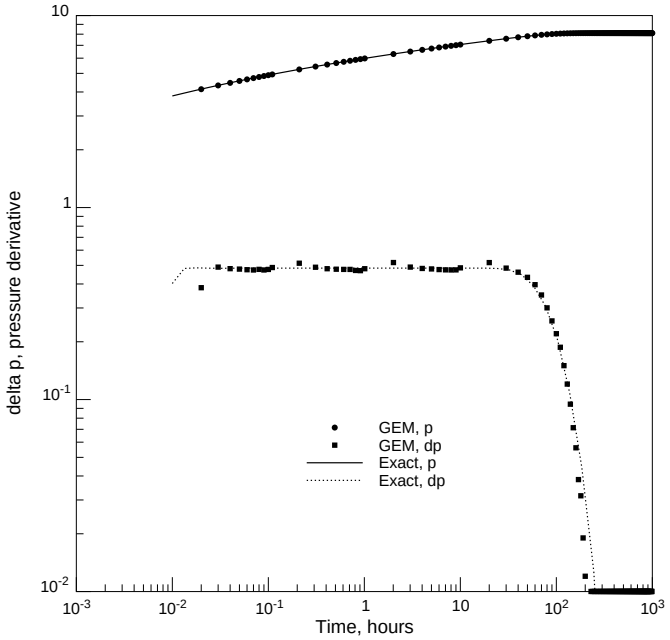

Figure 3.14: Example 4 - GEM simulation of well test in a reservoir with constant pressure boundaries

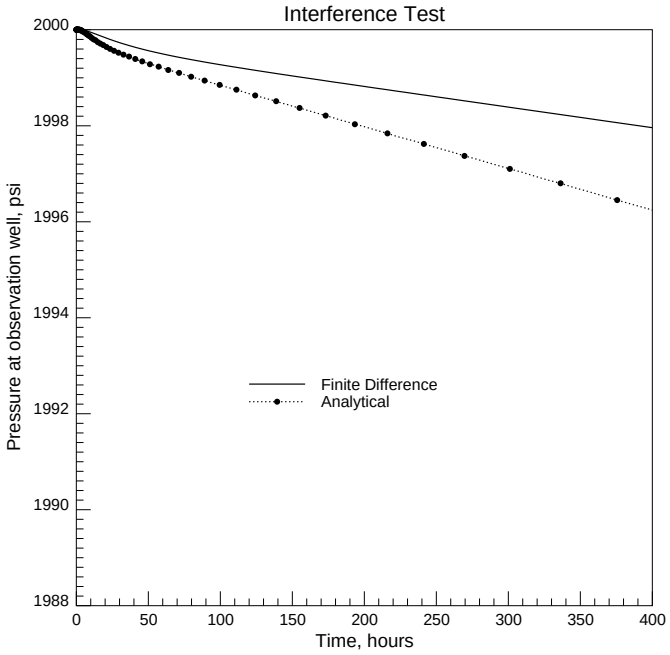

Figure 3.15: Example 5 - Finite difference simulation of an interference test in a closed reservoir

Table 3.5: Examples 6 and 7 - Reservoir properties

ϕ	0.3
μ	1cp
p_i	2000 psi
c_t	10e-06
r_w	0.3ft
h	50ft
Length	3000ft
Width	3000ft

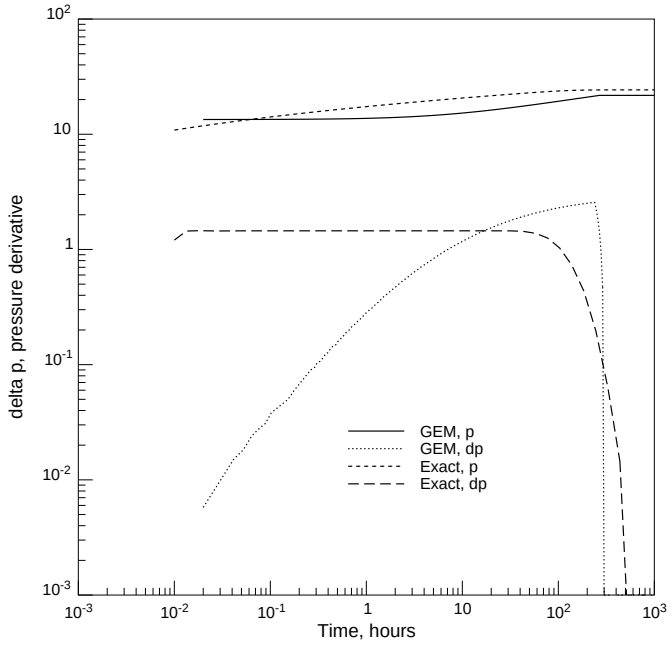

Figure 3.16: Example 6 - GEM simulation without singularity programming

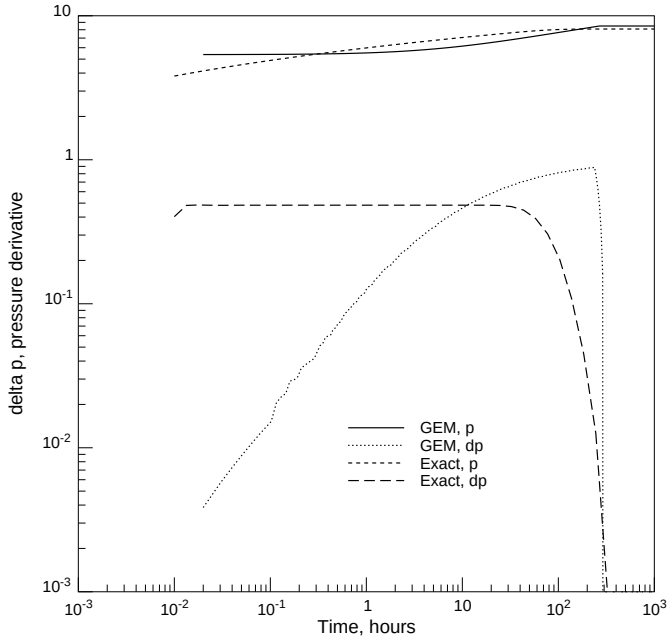

Figure 3.17: Example 7 - GEM simulation without singularity programming - example two

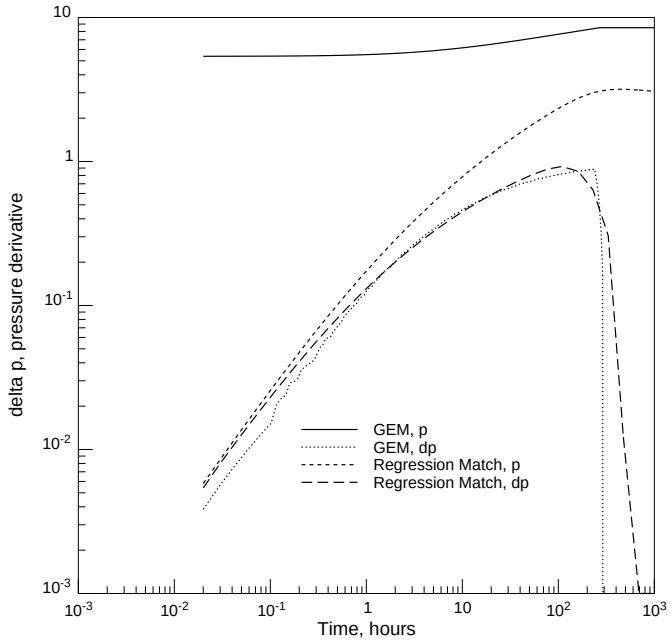

Figure 3.18: Example 6 - Artificial skin/storage effect

cases were considered. In the first case (Example 6), $k = 100md$ and $q_w = 100STB/d$ and in the second case (Example 7) $k = 150md$ and $q_w = 50STB/d$. The singularity in Example 6 is three times stronger than in Example 7. The pressure and pressure derivative curves computed when Example 6 and Example 7 were simulated using GEM without singularity programming are shown in Figures 3.16 and 3.17. The analytical versions of these curves are presented for comparison.

Figures 3.16 and 3.17 show that when singularity programming is not used the match to the pressure is not as precise as when singularity is applied (compare to Example 4, Figure 3.14). The early time behavior of the derivative curve is matched poorly. Figure 3.18 illustrates how this poorly matched derivative curve could be interpreted if it were treated as true data in a classical well test analysis. The match was performed on the derivative, and gave rise to the estimates shown in Table 3.6.

The values in Table 3.6 are clearly erroneous, they demonstrate the artificial well-bore storage effect that occurs in this method as the well drains the grid block it is located in. Singularity programming is successful in avoiding this artifical effect.

Table 3.6: Example 6 - Regression matched parameters

Parameter	Value	Confidence Interval	True Value
C	6.46 stb/psi	± 6.2e02 %	0 STB/psi
S	-7.62	± 2.7 %	0
k	48md	± 2.1e02%	50 md

3.3 Discussion

The simulated well test examples show that the combination of GEM and singularity programming can reproduce pressure transients accurately in comparison to analytical models. The proposed method was able to reproduce the pressure derivative curve much more accurately than conventional finite difference simulation. The combination of GEM and singularity programming was shown to be highly accurate for simulating interference tests as well as standard single-well pressure transient tests. The use of singularity programming was shown to be a key component of the proposed method. When singularity programming was replaced by the use of a Peaceman [50] well index the accuracy of the method suffered significantly. The Peaceman well index is not strictly appropriate for modeling pressure transient tests because it was derived for single-phase, steady-state, radial flow in a homogeneous reservoir. Sato [57] showed that singularity programming was a useful tool when applied in conjunction with the perturbation boundary element method. Russell and Wheeler[56] advocate the use of singularity programming in their finite element schemes. The well test modeled in Example 6 when singularity programming was not used was also simulated using Eclipse. Neither the GEM scheme nor the finite difference scheme used by Eclipse produced an accurate derivative match, however the GEM simulation demonstrates an important feature of boundary element methods. Example 3 shows that the effect of a closed boundary on the pressure derivative could not be reproduced accurately by Eclipse. Using nonuniform gridding exacerbated this problem and caused the infinite-acting radial flow period to be misrepresented in the pressure derivative curve. GEM in conjunction with singularity programming produced accurate matches to every

pressure transient considered without being hampered by numerical artifacts.

Chapter 4

Convection Diffusion Equation

The following section considers tracer flow in one- and two-dimensional media. The flow examples presented include both homogeneous and heterogeneous media problems.

In all cases the differential equation governing the flow is:

$$\nabla^2 c = \frac{1}{D}\left(v \cdot \nabla c + \frac{\partial c}{\partial t}\right) \tag{4.1}$$

where c is the tracer concentration, D is the diffusion coefficient and v is the velocity. The examples present calculations performed using DRBEM and GEM.

4.1 Theory

4.1.1 Dual Reciprocity Boundary Element Method

The Dual Reciprocity Boundary Element Method can be applied to the convection-diffusion equation in the same manner as the pressure diffusion equation described in Sections 2.3.1 and 2.3.2. For the convection-diffusion equation the right hand side b contains the convective and transient terms:

$$b = \frac{1}{D}\left(v \cdot \nabla c + \frac{\partial c}{\partial t}\right) \tag{4.2}$$

As in the case of the diffusion equation the right hand side is then expanded as the sum of a series of approximating functions, f_j:

$$b = \sum_{j=1}^{N+L} \alpha_j f_j \tag{4.3}$$

The expansion of the right hand side (Equation (4.3)) means that the left hand side of Equation (4.1) can be written as:

$$\nabla^2 c = \sum_{j=1}^{N+L} \alpha_j \nabla^2 \hat{c}_j \tag{4.4}$$

where

$$\nabla^2 \hat{c}_j = f_j \tag{4.5}$$

Multiplying Equation (4.4) by G, integrating over the domain and writing the result in matrix form gives:

$$Ac - Bq = \sum_{j=1}^{N+L} \alpha_j (A\hat{c}_j - B\hat{q}_j) \tag{4.6}$$

The terms in the A and B matrices are the same as for the diffusion equation case. Before Equation (4.6) can be solved for the concentration the weights α_j must be determined. The weights are determined by recalling that the weighted sum of the approximating functions is set equal to the right hand vector b.

$$b = \sum_{j=1}^{N+L} \alpha_j f_j = \frac{1}{D}\left(v_x \frac{\partial c}{\partial x} + v_y \frac{\partial c}{\partial y} + \frac{\partial c}{\partial t}\right) \tag{4.7}$$

This can be written is matrix form as:

$$F\alpha = \frac{1}{D}\left(v_x \frac{\partial c}{\partial x} + v_y \frac{\partial c}{\partial y} + \frac{\partial c}{\partial t}\right) \tag{4.8}$$

Premultiplying Equation (4.8) by F^{-1} allows α to be defined as:

$$\alpha = F^{-1}\frac{1}{D}\left(v_x \frac{\partial c}{\partial x} + v_y \frac{\partial c}{\partial y} + \frac{\partial c}{\partial t}\right) \tag{4.9}$$

For further progress to be made the spatial derivatives of concentration in Equation (4.9) must be expressed in terms of concentration. This can be acheived by defining

a second set of weights, β, which relate the approximating functions to the concentration.

$$c = F\beta \tag{4.10}$$

therefore

$$\beta = F^{-1}c \tag{4.11}$$

$$\frac{\partial c}{\partial x} = \frac{\partial F}{\partial x}\beta \tag{4.12}$$

Substituting Equation (4.11) into (4.12) gives:

$$\frac{\partial c}{\partial x} = \frac{\partial F}{\partial x}F^{-1}c \tag{4.13}$$

Combining Equations (4.13), (4.9) and (4.6) gives the final matrix equation for the DRBEM solution of the convection-diffusion equation:

$$Hc - Gq = \frac{1}{D}\left(H\hat{c} - G\hat{q}\right)F^{-1}\left(v_x\frac{\partial F}{\partial x}F^{-1}c + v_y\frac{\partial F}{\partial y}F^{-1}c + \frac{\partial c}{\partial t}\right) \tag{4.14}$$

This can be written more compactly by defining the matrices S and R as:

$$S = -\frac{1}{D}\left(H\hat{c} - G\hat{q}\right)F^{-1} \tag{4.15}$$

$$R = S\left(v_x\frac{\partial F}{\partial x}F^{-1}c + v_y\frac{\partial F}{\partial y}F^{-1}c\right) \tag{4.16}$$

The DRBEM scheme can then be written as:

$$(H + R)c + S\frac{\partial c}{\partial t} = Gq \tag{4.17}$$

4.1.2 Green Element Method

The Green Element Method can also be applied to the convection-diffusion equation, Equation (4.1). Initially the diffusion coefficent, D and the velocity, v are assumed to be constant. This assumption will ultimately be relaxed however. As in prior GEM derivations the procedure begins by multiplying the governing differential equation by G and integrating. This results in an integral form of the equation as shown as follows for different types of model.

One-Dimensional Model

The Green's function applied in the case of the convection-diffusion equation is the same as that used for the diffusion equation: The solution to Equation (2.72) is:

$$G(x_i, x) = \frac{1}{2}(|x_i - x| + le) \tag{4.18}$$

where le is an arbitrary constant taken to be the length of the element.
Equation (4.1) can be cast as an integral equation by substituting Equations (4.18) and (4.1) into Green's second identity, Equation (2.74). The resulting integral equation is:

$$c\left.\frac{\partial G}{\partial x}\right|_0^L - G\left.\frac{\partial c}{\partial x}\right|_0^L = \int_0^L \left(c\delta(x - x_i) - G\frac{1}{D}\left(v\frac{\partial c}{\partial x} + \frac{\partial c}{\partial t}\right)\right) dx \tag{4.19}$$

As in the transient diffusion case the final integral equation is derived from Equation (4.19) by noting the properties of the Dirac delta function:

$$-\lambda_i c(x_i) + \left[c\frac{\partial G}{\partial x} - G\frac{\partial c}{\partial x}\right]_0^L + \int_0^L G\frac{1}{D}\left(v\frac{\partial c}{\partial x} + \frac{\partial c}{\partial t}\right) dx = 0 \tag{4.20}$$

where $\lambda_i = 1$ at points within the domain and $\lambda_i = 0.5$ at the end nodes.
GEM proceeds by discretising the domain into elements. Equation (4.20) is evaluated as a summation over these elements:

$$\sum_{e=1}^{M}\left(-\lambda_i c(x_i) + \left[c\frac{\partial G}{\partial x} - G\frac{\partial c}{\partial x}\right]_{x_2}^{x_1} + \int_{x_1}^{x_2} G\frac{1}{D}\left(v\frac{\partial c}{\partial x} + \frac{\partial c}{\partial t}\right) dx\right) = 0 \tag{4.21}$$

where M is the total number elements.

Shape functions are now introduced to approximate c and $\frac{\partial c}{\partial x}$ (denoted as q) over the element in terms of the nodal values at the end of each element. In this case linear shape functions will be used:

$$c = N_1 c_1 + N_2 c_2 \tag{4.22}$$

$$q = N_1 q_1 + N_2 q_2 \tag{4.23}$$

Substituting the spatial derivative of the Green's function Equation (2.80), the Heaviside step function, Equation (2.81), and the shape functions, Equations (4.22)

and (4.23) into Equation (4.21) gives:

$$\sum_{e=1}^{M} -2\lambda_i c(x_i) + [H(x_2 - x_i) - H(x_i - x_2)]c_2$$

$$-[H(x_1 - x_i) - H(x_i - x_1)]c_1 - (|x_2 - x_i| + 1)q_2$$

$$+(|x_1 - x_i| + 1)q_1 + \int_{x_1}^{x_2} G\frac{1}{D}\left(N_1\frac{\partial c_1}{\partial t} + N_2\frac{\partial c_2}{\partial t} + \frac{v}{D}\left(N_1 q_1 + N_2 q_2\right)dx\right) = 0 \quad (4.24)$$

Equation (4.24) can be used to generate two separate equations depending whether $x_i = x_1$ or $x_i = x_2$. When $x_i = x_1$:

$$\sum_{e=1}^{M} -c_1 + c_2 + q_1 - (|x_2 - x_1| + 1)q_2$$

$$+\int_{x_1}^{x_2} G\frac{1}{D}\left(N_1\frac{\partial c_1}{\partial t} + N_2\frac{\partial c_2}{\partial t} + \frac{v}{D}\left(N_1 q_1 + N_2 q_2\right)dx\right) = 0 \quad (4.25)$$

When $x_i = x_2$:

$$\sum_{e=1}^{M} -c_2 + c_1 - q_2 + (|x_1 - x_2| + 1)q_1$$

$$+\int_{x_1}^{x_2} G\frac{1}{D}\left(N_1\frac{\partial c_1}{\partial t} + N_2\frac{\partial c_2}{\partial t} + \frac{v}{D}\left(N_1 q_1 + N_2 q_2\right)dx\right) = 0 \quad (4.26)$$

Equations (4.25) and (4.26) can be written more compactly as:

$$\sum_{e=1}^{M}\left(R_{ij}^e c_j + (L_{ij}^e + U_{ijl}\frac{v_j}{D})q_j + T_{ij}^e\frac{\partial c_j}{\partial t}\right) = 0 \quad (4.27)$$

where R_{ij}, L_{ij} and T_{ij} were defined in Chapter 2 by Equations (2.86), (2.87) and (2.88). U_{ijl} is defined by:

$$U_{ijl} = \int_{\Gamma^e} G(r, r_i)N_j N_l d\Gamma \quad (4.28)$$

$$U_{1jl} = \frac{l_e}{12}\begin{bmatrix} 4 + l_e & 2 + l_e \\ 2 + l_e & 4 + 3l_e \end{bmatrix} \quad (4.29)$$

$$U_{2jl} = \frac{l_e}{12}\begin{bmatrix} 4 + 3l_e & 2 + l_e \\ 2 + l_e & 4 + l_e \end{bmatrix} \quad (4.30)$$

Two-Dimensional Model

The integral form of the convection-diffusion equation, Equation (4.1), in two dimensions is:

$$\frac{\theta_i}{2\pi}c(r_i) + \int_\Gamma K_1(r,r_i)c(r_i)d\Gamma - \int_\Gamma K_2(r,r_i)\frac{\partial c(r_i)}{\partial n}d\Gamma = \int_\Omega G\frac{1}{D}\frac{\partial c}{\partial t}d\Omega + \int_\Omega G\frac{1}{D}\left(v_x\frac{\partial c}{\partial x} + v_y\frac{\partial c}{\partial y}\right)d\Omega \tag{4.31}$$

Since most of the terms in the current derivation are the same as the transient diffusion case this derivation will focus on the convective terms. The first step is to write the integral involving the convective terms as a sum of element integrals:

$$\int_\Omega G\frac{1}{D}\left(v_x\frac{\partial c}{\partial x} + v_y\frac{\partial c}{\partial y}\right)d\Omega = \sum_{e=1}^{M}\int_{\Omega^e} G\frac{1}{D}\left(v_x\frac{\partial c}{\partial x} + v_y\frac{\partial c}{\partial y}\right)d\Omega \tag{4.32}$$

The nodal concentrations are then interpolated using shape functions. The derivatives of the concentration are expressed in terms of the nodal concentrations and derivatives of the shape functions:

$$\frac{\partial c}{\partial x} = \frac{\partial N_j}{\partial x}c_j \tag{4.33}$$

$$\frac{\partial c}{\partial y} = \frac{\partial N_j}{\partial y}c_j \tag{4.34}$$

The right hand side of Equation (4.32) can be written more compactly as:

$$\sum_{e=1}^{M}\int_{\Omega^e} G\frac{1}{D}\left(v_x\frac{\partial c}{\partial x} + v_y\frac{\partial c}{\partial y}\right)d\Omega = \frac{1}{D}\left(v_xP_{ij}^e + v_yS_{ij}^e\right)c_j \tag{4.35}$$

where

$$P_{ij}^e = \iint_{\Omega^e} G(r,r_i)\frac{\partial N_j}{\partial x}d\Omega \tag{4.36}$$

$$S_{ij}^e = \iint_{\Omega^e} G(r,r_i)\frac{\partial N_j}{\partial y}d\Omega \tag{4.37}$$

Now that the form of the convective terms has been established the full GEM formulation can be written as:

$$\sum_{e=1}^{M}\left(R_{ij}^e c_j + L_{ij}^e q_j - \frac{1}{D}\left(v_xP_{ij}^e + v_yS_{ij}^e\right)c_j - T_{ij}^e\frac{\partial c_j}{\partial t}\right) = 0 \tag{4.38}$$

The time derivative is expanded as:

$$\frac{\partial c}{\partial t} = \frac{c^{m+1} - c^m}{\Delta t} \tag{4.39}$$

A two-level time integration scheme is applied to Equation (4.38) to give:

$$\sum_{e=1}^{M} \theta \left(R_{ij}^e c_j^{m+1} + L_{ij}^e q_j^{m+1} - \frac{1}{D} \left(v_x P_{ij}^e c_j^{m+1} + v_y S_{ij}^e c_j^{m+1} \right) \right) +$$
$$(1-\theta) \left(R_{ij}^e c_j^m + L_{ij}^e q_j^m - \frac{1}{D} \left(v_x P_{ij}^e c_j^m + v_y S_{ij}^e c_j^m \right) \right) - T_{ij}^e \frac{\partial c_j}{\partial t} = 0 \tag{4.40}$$

4.2 Results

4.2.1 Example 8: One-Dimensional Tracer Flow

The performance of DRBEM and GEM for solving one-dimensional tracer flow problems was assessed by simulating a variety of cases ranging from Peclét numbers of ten to 10,000. Since realistic reservoir engineering problems are likely to be convection dominated the performance of the methods at high Peclét numbers is of greatest interest. The problem posed was the solution of:

$$D\frac{\partial^2 c}{\partial x^2} - V\frac{\partial c}{\partial x} = \frac{\partial c}{\partial t} \tag{4.41}$$

The boundary conditions applied were:

$$c(0) = 1 \tag{4.42}$$

$$\frac{\partial c}{\partial x}(1) = 0 \tag{4.43}$$

The domain considered was $x[0, 1]$. The Peclét number was defined as:

$$Pe = \frac{VL}{D} \tag{4.44}$$

For this problem $L = 1$. The numerical solutions were computed on a one-dimensional grid with 40 nodes. The timestep was chosen to set the Courant number to 0.2 in each run. The Courant number is defined by:

$$Cr = \frac{V\Delta t}{\Delta x} \tag{4.45}$$

An analytical solution is available for this problem [41] when it is solved on a semi infinite one-dimensional domain with the boundary condition:

$$c(\infty, 0) = 0 \tag{4.46}$$

$$c(x,t) = \frac{1}{2}\left[erfc\left(\frac{1-Vt}{2\sqrt{Dt}}\right) + exp\left(\frac{V}{D}\right) erfc\left(\frac{1+Vt}{2\sqrt{Dt}}\right)\right] \tag{4.47}$$

The discrepancy between the numerical and analytical solutions at $Pe = 10$ in Figure 4.1 is because of the effect of imposing the boundary condition at $x = 1$.

For comparison purposes the results computed by a central finite difference method and an upwind finite difference method were also considered. Figures 4.1 and 4.2 show the tracer distribution at $t = 0.5$ days for the four Peclét numbers considered.

The central finite difference equation used was:

$$D\frac{c_{i-1}^{m+1} - 2c_i^{m+1} + c_{i-1}^{m+1}}{(\Delta x)^2} - V\frac{c_{i+1}^{m+1} - c_{i-1}^{m+1}}{2\Delta x} - \frac{c_i^{m+1}}{\Delta t} = \frac{c_i^m}{\Delta t} \tag{4.48}$$

Figure 4.1 shows that as the Peclét number increased DRBEM, GEM and the central finite difference method suffered from spurious numerical oscillations. The finite difference scheme and DRBEM experienced noticeable oscillations at a Peclét number of 1000, however the only oscillations that occur with GEM are very small and occur at a Peclét number of 10,000.

The oscillations can be removed by using an upwind form of the convective term:

$$D\frac{c_{i-1}^{m+1} - 2c_i^{m+1} + c_{i-1}^{m+1}}{(\Delta x)^2} - V\frac{c_i^{m+1} - c_{i-1}^{m+1}}{\Delta x} - \frac{c_i^{m+1}}{\Delta t} = \frac{c_i^m}{\Delta t} \tag{4.49}$$

Note that Equation (4.49) assumes the flow moves from node $i-1$ to i. The upwind finite difference scheme is compared to central finite differences and to the analytical solution in Figure 4.2.

Another feature of interest in any numerical model of tracer flow is how much numerical diffusion smoothes sharp fronts. Figure 4.1 shows that GEM recovers sharp tracer fronts more accurately than DRBEM or the central finite difference scheme. Upwind finite differences cause much more numerical diffusion than the oscillatory central finite difference scheme.

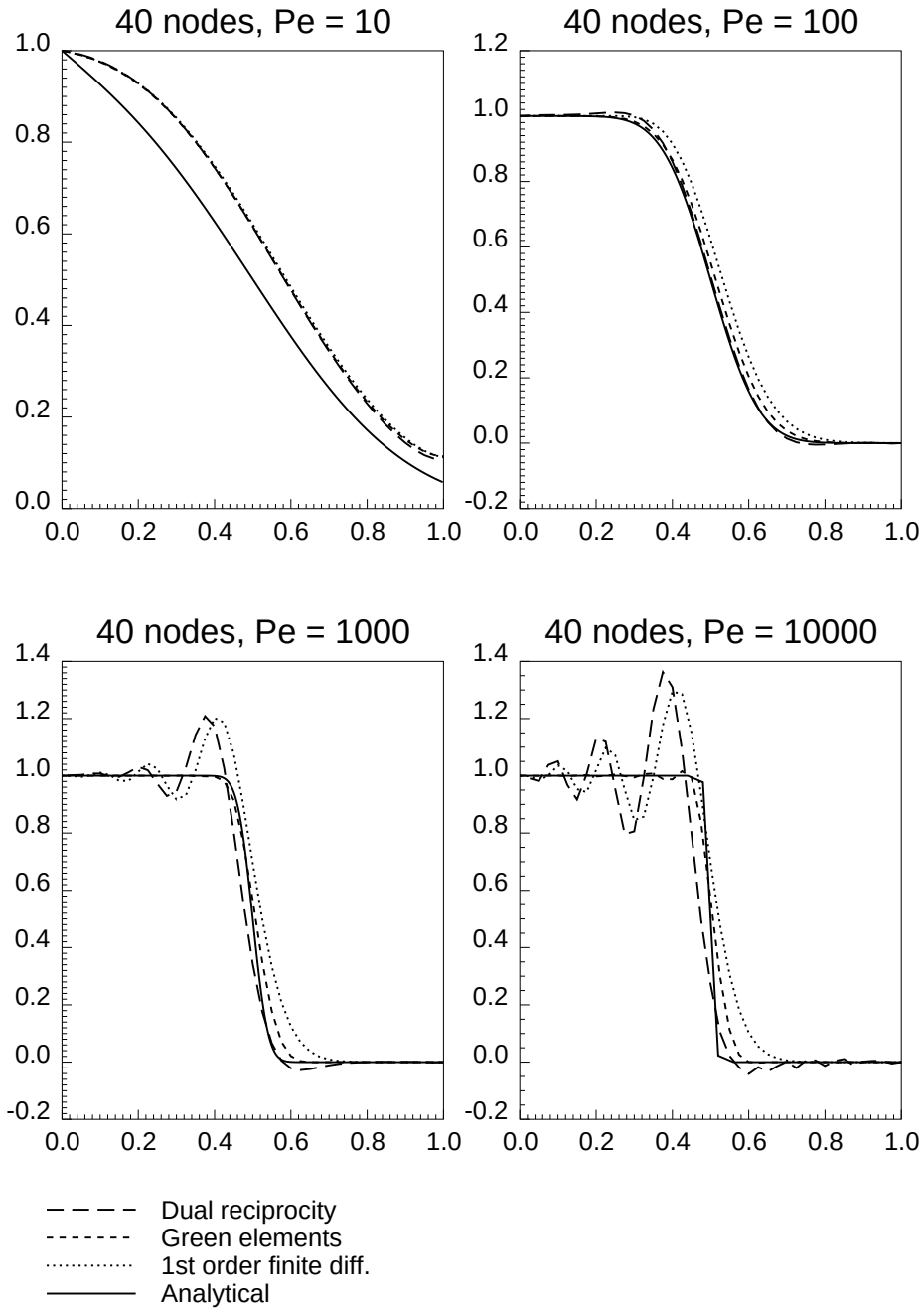

Figure 4.1: Example 7 - Comparison of DRBEM, GEM and finite difference schemes

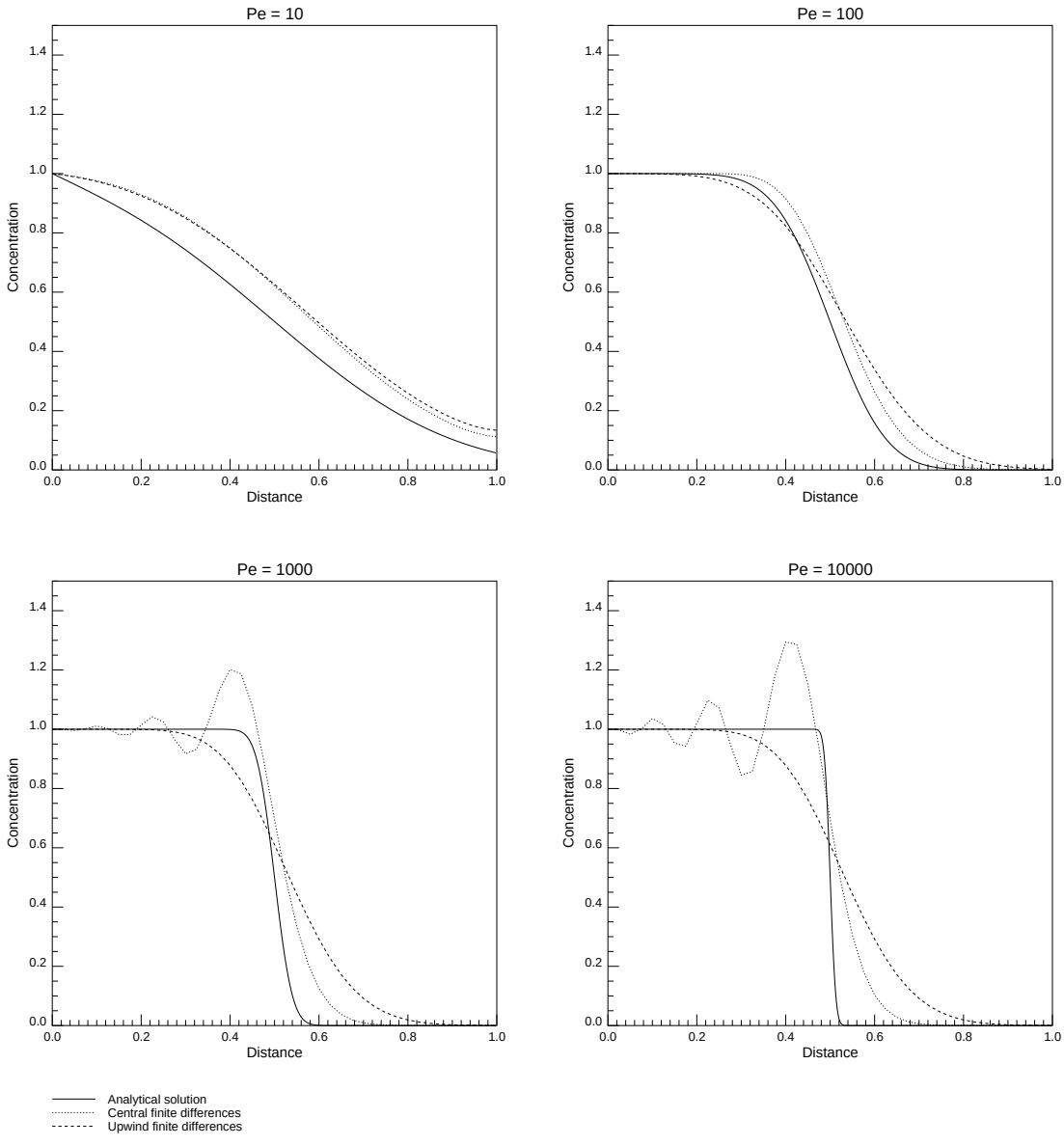

Figure 4.2: Example 7 - Upwind and central finite difference schemes

4.2.2 Example 9: Vertical Cross Section in a Heterogeneous Reservoir

Theory

To consider tracer flow in heterogeneous media the theory presented in Section 4.1.2 must be extended to handle a nonconstant velocity field. This can be done by simply reconsidering the treatment of the right hand side of Equation 4.35. When the velocity varies over the element the velocity distribution can be described in terms of the nodal velocity values and shape functions:

$$\sum_{e=1}^{M} \int_{\Omega^e} G \frac{1}{D} \left(v_x \frac{\partial c}{\partial x} + v_y \frac{\partial c}{\partial y} \right) d\Omega = \frac{1}{D} \left(v_x(j) W X^e_{ijl} + v_y(j) W Y^e_{ijl} \right) c_l \tag{4.50}$$

where

$$W X_{ijl} = \iint_{\Omega^e} G(r, r_i) N_j \frac{\partial N_l}{\partial x} d\Omega \tag{4.51}$$

$$W Y_{ijl} = \iint_{\Omega^e} G(r, r_i) N_j \frac{\partial N_l}{\partial y} d\Omega \tag{4.52}$$

Once vxP_{ij} is replaced by $vx_j WX_{ijl}$ and the vyS_{ij} is replaced by $vx_j WY_{ijl}$ the development of GEM for heterogeneous media is the same as for homogeneous media.

To apply GEM the convection-diffusion equation (4.1) is nondimensionalised using the following set of dimensionless variables:

$$c_D = \frac{c}{c_o} \tag{4.53}$$

$$x_D = \frac{x}{\sqrt{A}} \tag{4.54}$$

$$y_D = \frac{y}{\sqrt{A}} \tag{4.55}$$

$$t_D = \frac{Dt}{A} \tag{4.56}$$

The nondimensional form of the convection-diffusion equation is:

$$\frac{\partial^2 c_D}{\partial x_D^2} - \frac{\sqrt{A}}{D} \left(v_x \frac{\partial c_D}{\partial x_D} + v_y \frac{\partial c_D}{\partial y_D} \right) = \frac{\partial c_D}{\partial t_D} \tag{4.57}$$

Results

The GEM simulation of tracer flow in heterogeneous media is demonstrated by considering a 3000ft by 3000ft vertical cross section. The section was discretised into a 20 by 20 element mesh. The permeability of the cross section being considered is shown in Figure 4.3. The diffusivity, α, was chosen to be 30 ft. A representative velocity in the cross section is 1 ft/day. Taking, $D = \alpha v$, gives a value for D of $30 ft^2/day$.

The horizontal component of the velocity field used for this example is shown in Figure 4.4 in units of ft/day. The velocity was derived by solving the steady-state pressure diffusion equation with the following boundary conditions:

$$p(x_D = 0) = 2000psi \tag{4.58}$$

$$p(x_D = 1) = 1000psi \tag{4.59}$$

The concentration distribution in the cross section at 1500 days is shown in Figure 4.5. The tracer follows the pathways that would be expected i.e. it moves more rapidly through the high permeability zone in the upper part of the cross section and it is slower to move through the low permeability region in the bottom part of the cross section.

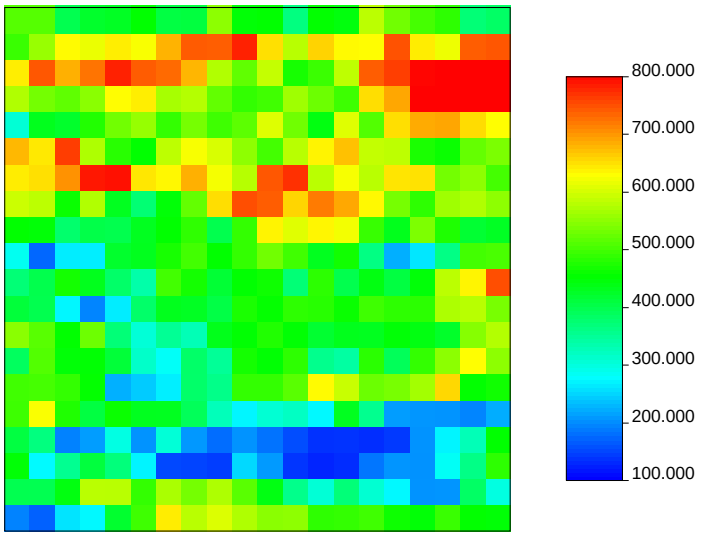

Figure 4.3: Example 8 - Permeability field

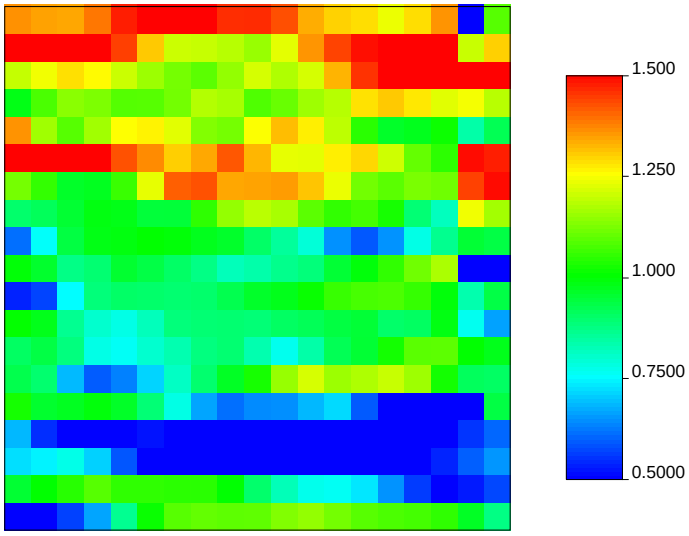

Figure 4.4: Example 8 - Horizontal velocity distribution

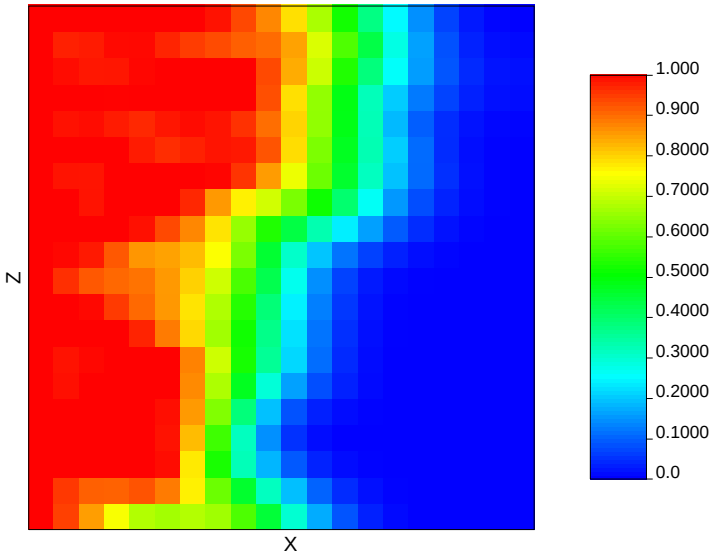

Figure 4.5: Example 8 - Concentration Map

Chapter 5

Oil-Water Reservoir Simulation

Chapters 3 and 4 demonstrated that GEM could produce accurate results to heterogeneous single phase well testing and tracer flow problems. In this chapter multiphase flow in heterogeneous media will be considered. The proposed method forms an IMPES pressure equation which is solved using GEM. Singularity programming is incorporated in the two-dimensional version of the method to capture the singularity at the well.

5.1 Theory

5.1.1 IMPES Scheme

The applicability of boundary element methods to multiple phase flow can be considered by using an approach similar to that used for single-phase flow in heterogeneous media in Chapter 3. A transformed form of the flow equations is required to cast the equation in a suitable form. The solution scheme is an IMPES scheme in which the pressure equation is solved using GEM. DRBEM could be used but GEM is preferred because of its sparse matrix structure. Fluxes between elements are then computed and the element saturations are updated accordingly.

The mass balance equations for oil and water flow problems are:

$$\nabla \cdot \left(\frac{k k_{ro}}{\mu_o} \nabla p \right) = \frac{\partial}{\partial t}(\phi S_o) \tag{5.1}$$

$$\nabla \cdot \left(\frac{k k_{rw}}{\mu_w} \nabla p \right) = \frac{\partial}{\partial t}(\phi S_w) \tag{5.2}$$

If the total compressibility remains constant with respect to pressure Equations (5.1) and (5.2) can be added together to give:

$$\nabla \cdot (k \lambda_t \nabla p) = \phi c_t \frac{\partial p}{\partial t} \tag{5.3}$$

where

$$\lambda_t = \left(\frac{k_{ro}}{\mu_o} + \frac{k_{rw}}{\mu_w} \right) \tag{5.4}$$

To cast this equation in a form suitable for solution with GEM a ∇^2 operator is extracted:

$$\nabla^2 p = -\nabla ln\left(k \lambda_t\right) \cdot \nabla p + \phi c_t \frac{\partial p}{\partial t} \tag{5.5}$$

5.1.2 Incorporation of Singularity Programming

When solving two-dimensional problems singularity programming was applied in conjunction with Equation (5.5) in a similar manner to the well testing case presented in Section 3.1.1. In dimensionless form the pressure satisifes:

$$\nabla^2 p_D = \frac{\lambda_t^o k_o}{\lambda_t k} \frac{\partial p_D}{\partial t_D} - \nabla ln\left(k \lambda_t\right) \cdot \nabla p_D \tag{5.6}$$

As before the singular component of the pressure satisfies:

$$\nabla^2 p_D^s = \frac{\partial p_D^s}{\partial t_D} \tag{5.7}$$

For a reservoir with multiple wells the singular component of the pressure is a sum of exponential integral solutions:

$$p_D^s = \sum_{i=1}^{nWells} -q_D^i Ei\left(\frac{r_{Di}^2}{4 t_D} \right) \tag{5.8}$$

To derive the equation governing the nonsingular component of the pressure Equation (5.7) is subtracted from Equation (5.6) giving:

$$\nabla^2 p_D - \nabla^2 p_D^s = \frac{\partial p_D^s}{\partial t_D} - \nabla ln\left(k\lambda_t\right) \cdot \nabla p_D \tag{5.9}$$

Finally, noting that $p_D = p_D^{ns} + p_D^s$ means that Equation (5.9) can be simplified to:

$$\nabla^2 p_D^{ns} = \frac{\lambda_t^0 k_0}{\lambda_t k} \frac{\partial p_D^{ns}}{\partial t_D} + \left(\frac{\lambda_t^0 k_0}{\lambda_t k} - 1\right) \frac{\partial p_D^s}{\partial t_D} - \nabla ln(\lambda_t k) \cdot \nabla (p_D^{ns} + p_D^s) \tag{5.10}$$

5.1.3 GEM Implementation

Equation (5.10) can be solved using GEM in a manner very similar to Equation (3.13) which governs the nonsingular component of the pressure in the single phase well testing problems. In fact the only change to the equation is the introduction of the λ_t premultiplying the permeability in the time derivative terms. Accordingly the GEM equation that can be used to solve Equation (5.10) implicitly for pressure is:

$$\sum_{e=1}^{M} \left(R_{ij} p_j^{m+1} + L_{ij} q_j^{m+1} - U_{ijl} \frac{\lambda_t^o k_o}{\lambda_t k_j} \frac{p^{m+1} - p^m}{\Delta t} - V_{ijl} ln k_j p_l^{m+1} + T_{ij} f_j^{m+1} \right) = 0 \tag{5.11}$$

where

$$f = \left(\frac{\lambda_t^0 k_0}{\lambda_t k} - 1\right) \frac{\partial p_D^s}{\partial t_D} - \nabla ln(\lambda_t k) \cdot \nabla p_D^s \tag{5.12}$$

The element matrices R,L,V,T and U have been defined previously in Equations (2.99),(2.100),(2.101), (3.22) and (2.108).

5.1.4 Saturation Update Procedure

The saturations are associated with elements centered around each pressure node. These saturation values are updated at each time step by first computing the fluid velocity normal to each face of the element and then moving an appropriate amount of each phase into the element.

In one dimension the GEM scheme computes the pressure gradients at each node as part of the solution. In two dimensions the pressure gradient is computed as a finite difference of adjacent pressure values. The pressure gradient is converted

Table 5.1: Example 10 - Reservoir and grid properties

Permeability	100md
Porosity	30%
Oil viscosity	1cp
Water viscosity	1cp
Length	2000ft
Thickness	20ft
Width	2.5ft
Number of gridblocks	20
Injection rate	50 STB/d

to velocity multiplying by the upstream mobility and the harmonic average of the adjacent permeability values. The scheme is explicit in saturation so the mobility values used are evaluated at the time level m and not $m+1$.

Note that the saturation update was not performed by solving a transport equation using GEM. This is because the saturation update is a purely convective process and GEM can only be applied to equations which include diffusive terms.

5.2 Results

5.2.1 Example 10: Buckley-Leverett Problem

Figure 5.1 shows a comparison between the watercut computed by a one-dimensional oil-water GEM solution, by the commercial black oil simulator IMEX and by the analytical Buckley-Leverett solution. The reservoir and grid properties are given in Table 5.1.

The relative permeabilities used are quadratic so all water saturations travel together as a piston-like shock.

$$k_{ro} = 1 - S_w^2 \tag{5.13}$$

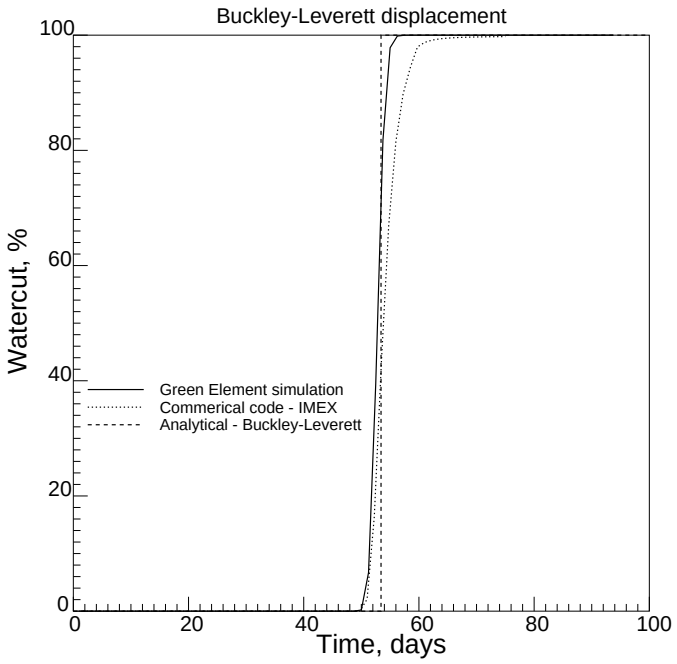

Figure 5.1: Example 10 - Comparison of GEM, analytical and finite difference solution to multiphase flow problem

$$k_{rw} = Sw^2 \tag{5.14}$$

Figure 5.1 shows that the predicted breakthrough time is the same for the GEM simulator and the commercial code. However GEM predicts the subsequent water production more accurately.

5.2.2 Example 11: Five-Spot Pattern

The simulation scheme proposed in Section 5.1.2 combines GEM and singularity programming to solve the pressure equation. To assess the performance of the scheme a five spot pattern was simulated. The reservoir and grid properties are given in Table 5.2.

Straight line relative permeabilities were used, i.e.:

$$k_{rw} = S_w \tag{5.15}$$

Table 5.2: Example 11 - Reservoir and grid properties

Permeability	250md
Porosity	30%
Oil viscosity	1cp
Water viscosity	1cp
Length	3000ft
Width	3000ft
Thickness	50ft
Number of elements	20 by 20
Injector position	1500, 1500ft
Injection rate	800 STB/d
Producer position 1	600, 600 ft
Producer position 2	600, 2400 ft
Producer position 3	2400, 600 ft
Producer position 4	2400, 2400 ft
Production rate per well	200 STB/d

$$k_{ro} = 1 - S_w \tag{5.16}$$

A reservoir simulation of this case was performed using a fine grid of 101 by 101 cells using the a streamline simulator (3DSL) [71]. This was taken to be the truth case. The reservoir was also simulated using Eclipse [25] and the GEM/singularity programming scheme on a 21 by 21 cell grid for comparison.

The results in Figure 5.2 show that neither method accurately recovers the true solution. Chapter 3 showed that using the combination of GEM and singularity programming was superior to an Eclipse simulation on the same grid for reproduction of the pressure response occuring in a well test. However when multiphase flow is considered these advantages are lost because the saturation update procedure still suffers from the adverse effects of numerical diffusion which smoothes the fluid front. Note that saturation update procedure is similar to what is used in finite difference simulation. In Chapter 4 GEM was shown to perform well for tracer flow. A GEM

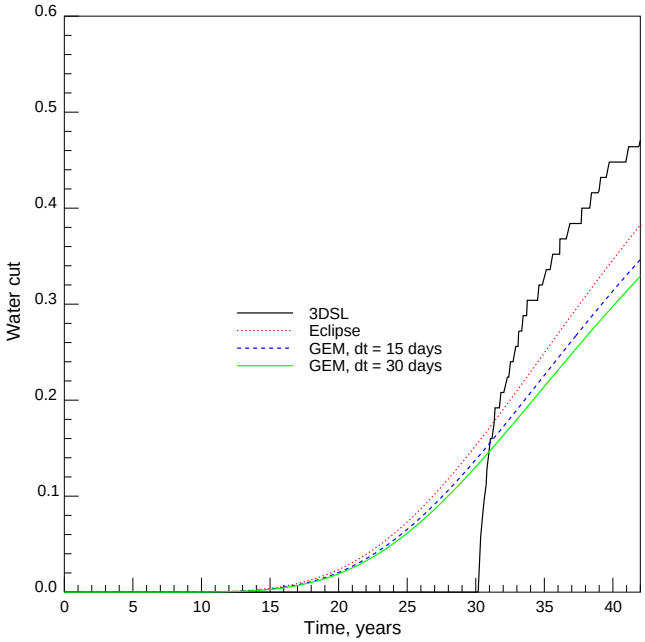

Figure 5.2: Example 11 - Watercut in a five-spot pattern

based saturation update method was not used however because GEM requires diffusive terms and can not be applied to a purely convective flow.

5.3 Mass Conservation

When fluxes are required from a GEM formulation Taigbenu [70] proposes obtaining those fluxes by differentiating the pressure distribution in terms of the shape functions used, e.g.:

$$\frac{\partial p}{\partial x} = \sum_{j=1}^{4} \frac{\partial N_j}{\partial x} p_j \tag{5.17}$$

When linear shape functions are used to interpolate both pressure and permeability over the elements there is a problem at the element boundaries. The C^0 continuity of the shape functions means there is no guarantee that the pressure derivatives computed by Equation 5.17 are continuous across element boundaries.

In an attempt to achieve a more conservative formulation of GEM, elements with higher order continuity were considered in this work. Two kinds of C^1 elements

were considered, Hermitian elements and Overhauser elements, as described in the following sections.

5.3.1 Hermitian Elements

Hermitian elements interpolate the pressure over an element in terms of the nodal pressures and the nodal pressure derivatives. This means there are three unknowns to be solved for every node. The shape functions for a one-dimensional element on $x[0, a]$ are [24]:

$$N_1^0 = 1 - 3\left(\frac{x}{a}\right)^2 + 2\left(\frac{x}{a}\right)^3 \tag{5.18}$$

$$N_1^1 = \left(\frac{x}{a}\right)\left(\left(\frac{x}{a}\right) - 1\right)^2 \tag{5.19}$$

$$N_2^0 = \left(\frac{x}{a}\right)^2\left(3 - 2\left(\frac{x}{a}\right)\right) \tag{5.20}$$

$$N_2^1 = \left(\frac{x}{a}\right)^2\left(\left(\frac{x}{a}\right) - 1\right) \tag{5.21}$$

$$p(x) = p_1 N_1^0 + q_1 N_1^1 + p_2 N_2^0 + q_2 N_2^1 \tag{5.22}$$

To use Hermitian elements an appropriate means to generate two extra equations at each internal node is required. Tomlinson et al. [72] derived a derivative boundary element formulation for Laplace's equation by differentiating the standard integral equation with respect to an initially arbitrary direction. In doing so some of the integrals involved become hypersingular. Tomlinson et al. manipulated the equations further to derive expressions involving at most weakly singular integrals. An analogous procedure for use with GEM could not be found here. The domain discretization used in GEM requires the corner-point singularities in each element to be handled accurately. Even if the two extra equations per node required to calculate the pressure derivatives had been available in weakly singular form it was not evident that the resulting derivatives would necessarily conserve mass.

5.3.2 Overhauser Elements

Overhauser elements were originally developed to provide C^1 continuity of the solutions from the boundary element method [23]. Unlike Hermitian elements only nodal pressure values are required. The one-dimensional Overhauser shape functions are produced by linearly blending two overlapping parabolas. The shape functions for a one-dimensional element $x[0, a]$ are:

$$N_1^{1D} = -\frac{1}{2}\left(\frac{x}{a}\right)^3 + \left(\frac{x}{a}\right)^2 - \frac{1}{2}\frac{x}{a} \tag{5.23}$$

$$N_2^{1D} = \frac{3}{2}\left(\frac{x}{a}\right)^3 - \frac{5}{2}\left(\frac{x}{a}\right)^2 + 1 \tag{5.24}$$

$$N_3^{1D} = -\frac{3}{2}\left(\frac{x}{a}\right)^3 + 2\left(\frac{x}{a}\right)^2 + \frac{1}{2}\frac{x}{a} \tag{5.25}$$

$$N_4^{1D} = \frac{1}{2}\left(\frac{x}{a}\right)^3 - \frac{1}{2}\left(\frac{x}{a}\right)^2 \tag{5.26}$$

The element is built from 16 nodes as shown in Figure 5.3. The pressure in the region between nodes 1 to 4 is interpolated in terms of the pressures at nodes 1 to 16, i.e.:

$$p(x, y) = \sum_{j=1}^{16} N_j p_j \tag{5.27}$$

When applied to the reservoir engineering problems being considered the use of Overhauser elements means that the pressure over an element is interpolated not only in terms of the nodal pressures of that element, but also in terms of the pressures in surrounding elements.

The shape functions for this two-dimensional case are products of one-dimensional shape functions e.g.:

$$N_5 = N_2^{1D}(x)N_1^{1D}(y) = \left(\frac{3}{2}\left(\frac{x}{a}\right)^3 - \frac{5}{2}\left(\frac{x}{a}\right)^2 + 1\right)\left(-\frac{1}{2}\left(\frac{y}{b}\right)^3 + \left(\frac{y}{b}\right)^2 - \frac{1}{2}\frac{y}{b}\right) \tag{5.28}$$

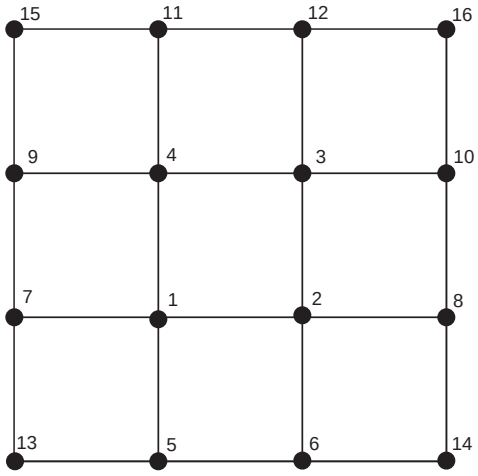

Figure 5.3: Overhauser element node numbering

$$N_{13} = N_1^{1D}(x)N_1^{1D}(y) = \left(-\frac{1}{2}\left(\frac{x}{a}\right)^3 + \left(\frac{x}{a}\right)^2 - \frac{1}{2}\frac{x}{a}\right)\left(-\frac{1}{2}\left(\frac{y}{b}\right)^3 + \left(\frac{y}{b}\right)^2 - \frac{1}{2}\frac{y}{b}\right) \tag{5.29}$$

When using Overhauser elements no extra equations are required but more element integrals are required in the original GEM equations to take account of the interdependence between the nodal values. The values for these integrals are given in Appendix A. With Overhauser elements the discontinuity in the pressure derivative between the element boundaries is gone. However the question of whether the fluxes into and out of an element conserve mass remains.

5.3.3 Example 12: Numerical Experiments

The question of local conservation over the elements was adressed using a simple two-dimensional test problem solving the steady state diffusion equation in a heterogeneous medium. The domain was a unit square and was represented by an 11 by 11 node mesh. No-flow boundary conditions were applied at the top and bottom and

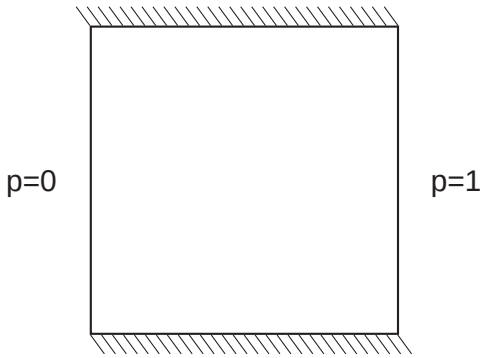

Figure 5.4: Example 12 - Test problem for numerical experiments

pressures were prescribed at the sides, as show in Figure 5.4.

$$p(0, y) = 0 \tag{5.30}$$

$$p(1, y) = 1 \tag{5.31}$$

A variety of heterogeneities was considered in an attempt to quantify the effect of heterogeneity on the conservation properties of the scheme. The last three heterogeneities considered have discontinuous permeability distributions. The distributions are shown in Figure 5.5.

The relative error is the sum of the absolute mass balance error over all the cells divided by the total flow through the reservoir. In this one-dimensional problem the total flow is the harmonic mean permeability multiplied by the applied pressure gradient (which is 1.0 in this case).

A similar set of numerical experiments was performed to assess the conservation properties of the one-dimensional GEM formulation. In this case the boundary conditions differ because for the problem to be properly posed one pressure and one pressure derivative must be prescribed as boundary conditions. The grid used consisted of ten one-dimensional elements. In this set of runs the boundary conditions used were:

$$p(0) = 0 \tag{5.32}$$

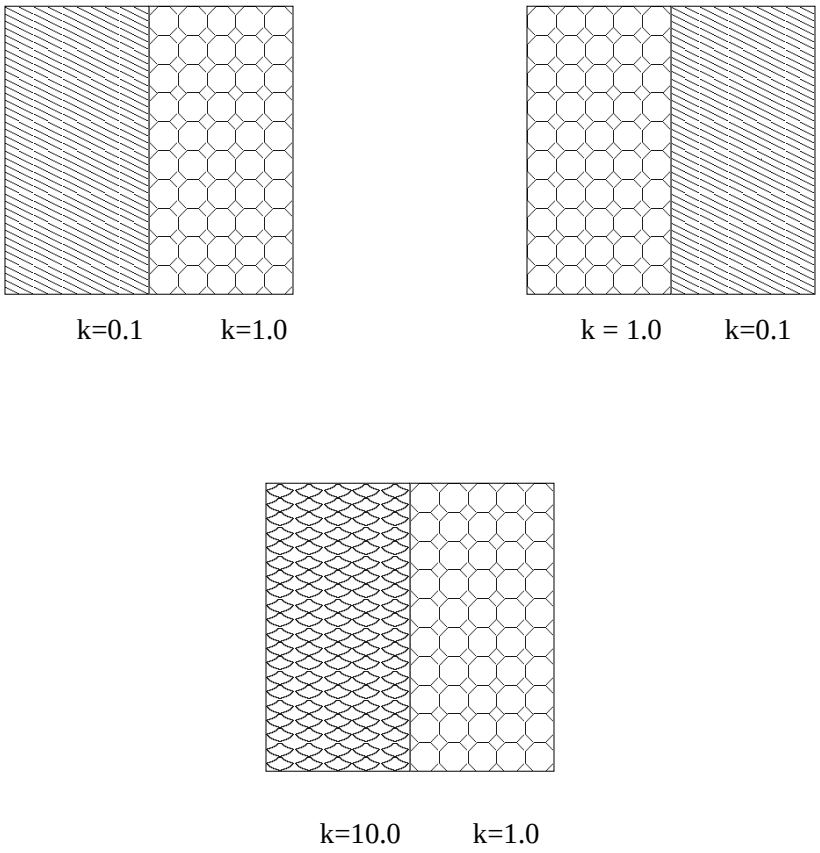

Figure 5.5: Example 12 - Discontinuous permeability distributions

Table 5.3: Example 12 - Mass conservation errors in two-dimensional heterogeneous media flow problem

Permeability variation	Absolute error	Harmonic Mean Permeability	Relative error
1	0	1.0	0
$exp(-x)$	0.000155	0.577	0.000269
$exp(-3x)$	0.000416	0.147	0.00282
$exp(-5x)$	0.000322	0.0292	0.0109
$1+x$	0.000437	1.43	0.000305
$1+x^2$	0.000868	1.27	0.000679
$2-x$	0.000488	1.43	0.000341
$exp(-(1-x))$	0.0000821	0.577	0.000142
$exp(-3(1-x))$	0.000299	0.147	0.00203
$exp(-5(1-x))$	0.000264	0.0292	0.00902
$\begin{cases} 1.0, & x < 0.5 \\ 0.1, & x \geq 0.5 \end{cases}$	0.0626	0.169	0.367
$\begin{cases} 0.1, & x < 0.5 \\ 1.0, & x \geq 0.5 \end{cases}$	0.0803	0.169	0.408
$\begin{cases} 10.0, & x < 0.5 \\ 1.0, & x \geq 0.5 \end{cases}$	0.0626	1.69	0.367

Table 5.4: Example 12 - Mass conservation errors in one-dimensional heterogeneous media flow problem

Permeability variation	Absolute error	Harmonic Mean Permeability	Relative error
1	0	1.0	0
$exp(-x)$	0.0003069	0.3678	0.000834
$exp(-3x)$	0.001122	0.0497	0.02259
$exp(-5x)$	0.0006913	0.006737	0.1026
$1+x$	0.0006247	2.0	0.0003124
$1+x^2$	0.0008321	2.0	0.0004160
$2-x$	0.003122	1.0	0.003122
$exp(-(1-x))$	0.0008349	1.0	0.0008349
$exp(-3(1-x))$	0.02307	1.0	0.02307
$exp(-5(1-x))$	0.11433	1.0	0.11433
$\begin{cases} 1.0, & x < 0.5 \\ 0.1, & x \geq 0.5 \end{cases}$	0.17033	0.1	1.703
$\begin{cases} 0.1, & x < 0.5 \\ 1.0, & x \geq 0.5 \end{cases}$	2.422	1.0	2.422
$\begin{cases} 10.0, & x < 0.5 \\ 1.0, & x \geq 0.5 \end{cases}$	1.703	1.0	1.703

$$\frac{dp}{dx}(1) = 1 \tag{5.33}$$

The results of these runs are summarized in Table 5.4.

The grid used is relatively coarse. When the grid was refined the mass conservation errors were reduced, but they were still present.

The results in Tables 5.4 and 5.3 show that the magnitude of the mass conservation errors increases as the domain becomes more heterogeneous. Perhaps suprisingly in some cases such as $k = exp(-(1-x))$ the errors are greater in the one-dimensional GEM model than in the two-dimensional GEM model. In the one-dimensional case the pressure derivatives are computed directly, in the two-dimensional case they are approximated using shape functions. The results also show that the mass conservation errors are greater when the permeability decreases in the direction of the flow. This

Table 5.5: Example 12 - Cases to demonstrate the effect of the flow direction

	Case A	Case B
Permeability, $x[0, 0.5]$	10	1
Permeability, $x[0.5, 1.0]$	1	10
Boundary condition, x=0	$p = 0$	$p = 0$
Boundary condition, x=1	$q = 1$	$q = 0.1$

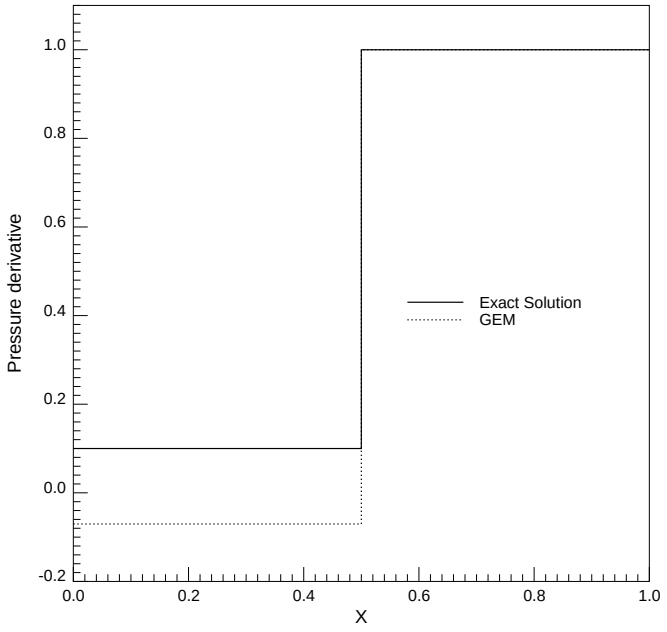

Figure 5.6: Example 12 - Pressure derivative distribution: Case A

can be demonstrated more clearly by comparing two cases using the one-dimensional version of GEM.

The discontinuity in the permeability distribution causes the pressure derivatives in both cases to be incorrect. However Figures 5.6 and 5.7 show this error is much more pronounced when the permeability decreases in the direction of flow.

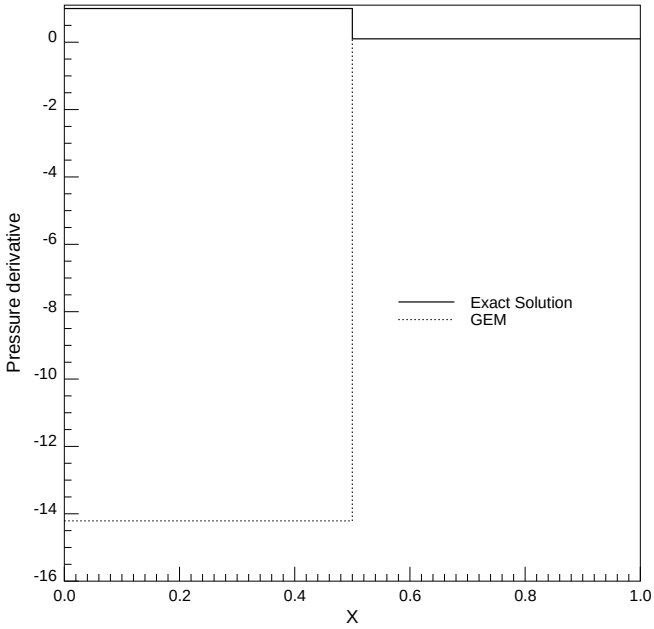

Figure 5.7: Example 12 - Pressure derivative distribution: Case B

5.3.4 Permeability Representation

Numerical Differentiation

In the treatment of flow in heterogeneous media applied in this work the heterogeneity is handled by a term of the form $\nabla lnk \cdot \nabla p$. In the standard approach to this term in a two-dimensional GEM model $\nabla lnk \cdot \nabla p$ is represented in discretized form as $V_{ijl} lnk_j q_l$, where:

$$V_{ijl} = \int_0^{l_e} G(r_i) \frac{dN_j}{dx} N_l \; dx \tag{5.34}$$

Equation 5.34 differentiates nodal values of $ln(k)$ numerically using the shape functions. The integrals are only performed over individual elements using the permeability values within that element. This causes an abrupt change in the value of $\frac{\partial ln(k)}{\partial x}$ across element boundaries.

To assess how significant this effect was, a GEM model was developed in which nodal values of $\frac{\partial ln(k)}{\partial x}$ could be specified. This means the $\nabla lnk \cdot \nabla p$ term is represented in discretized form as $V_{ijl} \frac{\partial ln(k_j)}{\partial x} q_l$. In the element interior these values would be interpolated to perform the integrals, i.e.:

$$V_{ijl} = \int_0^{le} G(r_i) N_j N_l \; dx \tag{5.35}$$

The first test case in the one-dimensional GEM model used the following permeability distribution:

$$k = \frac{1}{1+x} \tag{5.36}$$

therefore

$$\frac{\partial lnk}{\partial x} = \frac{-1}{1+x} \tag{5.37}$$

The boundary conditions were:

$$p(0) = 0 \tag{5.38}$$

$$\frac{\partial p}{\partial x}(1) = 2 \tag{5.39}$$

When the standard formulation was used the mass conservation error was 0.000312. Providing the code with the exact values of the derivative of the permeability resulted in a mass balance error of 0.02602. The mass balance error did not improve when exact values were specified for the derivative of the permeability at the nodes, because using exact nodal values does not necessarily improve the accuracy of the integral of ∇lnk over the element. For a element which is a unit square consider the following integral:

$$\int_0^1 \int_0^1 \nabla lnk \; dxdy \tag{5.40}$$

When the analytical expression is expressed for k in Equation (5.40) the integral becomes:

$$\int_0^1 \int_0^1 \frac{-1}{1+x} \; dxdy = 0.693147 \tag{5.41}$$

When the permeability is expressed in terms of shape functions and nodal value of the shape functions the integral in Equation (5.40) becomes:

$$\int_0^1 \int_0^1 \left(ln(k_1)\frac{\partial N_1}{\partial x} + ln(k_2)\frac{\partial N_2}{\partial x} + ln(k_3)\frac{\partial N_3}{\partial x} + ln(k_4)\frac{\partial N_4}{\partial x} \right) \; dxdy = 0.693147 \tag{5.42}$$

For this particular permeability variation using nodal values of $ln(k)$ and linear shape functions recovers the correct value of the integral. Using nodal values of $\frac{\partial ln(k)}{\partial x}$ gives:

$$\int_0^1 \int_0^1 \left(\frac{\partial ln(k_1)}{\partial x} N_1 + \frac{\partial ln(k_2)}{\partial x} N_2 + \frac{\partial ln(k_3)}{\partial x} N_3 + \frac{\partial ln(k_4)}{\partial x} N_4 \right) \; dxdy = 0.75 \quad (5.43)$$

Equations (5.40), (5.42) and (5.43) show that using nodal values of the permeability derivative does not necessarily improve the integral of ∇lnk over the element.

Overhauser Element Representation of Permeability

The standard one-dimensional GEM model uses linear shape functions to represent the permeability distribution and its derivative. This causes an abrupt change in the permeability derivative across element boundaries. A continuous derivative can be computed by using Overhauser elements instead of linear elements to describe the permeability, i.e.:

$$V_{ijl} = \int_0^{le} G(r_i) \frac{dN_j^{Ov}}{d_x} N_l \; dx \quad (5.44)$$

For a case in which the permeability is:

$$k = \begin{cases} 10, & x < 0.5 \\ 1, & x >= 0.5 \end{cases} \quad (5.45)$$

the resulting representations of $\nabla ln(k)$ on a ten element grid are shown in Figure 5.8.

Incorporating the Overhauser element description of permeability into the one-dimensional GEM model made no difference to the computed pressure derivatives, and therefore no change in the mass conservation achieved for this case. A small improvement in the computed pressure was achieved.

5.3.5 Theoretical Issues

If pressure is the only quantity of interest in a simulation then it is not necessary to use a conservative numerical scheme. Roache [54] states that nonconservative forms

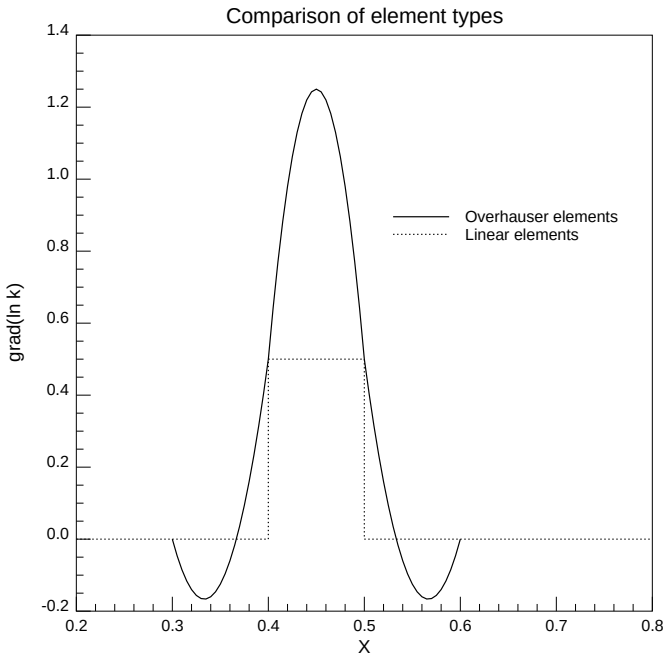

Figure 5.8: Comparison of Overhauser and linear element for permeability representation

of the variable coefficient diffusion equation can produce more accurate results than the conservative forms.

Trujillo [73] presents an analysis of the conservation properties of finite volume and the Galerkin finite element method for elliptic and parabolic equations. If this analysis is confined to steady-state flow the global conservation law is:

$$\int_{\Gamma} (k\nabla p) \cdot n \ d\Gamma = 0 \tag{5.46}$$

The weak form of the finite volume method is:

$$\int_{\Gamma^e} (k\nabla p) \cdot n \ d\Gamma = 0 \quad \forall \Gamma^e \tag{5.47}$$

Trujillo [73] states this implies the finite volume method is conservative because Equation (5.47) closely mimics the global conservation law given in (5.46).

The weak form of the Galerkin finite element does not mimic Equation (5.47) so accordingly this method is not conservative. Conservative finite element methods can be developed by using a mixed method that solves for both the pressure and the

components of the fluid velocities at each node. Mixed methods solve integral forms of:

$$v = -k\nabla p \tag{5.48}$$

$$\nabla \cdot v = 0 \tag{5.49}$$

The weak form that is the basis of GEM is:

$$c_i p(r_i) - \sum_{e=1}^{M} \int_{\Gamma^e} \left(p\frac{\partial G}{\partial n} - G\frac{\partial p}{\partial n} \right) d\Gamma + \int_{\Omega^e} G\, \nabla lnk \cdot \nabla p \, d\Omega = 0 \tag{5.50}$$

Equation (5.50) clearly does not offer local conservation of mass because it does not mimic Equation (5.46) at the element level.

5.3.6 Discussion

The results presented show that GEM is not a suitable scheme for multiple phase flow because of the mass conservation errors that occur. This problem is believed to be common to all boundary element based methods because they do not incorporate a conservation equation of the form of Equation (5.46) at the element level.

When the simulation scheme was coupled to a parameter estimation scheme and run in an iterative fashion, the conservation problems were amplified. In the runs that were performed the parameter estimation scheme tended to increase permeability contrasts which increases the mass conservation error, despite decreasing the objective function value.

Both reservoir heterogeneity and mobility contrast can cause mass conservation error. The Buckley-Leverett case presented in Section 5.2.1 works successfully with the particular set of relative permeability curves given in Equations (5.14) and (5.13). If total mobility varies significantly throughout the reservoir then errors do occur.

However there may be other viable avenues for the use of boundary element methods in multiple phase flow. One possibility is the development of a hybrid finite difference/boundary element simulator. Finite differences could be used in the reservoir and boundary elements could be used in small, homogeneous regions surrounding the wellbores. This would allow the model to retain the familiarity and flexibility of finite

differences while using boundary elements to capture the singularity at the well more rigorously.

Chapter 6

Parameter Estimation

This chapter demonstrates the use of a Gauss-Newton optimization method in conjunction with GEM to perform parameter estimation. In the example presented the scheme is used to determine the permeability distribution of a reservoir by matching pressure data from one producing well and three observation wells. Singularity programming is used in conjunction with GEM, requiring an extra parameter, k_o, the reference permeability used in the singular solution. This parameter is also matched using the Gauss-Newton method.

6.1 Gauss-Newton Method

The optimization method aims to achieve the best possible match between the calculated and observed pressure transients by minimizing the weighted least squares objective function, E:

$$E(k) = (d^{obs} - d^{cal})^T W (d^{obs} - d^{cal}) \tag{6.1}$$

where d^{obs} and d^{cal} are vectors of the observed and calculated pressure data and W is a weight matrix.

The Gauss-Newton method proceeds by taking the derivative of the objective function E to form the sensitivity matrix, G:

$$G_{ij} = \frac{\partial d_i^{cal}}{\partial k_j} \tag{6.2}$$

Using these definitions the gradient of the objective function is:

$$\nabla E = -2G^T W(d^{obs} - d^{cal}) \tag{6.3}$$

The Hessian matrix contains the derivatives of ∇E with respect to the permeability values, and is defined by:

$$H = \frac{\partial \nabla E}{\partial k} = 2G^T WG - 2\frac{\partial G^T}{\partial k} W(d^{obs} - d^{cal}) \tag{6.4}$$

The Gauss-Newton approximation to the Hessian of Equation (6.4) is:

$$H_{GN} = 2G^T WG \tag{6.5}$$

At each iteration of the Gauss-Newton algorithm the following equation is solved to find a descent direction:

$$H_{GN}\delta k = -\nabla E \tag{6.6}$$

6.1.1 Scaling of the Hessian

The Hessian is frequently ill-conditioned or even singular which causes numerical problems in the solution process. To avoid these problems a scaling technique is used. The scaling was described by Wang [74] and originally comes from work by Gill, Wright and Murray [20]. The first step is to construct a diagonal matrix F whose elements are the inverse of the square root of the corresponding diagonal elements of H_{GN}:

$$F_{ii} = (H_{GN_{ii}})^{-\frac{1}{2}} \tag{6.7}$$

Instead of solving Equation (6.6) the following scaled form of the equations is solved for $F^{-1}\delta k$:

$$(FH_{GN}F)\, F^{-1}\delta k = -F\nabla E \tag{6.8}$$

The solution δk can be found by rescaling $F^{-1}\delta k$ by F:

$$\delta k = F\left(F^{-1}\delta k\right) \tag{6.9}$$

6.2 Sensitivity Coefficients

An important step in the application of the Gauss-Newton method is the calculation of the sensitivity coefficients, G_{ij}. Computing the sensitivity coefficients by substitution, i.e. perturbing the permeability in one cell, redoing the well test simulation and computing the difference in the pressure response, is too slow for practical use. Landa [32] demonstrated how sensitivity coefficients could be computed accurately and efficiently from the Jacobian of a finite difference simulator, based on earlier work by Anterion et al. [2]. The current work used singularity programming and required the sensitivity to both the permeability values in each grid cell and to the reference permeability, k_o.

6.2.1 Sensitivity Coefficient for k_o

The sensitivity coefficient to the reference permeability k_o can be computed analytically as:

$$\frac{\partial p_D^s}{\partial k_o} = \frac{-1}{k_o} p_D^s - \frac{q_D}{k_o} exp\left(\frac{-r_D^2}{4t_D}\right) \tag{6.10}$$

The variation of this sensitivity cofficient with time is shown in Figure 6.1 for an example problem. The reservoir parameters used to compute this example are given in Table 6.1. The permeability in the model was homogeneous and equal to 250md. As expected the sensitivity to the reference permeability, which in this example was set to the permeability of the well block, is highest in the early part of the pressure transient data.

6.2.2 Sensitivity Coefficients for Grid Cell Permeabilities

The sensitivity coefficients for the grid cell permeabilities can be derived by differentiating the single-phase flow equations in matrix form. The flow equations can be written in the form:

$$A(k)p^{m+1} = b(k, p^m) \tag{6.11}$$

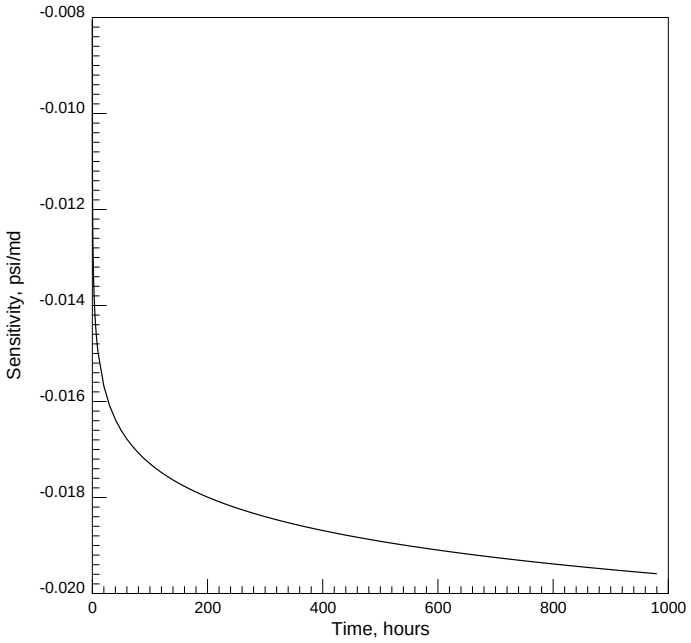

Figure 6.1: Example 13 - Variation of k_o sensitivity with time

Differentiating Equation (6.11) with respect to k gives:

$$\frac{\partial A}{\partial k}p^{m+1} + A\frac{\partial p^{m+1}}{\partial k} = \frac{\partial b}{\partial k} + \frac{\partial b}{\partial p^m}\frac{\partial p^m}{\partial k} \tag{6.12}$$

Rearranging Equation (6.12) generates an expression which can be used to solve for the sensitivity coefficients:

$$A\frac{\partial p^{m+1}}{\partial k} = \frac{\partial b}{\partial k} + \frac{\partial b}{\partial p^m}\frac{\partial p^m}{\partial k} - \frac{\partial A}{\partial k}p^{m+1} \tag{6.13}$$

As in Landa's [32] sensitivity coefficient generation approach for multiphase flow, this approach requires the solution of a matrix equation with multiple right hand sides to generate the sensitivity coefficients. There are of course computational costs involved in generating these right hand sides however the major cost is in solving the matrix equation. If a direct solver is used, then at each timestep the matrix A has already been factored to calculate the pressure solution. Computing each sensitivity only requires an additional back-substitution step.

Table 6.1: Example 13 - Reservoir and grid properties

ϕ	0.3
μ	1 cp
p_i	2000 psi
$q(producer)$	250 STB/d
$q(injector)$	250 STB/d
c_t	10e-06 psi^{-1}
r_w	0.3 ft
h	50 ft
Length	3000 ft
Width	3000 ft
Grid	11 by 11
dx	272.7 ft
dy	272.7 ft

6.3 Results

6.3.1 Example 13: Permeability Estimation

To demonstrate the performance of the proposed parameter estimation scheme a synthetic history matching example was constructed. The reservoir and grid properties are given in Table 6.1. The true reservoir permeability was a heterogeneous distribution shown in Figure 6.2. A production well was located at (1050ft, 1050ft) and an injection well was located at (1950ft, 1950ft). These locations are denoted by stars in Figure 6.2. Two years of pressure data from these two wells was matched to determine the reservoir permeability.

The parameter estimation algorithm succeeded in matching the pressure data from the two wells as shown in Figures 6.4 and 6.5. The estimated reservoir permeability distribution is shown in Figure 6.3. The matching process began with an initial distribution of random uncorrelated permeability values with a mean of 375md. The mean of the true permeability distribution is 275md. The overall permeability distribution estimated by the optimization procedure is not a close match. However the permeability of the cell containing the well and the overall permeability of the surrounding

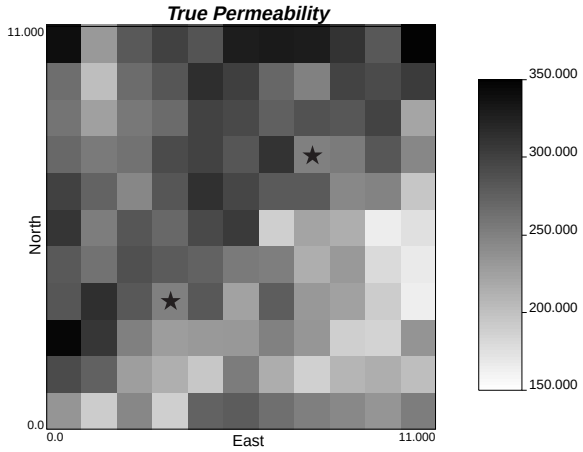

Figure 6.2: Example 13 - True permeability distribution

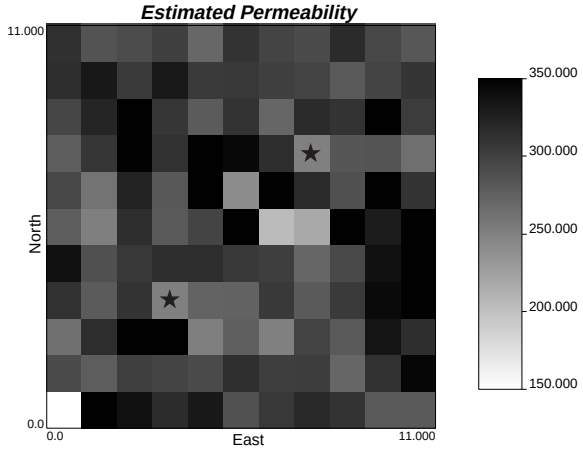

Figure 6.3: Example 13 - Estimated permeability distribution

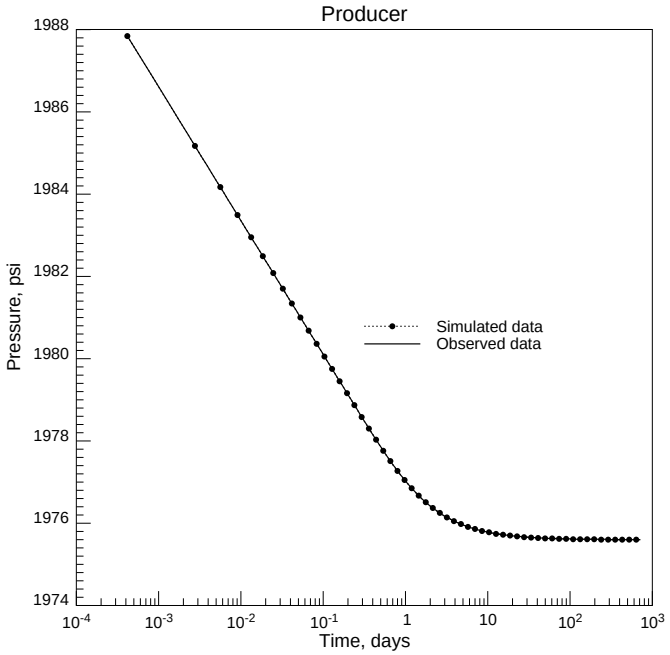

Figure 6.4: Pressure match at producer

cells are well matched.

The decrease of the objective function as the algorithm iterated is shown in Figure 6.6. Note that all the data are weighted equally, however the data are spaced more closely at early time, effectively giving that portion of the transient more weight. The change in the reference permeability is shown in Figure 6.7.

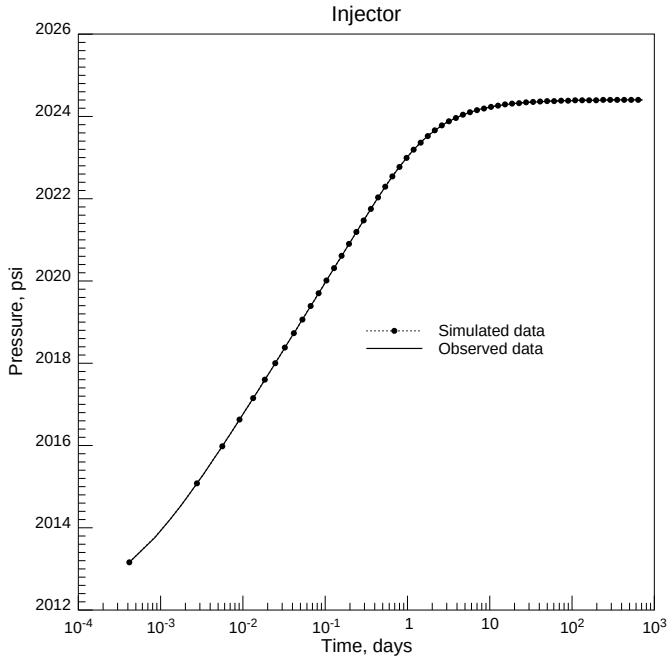

Figure 6.5: Pressure match at injector

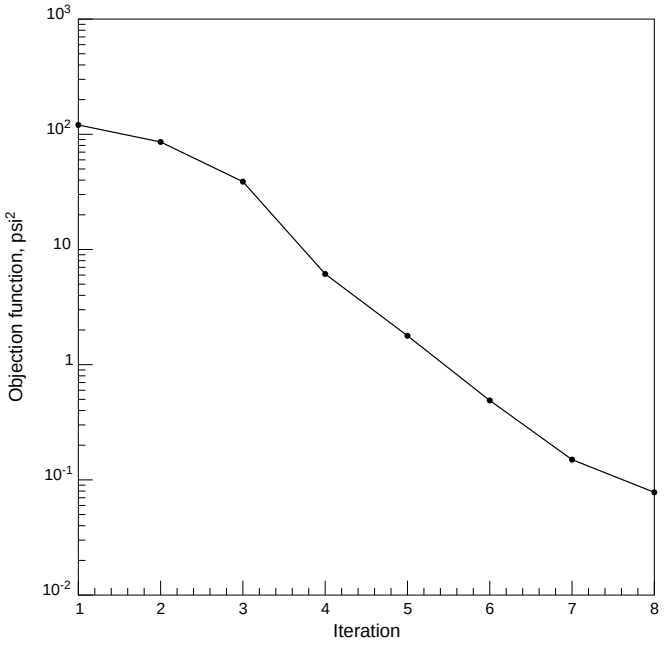

Figure 6.6: Objective function

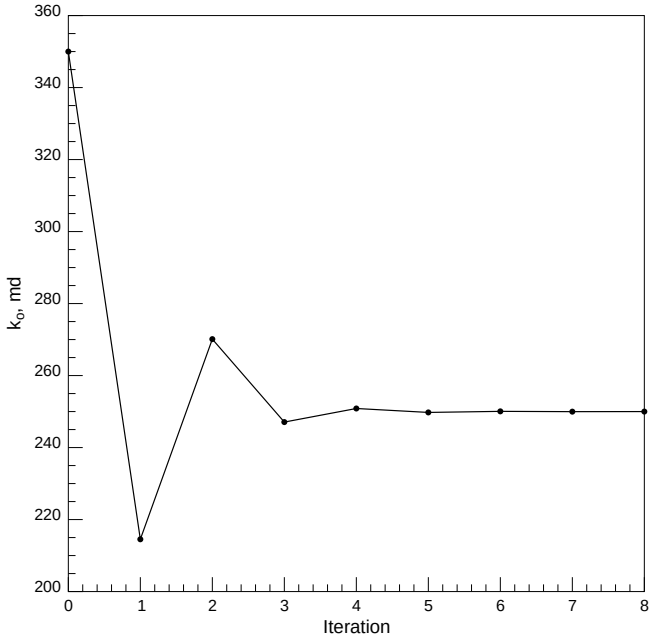

Figure 6.7: Example 13 - k_o estimates

Chapter 7

Concluding Remarks

7.1 Theoretical Issues

Both DRBEM and GEM can be applied to the reservoir engineering problems presented. GEM has been chosen as the preferred solution scheme however. GEM's chief advantage is the sparse matrix structure involved. GEM enters values in the same positions as a nine-point finite difference scheme would. The calculation of the weights, α, in DRBEM is computationally intensive for reservoir engineering problems with large numbers of nodes. For transient problems and tracer problems the inverse of the matrix F is required since the right hand side depends on the unknown pressure and concentration values. The matrix F is likely to be poorly conditioned [48]. F is an N by N (where N is the number of nodes in the problem) matrix which contains the value of each approximating function, f_j, evaluated at each node. There are also other computational issues associated with DRBEM and GEM that will be discussed here.

7.1.1 Element Integrations

Like the classical form of the boundary element method DRBEM requires quadrature rules to perform the integrations over the elements to assemble the matrix equation. To achieve high accuracy many points may be required in the quadrature, which

increases the computational cost. For two-dimensional problems with rectangular or triangular elements the corresponding integrals can be performed analytically using GEM.

7.1.2 DRBEM Approximating Functions

The essence of DRBEM is the expansion of the right hand side terms in the differential equation to be solved as the weighted sum of a set of approximating functions, f_j. As Goldberg [21] notes, the expectation is that if this summation is a good approximation of the right hand side terms then the corresponding particular solution is a good approximation to a particular solution of the differential equation. This makes the appropriate choice of the approximating functions an important part of DRBEM. At this point the best choice of approximating functions is still under discussion in the boundary element literature.

The most common choice of approximating functions is:

$$f_j = 1 + r_j \tag{7.1}$$

For a test problem governed by the Poisson equation Goldberg [21] showed that the choice of thin plate splines and multiquadrics gave higher accuracy than Equation (7.1). In the case of multiquadrics the error was up to three orders of magnitude less depending on the choice of c. Multiquadrics are defined by:

$$f = \sqrt{r^2 + c^2} \tag{7.2}$$

Partridge [48] compared the performance of Equation (7.1) to approximating functions defined by:

$$f_j = 1 + r_j^3 \tag{7.3}$$

and

$$f_j = 1, sin(x), sin(y), sin(2x), sin(x)sin(y), \ldots \tag{7.4}$$

Partridge [48] considered diffusive and convective problems and found that the best choice of approximating functions was problem dependent. The differential equation being solved, the geometry and gridding all played a role. Partridge's advice was to

choose whichever approximating function gave the best conditioning number in the matrix F.

The only approximating functions studied in this work were those defined by Equation (7.1). If DRBEM were to be pursued further for petroleum engineering applications the choice of approximating functions should be given more study.

7.2 Computational Costs Associated with Matrix Structure

If DRBEM, GEM and finite differences were applied to a problem on a given grid the size of the matrix equation which would result is the same for each method. However the structure of the matrices involved differs.

7.2.1 DRBEM

DRBEM produces a nonsymmetric, fully populated matrix equation. Bulgakov et al. [5] presented results that show that iterative matrix solvers can be applied successfully to the matrix equation that results from DRBEM. Bulgakov et al. considered transient diffusion in a homogeneous medium, and they compared the performance of preconditioned conjugate gradient squared (CGS) method and the general minimal residual (GMRES) method to a direct method. In one test problem with 961 grid points the direct method took 112 seconds to solve the matrix system whereas CGS took 6 seconds and GMRES took 3 seconds. The test problem used thin plate splines as approximating functions.

7.2.2 GEM

The matrix equation produced by GEM is sparse. In a two-dimensional problem the matrix equation has nine bands, as opposed to the five bands that would arise from a finite difference solution of the same problem. How much this affects the speed of the solver depends on the kind of solver used. If the solver is only sensitive to

Table 7.1: Cost comparison of GEM and finite difference matrix assembly

Number of nodes	Finite Difference, seconds	GEM, seconds
40 by 40	1	3
50 by 50	3	6
60 by 60	6	11

the bandwidth of the matrix, then the difference in speed will be small, because the bandwidth increases by only two. However if the solver is sensitive to the number of nonzero elements in the matrix the GEM matrix equation could take somewhat longer to solve than a matrix formulated using the finite difference method.

The cost of assembling the GEM matrix is higher than for finite differences, especially in the heterogeneous case because of the loops required to set up the $V_{ijl}lnk_jp_l$ term. To compare the cost of the two methods the diffusion equation was solved on a unit square using finite differences and GEM. The cost in seconds of assembling the matrix on a 275MHz DEC Alpha workstation is shown in Table 7.1.

The cost of assembling and solving the denser matrix involved in GEM is offset somewhat by the greater accuracy of the GEM scheme. Coarser grids can be used to give accurate simulations of well tests.

7.3 The Role of Singularity Programming

Singularity programming played an important role in achieving the accurate simulation of pressure transients in Chapter 3. When two well tests were modeled with GEM but without using singularity programming (see Figures 3.16 and 3.17) the results did suffer from an artifical wellbore storage effect. Sato [57] also found singularity programming to be important. Simulations of well tests using conventional finite difference simulators could potentially be improved by using singularity programming. This could be done in the same manner as this work, i.e. breaking the pressure into singular and nonsingular components and solving for the nonsingular component. An alternative to this approach, which could be implemented more easily

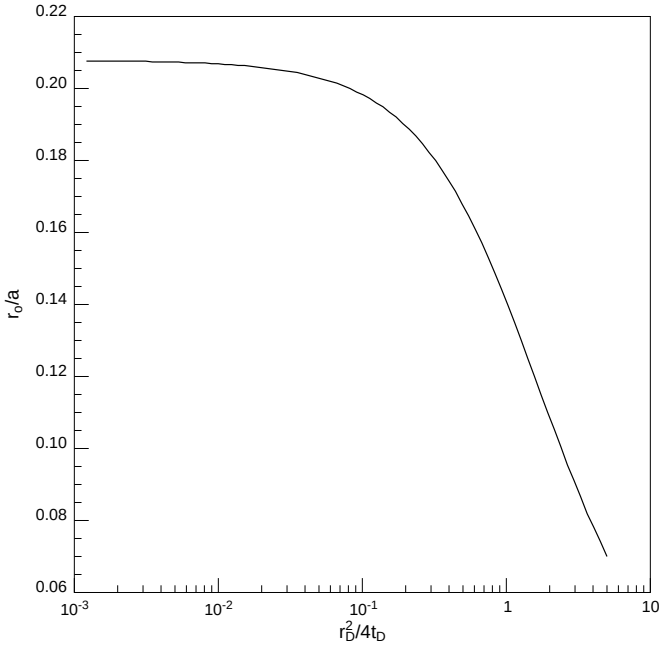

Figure 7.1: Effective radius for well index calculation

in an existing finite difference simulator, would be to reconsider the well index.

The Peaceman well index is not appropriate for the early part of the pressure transient because its derivation is based on the analytical solution to steady-state radial flow. The Peaceman index includes a calculation of a radius r_o at which the block pressure matches the pressure predicted by the analytical solution. For homogeneous isotropic media this radius is defined by:

$$\frac{r_o}{a} = exp\left(-\frac{\pi}{2}\right) = 0.208 \tag{7.5}$$

where a is the side length of the sqaure cell containing the well.

If this derivation is based on the analytical solution for transient radial flow (which was also the basis for the singularity programming applied in this work) a time varying well index can be derived. The derivation of this well index is given in Appendix B (see Equation B.6). The transient well index does reach an asymptotic value of $\frac{r_o}{a}$.

This work has not implemented the proposed transient well index in any finite difference simulator. It is an area that could be investigated further.

7.4 Contributions of This Work

This work presents the theory of DRBEM and GEM applied to three classes of reservoir engineering problems - well testing, tracer testing and multiphase flow in heterogeneous reservoirs. Unlike the perturbation boundary element method used by Sato [57] the computational effort involved in the methods presented in this work does not increase as the heterogeneity becomes more pronounced. GEM was chosen as the preferred method because it produces a sparse coefficient matrix.

To simulate well tests singularity programming was incorporated with GEM. The results were compared to analytical and finite difference solutions. The matches to analytical solutions were excellent, even on a coarse 11 by 11 grid. The finite difference simulations had numerical artifacts, including artificial wellbore storage and difficulty reproducing the flat pressure derivative associated with infinite acting radial flow when using a nonuniform grid.

Numerical tracer flow experiments showed that GEM was more appropriate than DRBEM for modeling tracer flows at high Peclet number. GEM gave a better representation of the tracer front and was less subject to spurious numerical oscillations.

An IMPES scheme based on GEM was developed for multiphase flow simulation. However the results demonstrated that GEM is not a conservative method. A version of GEM incorporating Overhauser elements produced solutions which have C^1 continuity but this was not enough to achieve local conservation of mass at the element level.

A parameter estimation scheme was developed to determine the reservoir permeability distribution from GEM simulations of well test data. This method also incorporated singularity programming. The scheme was applied to successfully match pressure data from multiple wells.

7.5 Future Applications of Boundary Element Based Methods in Reservoir Enginering

If boundary element based methods are to be used for multiphase flow they must be derived in such a way that they are locally conservative. This is a very fundamental issue because boundary element methods arise from a global statement of conservation of mass (in integral form), as opposed to the element-by-element mass conservation statements that form the basis of traditional finite difference schemes. If boundary element method solutions to multiphase flow problems are going to be sought in the future this issue must be considered carefully. Another possible approach would to be couple a boundary element based calculation for the near-wellbore region with a finite difference calculation in the remainder of the reservoir.

Another possible extension to this work would be to consider other singular solutions in the well testing problem. Storage, skin and fractured wells could potentially be treated this way. To do so the singular solution would have to be computed in Laplace space and inverted numerically before being coupled with the boundary element scheme.

Nomenclature

A	reservoir area
C	concentration
c	compressibility
D	diffusion coefficient
e	element index
F	matrix of approximating function values
f	approximating function, DRBEM
G	Green's function
h	reservoir thickness
i	source node position
j	dummy index, GEM
k	permeability
L	number of internal nodes, DRBEM
L	elemental matrix, GEM
l	dummy index, GEM
M	number of boundary nodes, DRBEM
m	timestep index
N	Lagrange interpolation function
Nel	number of elements
n	outward normal vector
p	pressure
Q	injection rate
q	flux

R	elemental matrix, GEM
R	matrix accounting for convective terms, DRBEM
r	position
S	intermediate matrix, DRBEM
u	transformed pressure variable, DRBEM
t	time
V	elemental matrix, GEM
v	velocity
WI	Peaceman well index
x	Cartesian coordinate
y	Cartesian coordinate

Greek

α	weight, DRBEM
α	dispersivity
β	secondary weight, DRBEM
Γ	boundary
δ	Dirac delta function
θ	internal angle of boundary, radians
θ	time integration parameter
μ	viscosity
ξ	local coordinate
η	local coordinate
θ	time integration parameter
ϕ	porosity
Ω	domain

Superscripts

$\hat{}$	particular solution, DRBEM
e	element
ns	non-singular
p	pressure
q	flux
s	singular

Subscripts

D	dimensionless
i	initial
o	oil
t	total
w	water

Bibliography

[1] Amoah, N., Morin, P. and Sabin, G,: "Analysis of Solute Transport Through Saturated Porous Aquifers Using the Dual Reciprocity Boundary Element Method", 18th World Conference on the Boundary Element Method, 1996, 619-628

[2] Anterion, F., Eymard, R., and Karcher, B.: "Use of Parameter Gradients for Reservoir History Matching", SPE 18433, SPE Symposium on Reservoir Simulation, Houston, TX, February 6-8, 1989

[3] Becker, A. A.: "The Boundary Element Method in Engineering", McGraw Hill, 1992

[4] Bokota, A. and Iskeria, S.: "An Analysis of the Diffusion-Convection Problem by the Boundary Element Method", Engineering Analysis with Boundary Elements, 15, 1995, 267-275

[5] Bulgakov, V., Sarler, B. and Kuhn, G.: "Iterative Solution of Systems of Equations in the Dual Reciprocity Boundary Element Method for the Diffusion Equations", International Journal for Numerical Methods in Engineering, 43, 1998, 713-732

[6] Carslaw, H. S and Jaegar, J. C.: "Conduction of Heat in Solids", 2nd edition, Clarendon Press, Oxford, 1959

[7] Chen, C. S., Marcozzi M. D. and Choi, S.: "The Method of Fundamental Solutions and Compactly Supported Radial Basis Functions: a Meshless Approach to 3D Problems", Proceedings of BEM 21, Oxford University, August 1999

[8] Cheng, A.H-D.: "Darcy's Flow with Variable Permeability. A Boundary Integral Solution", Water Resources Research, 1984, 20, 980-984

[9] Cheng, A.H-D. and Ouazar, D.: "Groundwater Flow", Chapter 8 of "Boundary Element Techniques in Geomechanics", edited by G.D. Manolis and T.G. Davies, Elsevier, 1993

[10] Cruse, T.A.: "Numerical Solutions in Three Dimensional Elastostatics", Int. J. Solids and Structures, 5, 1259-1274, 1969

[11] Dake, L. P.: "Fundamentals of Reservoir Engineering", Elsevier Science, Amsterdam, 1978

[12] El Harrouni, K., Ouazar, D. and Wrobel, L. C.: "About the Identifiability of Inverse Problems with Boundary Element Method", Proceedings of the International Conference on Boundary Element Methods, 1993, 399-410

[13] El Harrouni, K., Ouazar, D., Wrobel, L. C. and Cheng, A.H-D.: "Global Interpolation Function Based DRBEM Applied to Darcy's Flow in Hetereogeneous Media", Engineering Analysis with Boundary Elements, 1996, 281-285

[14] El Harrouni, K., Ouazar, D., Walters, G. A. and Cheng, A.H-D.: "Groundwater Optimization by Genetic Algorithm and Dual Reciprocity Boundary Element Method", Engineering Analysis with Boundary Elements, 1996, 287-296

[15] El Harrouni, K., Ouazar, D., Wrobel L. C. and Cheng, A.H-D.: "Groundwater Parameter Estimation by Optimization and DRBEM", Engineering Analysis with Boundary Elements, 1997, 97-103

[16] El Harrouni, K., Ouazar, D., Wrobel L. C. and Cheng, A.H-D.: "Uncertainty Analysis of Groundwater Flow with DRBEM", Engineering Analysis with Boundary Elements, 1997, 217-221

[17] El Harrouni, K., Ouazar, D., Wrobel L. C. and Cheng, A.H-D.: "Aquifer Parameter Estimation by Extended Kalman Filtering and Boundary Elements", Engineering Analysis with Boundary Elements, 1997, 231-237

[18] Eldho, R.I.: "Pollutant Dispersion Analysis in Porous Media using Dual Reciprocity Boundary Element Method" in "Development and Application of Computer Techniques to Enivronmental Studies VI", Computational Mechanics Publications, Southhampton, 121-130, 1996

[19] Gelhar, I. W.: "Stochastic Subsurface Hydrology from Theory to Applications", Water Resources Research, 22, 9, 1986, 135 -145

[20] Gill, P. E., Murray, W. and Wright, M. H.: "Practical Optimization", Academic Press Inc., San Diego, California

[21] Goldberg, M. A., Chen, C. S., Bowman, H. and Power, H.: "Some Comments on the use of Radial Basis Functions in the Dual Reciprocity Method", Computational Mechanics, 21, 1998, 141-148

[22] Gringarten, A. C. and Ramey, H. J., Jr.: "The Use of Source and Green's Functions in Solving Unsteady-Flow Problems in Reservoirs", SPEJ, October 1973, 285-296

[23] Hall, W. S. and Hibbs, T. T.: "Continuous, quadrilateral, and triangular surface patches" in "Applied Surface Modelling" Creasy, C. F. M. and Craggs, C. (editors), 1990, 139

[24] Hunter, P. and Pullan, A.: "FEM/BEM notes", Department of Engineering Science, University of Auckland, 1998
http://www.esc.auckland.ac.nz/Academic/Texts/FEM-BEM-notes.html

[25] Intera Information Technologies Ltd.: "Eclipse 100 Reference Manual", 96a Release

[26] Jaswon, M. A. "Integral Equation Methods in Potential Theory, I" Proc. Roy. Soc. Ser. A, 1963, 275, 23-32

[27] Kikani, J. and Horne, R. N.: "Application of Boundary Element Method to Reservoir Engineering Problems", Journal of Petroleum Science and Engineering, 1989, 229-241

[28] Kikani, J. and Horne, R. N.: "Pressure-Transient Analysis of Arbitrarily Shaped Reservoirs With the Boundary Element Method", SPE Formation Evaluation, 1992, 53-60

[29] Koh, L. S. and Tiab, D.: "A Boundary Element Algorithm for Modelling 3D Horizontal Wells Problems Using 2D Grids", SPE Petroleum Computer Conference, New Orleans, LA, 11-14 July 1993, 91-106

[30] Koro, K. and Abe, K.: "H-Hierarchial Adaptive BEM with Haar Wavelet Functions for Two-Dimensional Laplace Problems", Proceedings of BEM 21, Oxford University, August 1999

[31] Lafe, O. E., and Cheng, A.H-D.: "A Perturbation Boundary Element Code for Steady State Groundwater Flow in Heterogeneous Aquifers", Water Resources Research, 1987, 23(6), 1079-1084

[32] Landa, J.: "Reservoir Parameter Estimation Constrained to Pressure Transients, Performance History and Distributed Saturation Data", Ph.D. Dissertation, Stanford U., 1997

[33] Layne, M. A., Numbere, D. T. and Koederitz L. F." "Future Performance Prediction for Water Drive Gas Reservoirs", SPE Annual Technical Conference and Exhibition, Houston, 1993

[34] Liggett, J. A. and Liu, P.L-F.: "Unsteady Free Surface Flow through a Zoned Dam using Boundary Integration", Symposium on Applications of Computer Methods, Los Angeles, CA, August 23-26, 1977

[35] Liggett, J. A. and Liu, P.L-F.: "Unsteady Flow in Confined Aquifers - A Comparison of Two Boundary Integral Methods", Water Resources Research, 1979, 15(4), 861-866

[36] Liggett, J. A. and Liu, P.L-F.: *The Boundary Integral Equation Method for Porous Media Flow*, George Allen and Unwin, London, 1983

[37] Lin, J.: "*An Image Well Method for Bounding Arbitrary Reservoir Shapes in the Streamline Model*", Ph.D. Dissertation, U. of Texas, Austin, 1972

[38] Masukawa, J. and Horne, R. N.: "Application of the Boundary Integral Method to Immiscible Displacement Problems", SPE Reservoir Engineering, August 1988, 1069-77

[39] Numbere, D. T. and Tiab, D.: "An Improved Streamline-Generating Technique that Uses the Boundary (Integral) Element Method", SPE Reservoir Engineering, August 1988, 1061-68

[40] Numbere, D. T. and Erkal, A.: "A Model for Tracer Flow in Heterogeneous Porous Media", SPE Asia Pacific Conference on Integrated Modelling for Asset Management", Kuala Lumpur, March 23-24, 1998

[41] Ogata, A. and Banks, R. B.: "A Solution of the Differential Equation of Longitudinal Dispersion in Porous Media", US Geological Survey Professional Paper 411-A

[42] Onyejekwe, O. O.: "A Green Element Solution of the Diffusion Equation", Proc. 34th Heat Transfer and Fluid Mechanics Institute, June 1-2, California State U., Sacremento, CA, 1995

[43] Onyejekwe, O. O.: "Green Element Description of Mass Transfer in Reacting Systems" Numerical Heat Transfer, Part B, 30, 1996, 483-498

[44] Onyejekwe, O. O.: "A Green Element Treatment of Isothermal Flow with Second Order Reaction", Int. Comm. Heat Mass Transfer, 24, 1997, 251-264

[45] Onyejekwe, O. O.: "A Boundary Element-Finite Element Equations Solution to Flow in Heterogeneous Porous Media", Transport in Porous Media, 31, 1998, 293-312

[46] Onyejekwe, O. O.: "Boundary Integral Procedures for Unsaturated Flow Problems", Transport in Porous Media, 31, 1998, 313-330

[47] Onyejekwe, O. O.: Personal communication, June 4, 1998

[48] Partridge, P. W.: "Dual Reciprocity BEM: Local Versus Global Approximation Functions for Diffusion, Convection and Other Problems", Engineering Analysis with Boundary Elements, 14, 1994, 349-356

[49] Partridge, P. W., Brebbia, C. A. and Wrobel, L. C.: "The Dual Reciprocity Boundary Element Method", Elsevier Applied Science, 1992

[50] Peaceman, D. W.: "Interpretation of Well-Block Pressures in Numerical Reservoir Simulation", SPEJ, 253, 1978, 183-194

[51] Pecher, R. and Stanislav, J. F.: "Boundary Element Techniques in Petroleum Reservoir Simulation", Journal of Petroleum Science and Engineering, 17, 1997, 353-366

[52] Petroway Inc.: Automate for Windows, version 1.8 Elsevier Applied Science, 1994

[53] Rizzo, F. J.: "An Integral Equation Approach to Boundary Value Problems of Classical Elastostatics", Q.J. Appl. Math, 1967, 25, 83-95

[54] Roache, P. J.: "Computational Fluid Dynamics", Hermosa Publishers, 1973

[55] Roy, R. V. and Grilli, S. T.: "Probablistic Analysis of Flow in Random Porous Media by Stochastic Boundary Element Methods", Engineering Analysis with Boundary Elements, 19, 1997, 237-255

[56] Russell, T. F. and Wheeler, M. F.: "Finite Element and Finite Difference Methods for Continuous Flows in Porous Media" in "The Mathematics of Reservoir Simulation", Frontiers in Applied Mathematics, SIAM, Philadlphia, 1983

[57] Sato, K.: *Accelerated Perturbation Boundary Element Model for Flow Problems in Heterogeneous Reservoirs*, Ph.D. Dissertation, Stanford U., 1992

[58] Sato, K. and Horne, R. N.: "Perturbation Boundary Element Method for Heterogeneous Reservoirs: Part 1 - Steady-State Flow Problems", SPE Formation Evaluation, 1993, 306-314

[59] Sato, K. and Horne, R. N.: "Perturbation Boundary Element Method for Heterogeneous Reservoirs: Part 2 - Transient Flow Problems", SPE Formation Evaluation, 1993, 315-322

[60] Sato, K. and Abbaszadeh, M.: "Tracer Flow and Pressure Performace of Reservoir Containing Distributed Thin Bodies", SPE Annual Technical Conference and Exhibition, New Orleans, Sept. 25-28, 1996

[61] Singh, K. M. and Kalra, M. S.: "Time Integration in the Dual Reciprocity Boundary Element Analysis of Transient Diffusion", Engineering Analysis with Boundary Elements, 1996, 18, 73-102

[62] Stehfest, H.: "Algorithm 368 - Numerical Inversion of Laplace Transforms [D5]", *Comm. of ACM* 1970, 47-49

[63] Symm, G. T.: "Integral Equation Methods in Potential Theory, II", Proc. Roy. Soc. Ser. A, 1963, 275, 33-46

[64] Taigbenu, A. E.: "A More Efficient Implementation of the Boundary Element Theory", Proc. 5th International Conference on Boundary Element Technology (BETECH 90), Newark, Delaware, 1990, 355-366

[65] Taigbenu, A. E.: "The Use of a Higher Interpolation Function in COnjuction with the Green Element Method (GEM)", Proc. Int. Conf. on Computer Meth. Water Resources, Rabat, Morocco, October 9-11, 1991, 293-305

[66] Taigbenu, A. E.: "The Green Element Method", International Journal for Numerical Methods in Engineering, 1995, 38, 2241-2263

[67] Taigbenu, A. E. and Onyejekwe, O. O.: "Green Element Simulations of the Transient Nonlinear Unsaturated Flow Equation", Appl. Math. Modelling, 19, 1995, 675-684

[68] Taigbenu, A. E.: "Transient 1D Transport Equation Simulated by a Mixed Green Element Formulation", International Journal for Numerical Methods in Fluids, 25, 1997, 437-454

[69] Taigbenu, A. E. and Onyejekwe, O. O.: "Green's Function-Based Integral Approach to Linear Transient Boundary-Value Problems and their Stability Characteristics (I)", Appl. Math. Modelling, 22, 1998, 687-702

[70] Taigbenu, A. E.: "The Green Element Method", Kluwer Academic Publishers, 1999

[71] Thiele, M. R., Batycky, R. P. and Blunt, M. J.: "A Streamline-Based 3D Field-Scale Compositional Reservoir Simulator", SPE Annual Technical Conference and Exhibition, San Antonio, Texas, 1997

[72] Tomlinson, K., Bradley, C. and Pullan A.: "On the Choice of a Derivative Boundary Element Formulation Using Hermite Interpolation", Internation Journal for Numerical Methods in Engineering, 39, 1996, 451-468

[73] Trujillo, R. V.: "Error Analysis of the Finite Volume Element Method for Elliptic and Parabolic Partial Differential Equations", Ph.D. thesis (Applied Mathematics), University of Colorado at Denver, 1996

[74] Wang, P.: "Integrating Resistivity Data into the Parameter Estimation Problem", M.S. report, Stanford U., June 1999

[75] Wolfram Research Inc." "Mathematica", version 4, 1999

[76] Wrobel, L. C., Brebbia, C. A. and Nardini D.: "The Dual Reciprocity Boundary Element Method Formulation for Transient Heat Conduction", Proc. 6th Int. Conf. Finite Elements in Water Resources, Lisbon, 1986

[77] Wrobel, L. C., and DeFigueirdo, D. B.: "A Dual Reciprocity Boundary Element Formulation for Convection-diffusion Problems with Variable Velocity Fields", Engineering Analysis with Boundary Elements, 1991, 8, 312

[78] Zhang, W. and Zeng P.: "A Boundary Element Method Applied to Pressure Transient Analysis of Irregularly Shaped Double-Porosity Reservoir", unsolicited manuscript, SPE 25284, May 1992

Appendix A

GEM Implementation Details

The equation describing the GEM approach to a certain differential equation can be written simply in index notation. For example the equation for the transient pressure diffusion equation in a heterogeneous medium is:

$$\sum_{e=1}^{M}\left(R_{ij}p_j + L_{ij}q_j - V_{ijl}lnk_j p_l + U_{ijl}\gamma_j\frac{\partial p_j}{\partial t}\right) = 0 \tag{A.1}$$

To implement a computer program to assemble and solve this matrix equation requires careful consideration of some details:
- the treatment of the pressure derivative term, q
- the matrix assembly procedure
- the evaluation of the element integrals, in this case R_{ij}, L_{ij}, V_{ijl} and T_{ij}

A.1 Treatment of the Normal Derivative of Pressure

The first key step in the implementation of GEM is to acknowledge that q, the normal derivative of p, is discontinuous at the corners of the elements. So each node in a two-dimensional problem has three unknowns which are the nodal pressure and two pressure derivatives, one in the x direction and one in the y direction. However when

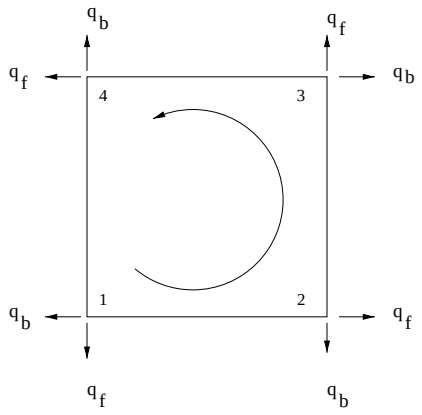

Figure A.1: Components of the normal derivative

programming the method it is more convenient to denote the components of q as q_b and q_f, i.e. before the node and after the node, instead of q_x and q_y. The element integrals are performed in an anticlockwise direction so the directions of the q_b and q_f depend on the position of the node within the element as shown in Figure A.1. According the corresponding element integral L_{ij} is broken up into two terms L^b_{ij} and L^f_{ij}.

A.1.1 Treatment of the Normal Derivative on External Segments of the Boundary

When setting the boundary conditions it is also important to make sure that the three unknowns at each node are correctly set. At nodes where the boundary of the computational domain is smooth either pressure or pressure derivative is set. If the pressure derivative is set both components are set equal to each other as shown in Figure A.2. If a node is at the corner of the problem domain then two of the three unknowns can be set as boundary conditions, either one pressure and one component of its derivative or both components of the derivative. This shown is Figure A.3.

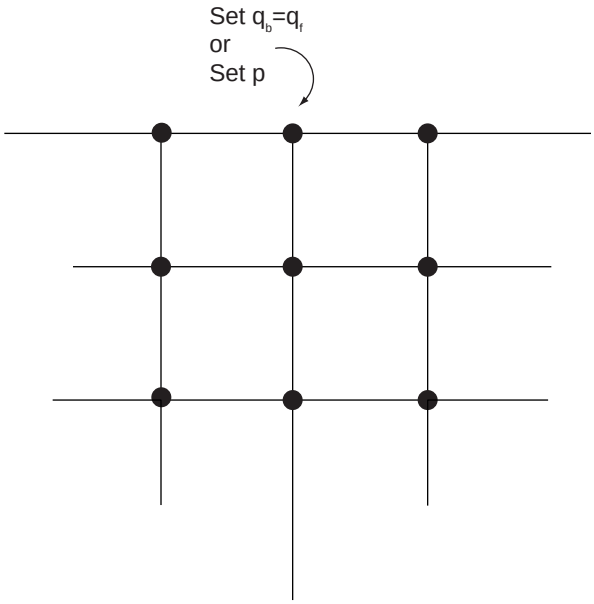

Figure A.2: Treatment of the normal derivative at a smooth boundary

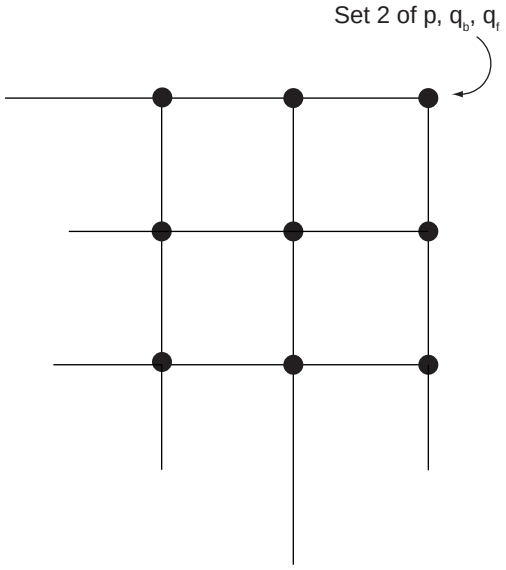

Figure A.3: Treatment of the normal derivative at a corner

A.1.2 Treatment of the Normal Derivative on Internal Segments of the Boundary

At internal nodes the pressure derivative is eliminated from the matrix equation (Equation (A.1) for example) by expanding it in terms of the derivatives of the shape functions and the nodal pressure values on the element. When the shape functions are linear this is a familiar finite difference approximation. The approach used in this work (and by Onyejekwe [47]) was to modify the R_{ij} terms for to take account of this. The procedure for regular elements with side length D is:

```
Loop over elements, M = 1, Nelements
      Loop over nodes within element, K = 1 to 4
           Is line segment from node K to K+1 in the interior?
              If yes modify R matrix for element M as follows
                  Is segment opposite from (K,K+1) on the
                  boundary?
                     If yes expand normal derivative in terms
                     of nodal pressures on this element (M):
                         R(M,K+2,K) = R(M,K+2,K)
                                           - LF(M,K+2,K)/D
                         R(M,K+2,K-1) = R(M,K+2,K-1)
                                             + LF(M,K+2,K)/D
                         R(M,K+3,K) = R(M,K+3,K)
                                           - LF(M,K+3,K)/D
                         R(M,K+3,K-1) = R(M,K+3,K-1)
                                             + LF(M,K+3,K)/D
                         R(M,K+2,K+1) = R(M,K+2,K+1)
                                             - LB(M,K+2,K+1)/D
                         R(M,K+2,K+2) = R(M,K+2,K+2)
                                             + LB(M,K+2,K+1)/D
                         R(M,K+3,K+1) = R(M,K+3,K+1)
                                             - LB(M,K+3,K+1)/D
```

```
    R(M,K+3,K+2) = R(M,K+3,K+2)
                          + LB(M,K+3,K+1)/D
If no expand normal derivative in terms
of nodal pressure on this element and
neighbouring element (L):
    R(M,K+2,K) = R(M,K+2,K)
                        - LF(M,K+2,K)*(3/2D)
    R(M,K+2,K-1) = R(M,K+2,K-1)
                          + LF(M,K+2,K)*(2/D)
    R(M,K+3,K) = R(M,K+3,K)
                        - LF(M,K+3,K)*(3/2D)
    R(M,K+3,K-1) = R(M,K+3,K-1)
                          + LF(M,K+3,K)*(2/D)
    R(M,K+2,K+1) = R(M,K+2,K+1)
                       - LB(M,K+2,K+1)*(3/2D)
    R(M,K+2,K+2) = R(M,K+2,K+2)
                          + LB(M,K+2,K+1)*(2/D)
    R(M,K+3,K+1) = R(M,K+3,K+1)
                        - LB(M,K+3,K+1)*(3/2D)
    R(M,K+3,K+2) = R(M,K+3,K+2)
                          + LB(M,K+3,K+1)*(2/D)
    LL = local node number in element L of
         the start of segment (K+2,K+3)
    R(L,K+2,LL-1) = R(L,K+2,LL-1)
                           - LF(M,K+2,K)*(1/2D)
    R(L,K+3,LL-1) = R(L,K+3,LL-1)
                           - LF(M,K+3,K)*(1/2D)
    R(L,K+2,LL-2) = R(L,K+2,LL-2)
                           - LB(M,K+2,K)*(1/2D)
    R(L,K+3,LL-2) = R(L,K+3,LL-2)
                           - LB(M,K+3,K)*(1/2D)
```

```
                End if
             If no do not modify R matrix for element M
          End if
      End node (K) loop
End element (M) loop
```

In the algorithm shown above for modifying the R_{ij} terms note that the indices i and j can not exceed 4. If $K = 4$ then $K + 1 = 1$, $K + 2 = 2$ etc.

A.2 Matrix Assembly

Once the element matrix R has been modified to handle the expansion of normal derivative of the pressure in terms of nodal pressure values the assembly of the matrix equation in the form $Ax = b$ is relatively straightforward. The assembly is performed in an element-by-element fashion as shown in the following procedure:

```
Loop over elements, M = 1, Nelements
      Loop over local node numbers within element for source point,
      L = 1 to 4
            I = Global node number of L
            Loop over local node numbers within element for field
            point, K = 1 to 4
                  J = Global node number of K
                  Is pressure an unknown variable at node J?
                     If yes include R terms
                          A(I,J) = A(I,J) + R(M,L,K)
                     Is permeability heterogeneous?
                     If yes include V terms
                         Loop over local node numbers, NU = 1 to 4
                              NJ = Global node number of NU
                              A(I,J) = A(I,J)
                                        - V(M,L,K,NU)*Log(Perm(NJ))
```

```
                    Include time derivative term
                        Loop over local node numbers, NU = 1 to 4
                             NJ = Global node number of NU
                             A(I,J) = A(I,J)
                                       + U(M,L,K,NU)*Gamma(NJ)/dt
                Is qf an unknown variable at node J?
                     If yes include LF term
                         A(I,J) = A(I,J) - LF(M,L,K)
                 Is qb an unknown variable at node J?
                     If yes include LB term
                         A(I,J) = A(I,J) - LB(M,L,K+1)
            End field point loop (K)
        End source point loop (L)
End element loop (M)
```

This procedure assumes that time is treated in a fully implicit fashion.

The right hand side is assembled in a similar fashion.

```
Loop over elements, M = 1, Nelements
      Loop over local node numbers within element for source point,
           L = 1 to 4
           I = Global node number of L
           Loop over local node numbers within element for field
           point, K = 1 to 4
                J = Global node number of K
                Is pressure a known variable at node J?
                   If yes include R terms
                        B(I) = B(I) - R(M,L,K)*P(J)
                   Is permeability heterogeneous?
                   If yes include V terms
                       Loop over local node numbers, NU = 1 to 4
                            NJ = Global node number of NU
```

```
                              B(I) = B(I)
                                    + V(M,L,K,NU)*Log(Perm(NJ))*P(J)
                        Include time derivative term
                            Loop over local node numbers, NU = 1 to 4
                                 NJ = Global node number of NU
                                 B(I) = B(I)
                                       - U(M,L,K,NU)*Gamma(NJ)/dt
                    Is qf a known variable at node J
                        If yes include LF term
                           B(I) = B(I) + LF(M,L,K)*QF(J)
                    Is qb a known variable at node J
                        If yes include LB term
                           B(I) = B(I) + LB(M,L,K+1)*QB(J)
                    End field point loop (K)
            End source point loop (L)
End element loop (M)
```

A.3 GEM Element Integrals for Linear Rectangular Elements

To assemble and solve the matrix equation produced by GEM expressions for the element integrals must be evaluated. Every problem involves diffusive terms denoted by R and L. The analytical expressions for the R and L are:

$$R_{ij} = \int_{\Gamma_e} \frac{\partial G(r, r_i)}{\partial n} N_j \; d\Gamma - \delta_{ij} \, \theta_i \tag{A.2}$$

$$L_{ij} = - \int_{\Gamma_e} G(r, r_i) N_j \; d\Gamma \tag{A.3}$$

Transient problems in homogeneous media require the element matrix T to be evaluated:

$$T_{ij} = \iint_{\Omega_e} G(r, r_i) N_j \; d\Omega \tag{A.4}$$

For transient problems in heterogeneous media the matrix U multiplies the time derivative term:

$$U_{ijl} = \int\int_{\Omega^e} G(r, r_i) N_j N_l \; d\Omega \tag{A.5}$$

For heteroegeneous problems a $\nabla lnk \cdot \nabla p$ term appears. In discrete form this requires the element matrix V:

$$V_{ijl} = \int\int_{\Omega_e} G(r, r_i) \left[\frac{\partial N_j}{\partial x} \frac{\partial N_l}{\partial x} + \frac{\partial N_j}{\partial y} \frac{\partial N_l}{\partial y} \right] \; d\Omega \tag{A.6}$$

When considering convective transport in two dimensions the convective terms involve the element matrices P and S.

$$P_{ij} = \int\int_{\Omega^e} G(r, r_i) \frac{\partial N_j}{\partial x} \; d\Omega \tag{A.7}$$

$$S_{ij} = \int\int_{\Omega^e} G(r, r_i) \frac{\partial N_j}{\partial y} \; d\Omega \tag{A.8}$$

The values of the elements in these matrices are given in the following sections for a rectangular element with side lengths a and b. The terms in (A.2) to (A.8) can be evaluated analytically (with the exception of (A.5). Equations (A.9) to (A.12), (A.18) to (A.25) and (A.50) to (A.53) were originally published by Taigbenu [70].

A.3.1 Diffusive Terms

$$R_{11} = -\frac{\pi}{2} \tag{A.9}$$

$$R_{12} = -\frac{a}{2b} ln \left(\frac{a^2 + b^2}{a^2} \right) + tan^{-1} \left(\frac{b}{a} \right) \tag{A.10}$$

$$R_{13} = \frac{a}{2b} ln \left(\frac{a^2 + b^2}{a^2} \right) + \frac{b}{2a} ln \left(\frac{a^2 + b^2}{b^2} \right) \tag{A.11}$$

$$R_{14} = -\frac{b}{2a} ln \left(\frac{a^2 + b^2}{b^2} \right) + tan^{-1} \left(\frac{a}{b} \right) \tag{A.12}$$

The remaining terms in the R matrix can be determined from the following relationships which arise from symmetry considerations:

$$R_{23} = R_{14} \tag{A.13}$$

$$R_{24} = R_{13} \tag{A.14}$$

$$R_{34} = R_{12} \tag{A.15}$$

$$R_{ii} = R_{11} \tag{A.16}$$

$$R_{ji} = R_{ij} \tag{A.17}$$

Taigbenu [70] splits the element matrix, L_{ij} which accounts for the flux term, into two parts. These are L^b_{ij} and L^f_{ij} which account for the flux before and after the node respectively when the integration is performed in an anti-clockwise direction. The terms in these matrices are:

$$L^b_{11} = -b\frac{(lnb^2 - 3)}{4} \tag{A.18}$$

$$L^b_{12} = -a\frac{(lna^2 - 1)}{4} \tag{A.19}$$

$$L^b_{13} = -\frac{1}{4}\left[b\ ln(a^2 + b^2) + \frac{a^2}{b}ln\frac{(a^2 + b^2)}{a^2} - b\right] \tag{A.20}$$

$$L^b_{14} = -\frac{1}{4}\left[a\ ln(a^2 + b^2) - \frac{b^2}{a}ln\frac{(a^2 + b^2)}{b^2} - 3a + 4b\,tan^{-1}\frac{a}{b}\right] \tag{A.21}$$

$$L^f_{11} = -a\frac{(lna^2 - 3)}{4} \tag{A.22}$$

$$L^f_{12} = -\frac{1}{4}\left[b\ ln(a^2 + b^2) - \frac{a^2}{b}ln\frac{(a^2 + b^2)}{a^2} - 3b + 4a\,tan^{-1}\frac{b}{a}\right] \tag{A.23}$$

$$L^f_{13} = -\frac{1}{4}\left[a\ ln(a^2 + b^2) + \frac{b^2}{a}ln\frac{(a^2 + b^2)}{b^2} - a\right] \tag{A.24}$$

$$L^f_{14} = -b\frac{(lnb^2 - 1)}{4} \tag{A.25}$$

The remaining terms in the matrices L^f and L^b can be using the following relationships:

$$L^f_{21} = L^b_{12} \tag{A.26}$$
$$L^f_{22} = L^b_{11} \tag{A.27}$$
$$L^f_{23} = L^b_{14} \tag{A.28}$$
$$L^f_{24} = L^b_{13} \tag{A.29}$$
$$L^f_{31} = L^f_{13} \tag{A.30}$$
$$L^f_{32} = L^f_{14} \tag{A.31}$$
$$L^f_{33} = L^f_{11} \tag{A.32}$$
$$L^f_{34} = L^f_{12} \tag{A.33}$$
$$L^f_{41} = L^b_{14} \tag{A.34}$$
$$L^f_{42} = L^b_{13} \tag{A.35}$$
$$L^f_{43} = L^b_{12} \tag{A.36}$$
$$L^f_{44} = L^b_{11} \tag{A.37}$$

$$L^b_{21} = L^f_{12} \tag{A.38}$$
$$L^b_{22} = L^f_{11} \tag{A.39}$$
$$L^b_{23} = L^f_{14} \tag{A.40}$$
$$L^b_{24} = L^f_{13} \tag{A.41}$$
$$L^b_{31} = L^b_{13} \tag{A.42}$$
$$L^b_{32} = L^b_{14} \tag{A.43}$$
$$L^f_{33} = L^b_{11} \tag{A.44}$$
$$L^f_{34} = L^b_{12} \tag{A.45}$$
$$L^f_{41} = L^f_{14} \tag{A.46}$$

$$L^f_{42} = L^f_{13} \tag{A.47}$$

$$L^f_{43} = L^f_{12} \tag{A.48}$$

$$L^f_{44} = L^f_{11} \tag{A.49}$$

A.3.2 Time Derivative Terms

The examples presented in Chapter 3 (Pressure Transient Analysis) and Chapter 4 (Convection Diffusion Equation) were for homogeneous media so they used the element matrix T to multiply the time derivative terms. Note that in both cases the theory can handle heterogeneous media in which case the element matrix U would be required. The matrix elements in T are:

$$\begin{aligned} T_{11} &= \frac{1}{ab}\left(-0.520833a^2b^2 + 0.16667\left(ab^3\arctan(\frac{a}{b}) + a^3b\arctan(\frac{b}{a})\right)\right. \\ &+0.02083333\left(a^4log(a^2) + b^4log(b^2) - a^4log(a^2+b^2) - b^4log(a^2+b^2)\right) \\ &\left.+0.125a^2b^2log(a^2+b^2)\right)\big) \end{aligned} \tag{A.50}$$

$$\begin{aligned} T_{12} &= \frac{1}{ab}\left(-0.395833a^2b^2 + 0.3333a^3b\arctan(\frac{b}{a})+\right. \\ &0.0625a^4\left(log(a^2) - log(a^2+b^2)\right) \\ &+0.125a^2b^2log(a^2+b^2) + 0.0625a^4\left(log(a^2) - log(a^2+b^2)\right) \\ &\left.+0.0208333\left(b^4log(a^2+b^2) - b^4log(b^2)\right)\right) \end{aligned} \tag{A.51}$$

$$\begin{aligned} T_{13} &= \frac{1}{ab}\left(-0.1875a^2b^2 + 0.0625\left((a^4+b^4)log(a^2+b^2) - a^4log(a^2)\right.\right. \\ &\left.\left.-b^4log(b^2)\right) + 0.125a^2b^2log(a^2+b^2)\right) \end{aligned} \tag{A.52}$$

$$\begin{aligned} T_{14} &= \frac{1}{ab}\left(-0.395833a^2b^2 + 0.33333ab^3\arctan(\frac{a}{b})\right. \\ &+0.02083333a^4\left(log(a^2+b^2) - log(a^2)\right) + 0.0625b^4\left(log(b^2)\right. \\ &\left.\left.-log(a^2+b^2)\right) + 0.125a^2b^2log(a^2+b^2)\right) \end{aligned} \tag{A.53}$$

The symmetry arguments that define the remaining terms in the T matrix are:

$$T_{23} = T_{14} \tag{A.54}$$

$$T_{24} = T_{13} \tag{A.55}$$

$$T_{34} = T_{12} \tag{A.56}$$

$$T_{ii} = T_{11} \tag{A.57}$$

$$T_{ji} = T_{ij} \tag{A.58}$$

Chapters 5 (Oil-Water Reservoir Simulation) and 6 (Parameter Estimation) presented examples involving flow in heterogeneous media. This requires the element matrix U multiplying the time derivative terms. The terms in the U matrix were not computed analytically. If analytical expressions were required they could be probably be derived by beginning from expressions for the following integral presented by Taigbenu [70]:

$$\frac{1}{2}\int_0^b\int_0^a \left(\frac{x}{a}\right)^i \left(\frac{y}{b}\right)^j ln(x^2+y^2)dxdy \tag{A.59}$$

However in this work the U matrix was computed using Mathematica's [75] Gauss-Kronrod numerical integration. For square elements with dimensionless lengths of 0.05 the terms in the U matrix are:

$$U_{1jl} = \begin{bmatrix} -0.00114098 & -0.000501048 & -0.000232431 & -0.000501048 \\ -0.000501048 & -0.000899393 & -0.00043014 & -0.000232431 \\ -0.000232431 & -0.00043014 & -0.000815155 & -0.00043014 \\ -0.000501048 & -0.000232431 & -0.00043014 & -0.000899393 \end{bmatrix} \tag{A.60}$$

$$U_{2jl} = \begin{bmatrix} -0.000899393 & -0.000501048 & -0.000232431 & -0.00043014 \\ -0.000501048 & -0.00114098 & -0.000501048 & -0.000232431 \\ -0.000232431 & -0.000501048 & -0.000899393 & -0.00043014 \\ -0.00043014 & -0.000232431 & -0.00043014 & -0.000815155 \end{bmatrix} \tag{A.61}$$

$$U_{3jl} = \begin{bmatrix} -0.000815155 & -0.00043014 & -0.000232431 & -0.00043014 \\ -0.00043014 & -0.000899393 & -0.000501048 & -0.000232431 \\ -0.000232431 & -0.000501048 & -0.00114098 & -0.000501048 \\ -0.00043014 & -0.000232431 & -0.000501048 & -0.000899393 \end{bmatrix} \tag{A.62}$$

$$U_{4jl} = \begin{bmatrix} -0.000899393 & -0.00043014 & -0.000232431 & -0.000501048 \\ -0.00043014 & -0.000815155 & -0.00043014 & -0.000232413 \\ -0.000232431 & -0.00043014 & -0.000899393 & -0.000501048 \\ -0.000501048 & -0.000232431 & -0.000501048 & -0.00114098 \end{bmatrix} \quad \text{(A.63)}$$

A.3.3 Heterogeneity Term

The theory presented in Chapter 3 (Pressure Transient Analysis) and the examples presented in Chapter 5 (Oil-Water Reservoir Simulation) and Chapter 6 (Parameter Estimation) require the element matrix V which corresponds to the $\nabla lnk \cdot \nabla p$ term. The terms in V are:

$$\begin{aligned} V_{111} &= \frac{1}{a^2b^2}\left(0.5a^2b^2\left(\arctan(\frac{a}{b}) + \arctan(\frac{b}{a})\right)\right. \\ &\quad \left. +ab\left(-0.611111(a^2+b^2) + 0.166667(a^2\log(a^2) + b^2\log(b^2))\right)\right) \end{aligned} \quad \text{(A.64)}$$

$$\begin{aligned} V_{112} &= \frac{1}{a^2b^2}\left(\left(0.166667a^4 - 0.5a^2b^2\right)\arctan(\frac{b}{a}) + ab\left(-0.305556a^27\right.\right. \\ &\quad +0.61111b^2 - 0.16667a^2log(a^2) - 0.08333b^2\left(log(a^2+b^2) + log(b^2)\right) \\ &\quad \left.\left. +0.25a^2log(a^2+b^2)\right)\right) \end{aligned} \quad \text{(A.65)}$$

$$\begin{aligned} V_{113} &= \frac{1}{a^2b^2}\left(0.305556\left(a^3b + ab^3\right) - 0.166667\left(b^4\arctan(\frac{a}{b}) + a^4\arctan(\frac{b}{a})\right)\right. \\ &\quad +0.0833333\left(a^3blog(a^2) + ab^3log(b^2)\right) \\ &\quad \left. -0.1666667\left(a^3blog(a^2+b^2) + ab^3log(a^2+b^2)\right)\right) \end{aligned} \quad \text{(A.66)}$$

$$\begin{aligned} V_{114} &= \frac{1}{a^2b^2}\left(\left(-0.5a^2b^2 + 0.166667b^4\right)\arctan(\frac{a}{b}) + ab\left(0.61111a^2\right.\right. \\ &\quad -0.3055556b^2 - 0.08333333a^2log(a^2) - 0.16666667b^2log(b^2) \\ &\quad \left.\left. -0.0833333a^2log(a^2+b^2) + 0.25b^2log(a^2+b^2)\right)\right) \end{aligned} \quad \text{(A.67)}$$

$$V_{121} = V_{112} \quad \text{(A.68)}$$

$$V_{122} = \frac{1}{a^2b^2}\left(a\left(-0.277778a^2b - 0.61111b^3 + (0.16667a^3 + 0.5ab^2)\arctan(\frac{b}{a}) + 0.166667a^2blog(a^2) + 0.166667b^3log(a^2+b^2)\right)\right) \quad (A.69)$$

$$V_{123} = \frac{1}{a^2b^2}\left(0.16667b^4\arctan(\frac{a}{b}) - 0.166667a^4\arctan(\frac{b}{a}) + ab\left(0.277778a^2 - 0.305556b^2 - 0.083333a^2log(a^2) + 0.0833333(b^2-a^2)log(a^2+b^2)\right)\right) \quad (A.70)$$

$$V_{124} = \frac{1}{a^2b^2}\left(0.30556(a^3b+ab^3) - 0.166667\left(b^4\arctan(\frac{a}{b}) + a^4\arctan(\frac{b}{a})\right) + 0.083333(a^3blog(a^2) + ab^3log(b^2)) - 0.16667(a^3blog(a^2+b^2) + ab^3log(a^2+b^2)\right) \quad (A.71)$$

$$V_{131} = V_{113} \quad (A.72)$$

$$V_{132} = V_{123} \quad (A.73)$$

$$V_{133} = \frac{1}{a^2b^2}\left(0.166667\left(b^4\arctan(\frac{a}{b}) + a^4\arctan(\frac{b}{a})\right) + ab\left(-0.27778(a^2+b^2) + 0.166667(a^2+b^2)log(a^2+b^2)\right)\right) \quad (A.74)$$

$$V_{134} = \frac{1}{a^2b^2}\left(0.166667\left(a^4\arctan(\frac{b}{a}) - b^4\arctan(\frac{a}{b})\right) + a\left(-0.305556a^2b + 0.277778b^3 + 0.0833333(a^2blog(a^2+b^2) - b^3log(a^2+b^2) - b^3log(b^2)\right)\right) \quad (A.75)$$

$$V_{141} = V_{114} \quad (A.76)$$

$$V_{142} = V_{124} \quad (A.77)$$

$$V_{143} = V_{134} \quad (A.78)$$

$$V_{144} = \frac{1}{a^2b^2}\left(\left(0.5a^2b^2 + 0.166667b^4\right)\arctan(\frac{a}{b}) + ab\left(-0.611111a^2 - 0.277778b^2 + 0.166667(b^2log(b^2) + a^2log(a^2+b^2))\right)\right) \quad (A.79)$$

A.3.4 Convective Terms

Chapter 4 requires element matrices P and S to handle the convective terms in the x and y directions. The terms in P and S are:

$$\begin{aligned} P_{11} &= \frac{1}{ab}\Big(0.916667ab^2 - 0.16667b^3\arctan(\frac{a}{b}) - 0.5a^2b\arctan(\frac{b}{a}) \\ &\quad -0.083333a^3log(a^2) + 0.08333a^3log(a^2+b^2) \\ &\quad -0.25ab^2log(a^2+b^2)\Big) \end{aligned} \tag{A.80}$$

$$P_{12} = -P_{11} \tag{A.81}$$

$$\begin{aligned} P_{13} = \ &= \frac{1}{ab}\Big(-0.583333ab^2 + 0.3333b^3\arctan(\frac{a}{b}) - 0.08333a^3log(a^2) \\ &\quad +0.08333a^3log(a^2+b^2) + 0.25ab^2log(a^2+b^2)\Big) \end{aligned} \tag{A.82}$$

$$P_{14} = -P_{13} \tag{A.83}$$

$$P_{21} = -P_{12} \tag{A.84}$$

$$P_{22} = -P_{11} \tag{A.85}$$

$$P_{23} = -P_{14} \tag{A.86}$$

$$P_{24} = -P_{13} \tag{A.87}$$

$$P_{31} = -P_{13} \tag{A.88}$$

$$P_{32} = -P_{14} \tag{A.89}$$

$$P_{33} = -P_{11} \tag{A.90}$$

$$P_{34} = -P_{12} \tag{A.91}$$

$$P_{41} = P_{14} \tag{A.92}$$

$$P_{42} = P_{13} \tag{A.93}$$

$$P_{43} = P_{12} \tag{A.94}$$

$$P_{44} = P_{11} \tag{A.95}$$

$$S_{11} = \frac{1}{ab}\Big(0.916667a^2b - 0.16667a^3\arctan(\frac{b}{a}) - 0.5ab^2\arctan(\frac{a}{b}) \\ -0.083333b^3log(b^2) + 0.08333b^3log(a^2+b^2) \\ -0.25a^2blog(a^2+b^2)\Big) \tag{A.96}$$

$$S_{12} = = \frac{1}{ab}\Big(0.583333a^2b - 0.3333a^3\arctan(\frac{b}{a}) + 0.08333b^3log(b^2) \\ -0.08333b^3log(a^2+b^2) - 0.25a^2blog(a^2+b^2)\Big) \tag{A.97}$$

$$S_{13} = -S_{12} \tag{A.98}$$

$$S_{14} = -S_{11} \tag{A.99}$$

$$S_{21} = S_{12} \tag{A.100}$$

$$S_{22} = S_{11} \tag{A.101}$$

$$S_{23} = S_{14} \tag{A.102}$$

$$S_{24} = S_{13} \tag{A.103}$$

$$S_{31} = -S_{13} \tag{A.104}$$

$$S_{32} = -S_{14} \tag{A.105}$$

$$S_{33} = -S_{11} \tag{A.106}$$

$$S_{34} = -S_{12} \tag{A.107}$$

$$S_{41} = -S_{14} \tag{A.108}$$

$$S_{42} = -S_{13} \tag{A.109}$$

$$S_{43} = -S_{12} \tag{A.110}$$

$$S_{44} = -S_{11} \tag{A.111}$$

A.4 Overhauser Element Matrices

Chapter 5 (Oil-Water Reservoir Simulation) investigated the use of Overhauser elements to provide C^1 continuity of the pressure. To do so the element matrices for terms involving the pressure must be recomputed. When Overhauser elements are used 16 positions must be considered for the field node of the Green's function.

A.4.1 Diffusion Term

The definition of the R matrix remains the same:

$$R_{ij} = \int_{\Gamma_e} \frac{\partial G(r, r_i)}{\partial n} N_j \; d\Gamma - \delta_{ij}\, \theta_i \tag{A.112}$$

However since the shape functions N_j are no longer linear the values of the terms in the R matrix become:

$$R_{1,1} = -\frac{\pi}{2} \tag{A.113}$$

$$\begin{aligned} R_{1,2} = \; & \frac{1}{b^3}\left(-1.75a^2b + (2.5a^2b + b^3)tan^{-1}\left(\frac{b}{a}\right) + 0.75a^3log(a^2)\right. \\ & \left.-0.75a^3log(a^2+b^2)\right) \end{aligned} \tag{A.114}$$

$$\begin{aligned} R_{1,3} = \; & -\frac{b}{a^3}\left(-1.25a^2 + 2ab\, tan^{-1}\left(\frac{a}{b}\right) + (0.25a^2 + 0.75b^2)log(b^2)\right. \\ & \left.-0.25a^2log(a^2+b^2) - 0.75b^2log(a^2+b^2)\right) + \frac{a}{b^3}\left(1.25b^2\right. \\ & -2ab\, tan^{-1}\left(\frac{b}{a}\right) + (-0.75a^2 - 0.25b^2)log(a^2) + 0.75a^2log(a^2+b^2) \\ & \left.+0.25b^2log(a^2+b^2)\right) \end{aligned} \tag{A.115}$$

$$\begin{aligned} R_{1,4} = \; & -\frac{1}{a^3}\left(1.75a^2b + (-a^3 - 2.5ab^2)atan^{-1}\left(\frac{a}{b}\right)\right. \\ & \left.-0.75b^3log(b^2) + 0.75b^3log(a^2+b^2)\right) \end{aligned} \tag{A.116}$$

$$\begin{aligned} R_{1,6} = \; & \frac{a}{b^3}\left(0.75b^2 - ab\, tan^{-1}\left(\frac{b}{a}\right) + (-0.25a^2 + 0.25b^2)log(a^2)\right. \\ & \left.+0.25a^2log(a^2+b^2) - 0.25b^2log(a^2+b^2)\right) \end{aligned} \tag{A.117}$$

$$R_{1,9} = -\frac{b}{a^3}\left(-0.75a^2 + ab\,tan^{-1}\left(\frac{a}{b}\right) + (-0.25a^2 + 0.25b^2)log(b^2) + 0.25a^2log(a^2+b^2) - 0.25b^2log(a^2+b^2)\right) \quad \text{(A.118)}$$

$$R_{1,10} = -\frac{b}{a^3}\left(-0.5ab\,tan^{-1}\left(\frac{a}{b}\right) - 0.25b^2log(b^2) + 0.25(a^2 + b^2log(a^2+b^2))\right) \quad \text{(A.119)}$$

$$R_{1,12} = \frac{a}{b^3}\left(0.5abtan^{-1}\left(\frac{b}{a}\right) + 0.25a^2log(a^2) - 0.25(b^2 + a^2log(a^2+b^2))\right) \quad \text{(A.120)}$$

$$R_{2,5} = R_{2,10} = R_{3,8} = R_{3,11} = R_{4,7} = R_{4,12} = R_{1,6} \quad \text{(A.121)}$$

$$R_{2,9} = R_{2,11} = R_{3,5} = R_{3,7} = R_{4,6} = R_{4,8} = R_{1,10} \quad \text{(A.122)}$$

$$R_{i,i} = R_{1,1} \qquad i = 2,3,4 \quad \text{(A.123)}$$

$$R_{j,i} = R_{i,j} \qquad i,j = 2,3,4 \quad \text{(A.124)}$$

All unspecified $R_{i,j}$ are zero.

A.4.2 Heterogeneity Term

The element integrals for the V_{ijl} term were computed numerically. The expression for V_{ijl} is the same as the linear element case give in Equation (A.6) however the index j run from 1 to 16, not 1 to 4 as in the linear element case. For an example with square elements with a dimensionless length of 0.1 the values in the V matrix

are:

$$V_{1jl} = \begin{bmatrix} -2.09234 & 0.58505 & 0.922237 & 0.058505 \\ 0.645954 & -1.97027 & 0.394723 & 0.929591 \\ 0.933995 & 0.422682 & -1.77936 & 0.422682 \\ 0.645954 & 0.929591 & 0.394723 & -1.97027 \\ 0.0391273 & -0.0772963 & -0.0355966 & 0.0737657 \\ -0.0793216 & 0.0637974 & 0.0533784 & -0.0378542 \\ 0.0391273 & 0.0737657 & -0.035966 & -0.0772963 \\ 0.0209646 & 0.0838252 & -0.0537365 & -0.0510534 \\ -0.0793216 & -0.0378542 & 0.0533784 & 0.0637974 \\ -0.051836 & -0.0557618 & 0.0725998 & 0.034998 \\ 0.0209646 & -0.0510534 & -0.0537365 & 0.0838252 \\ -0.051836 & 0.034998 & 0.0725998 & -0.0557618 \end{bmatrix} \tag{A.125}$$

$$V_{2jl} = \begin{bmatrix} -1.97027 & 0.394723 & 0.929591 & 0.645954 \\ 0.422682 & -1.77936 & 0.422682 & 0.645954 \\ 0.0929591 & 0.645954 & -1.97027 & 0.645954 \\ 0.58505 & 0.922237 & 0.58505 & -2.09234 \\ 0.083252 & -0.0537365 & -0.0510534 & 0.0209646 \\ -0.0557618 & 0.0725998 & 0.034998 & -0.051836 \\ 0.0838252 & 0.0209646 & -0.0510534 & -0.0537365 \\ 0.0737657 & 0.0391273 & -0.0772963 & -0.0355966 \\ -0.0557618 & -0.051836 & 0.034998 & 0.0725998 \\ -0.0378542 & -0.0793216 & 0.0637974 & 0.0533784 \\ 0.034998 & -0.051836 & -0.0557618 & 0.0725998 \\ -0.0510534 & 0.0209646 & 0.0838252 & -0.0537365 \end{bmatrix} \tag{A.126}$$

$$V_{3jl} = \begin{bmatrix} -1.77936 & 0.422682 & 0.933995 & 0.422682 \\ 0.394723 & -1.97027 & 0.645954 & 0.929591 \\ 0.0922237 & 0.58505 & -2.09234 & 0.58505 \\ 0.394723 & 0.929591 & 0.645954 & -1.97027 \\ 0.07259978 & -0.0557618 & -0.051836 & 0.034998 \\ -0.0537365 & 0.0838252 & 0.0209646 & -0.0510534 \\ 0.0725998 & 0.034998 & -0.051836 & -0.0557618 \\ 0.0533784 & 0.0637974 & -0.0793216 & -0.0378542 \\ -0.0537365 & -0.0510534 & 0.0209646 & 0.0838252 \\ -0.0355966 & -0.0772963 & 0.0391273 & 0.0737657 \\ 0.0533784 & -0.0378542 & -0.0793216 & 0.0637974 \\ -0.0355966 & 0.0737657 & 0.031273 & -0.0772933 \end{bmatrix} \quad \text{(A.127)}$$

$$V_{4jl} = \begin{bmatrix} -1.97027 & 0.394723 & 0.929591 & 0.645954 \\ 0.422682 & -1.77936 & 0.422682 & 0.933995 \\ 0.929591 & 0.394723 & -1.97027 & 0.645954 \\ 0.58505 & 0.922237 & 0.58505 & -2.09234 \\ 0.0838252 & -0.0537365 & -0.0510534 & 0.0209646 \\ -0.0557618 & 0.0725998 & 0.034998 & -0.051836 \\ 0.0637974 & 0.0533784 & -0.0378542 & -0.0793216 \\ 0.034998 & 0.0725998 & -0.0557618 & -0.051836 \\ -0.0772963 & -0.0355966 & 0.0737657 & 0.0391273 \\ -0.0510534 & -0.0537365 & 0.0838252 & 0.0209646 \\ 0.0737657 & -0.0355966 & -0.0772963 & 0.0391273 \\ -0.0378542 & 0.0533784 & 0.0637974 & -0.0793216 \end{bmatrix} \quad \text{(A.128)}$$

Appendix B

Transient Well Index

This apppendix presents a derivation of a transient well index proposed in Chapter 7 (Concluding Remarks). The derivation is based on the derivation of the Peaceman well index [50] however it does not make the assumption of steady-state flow. The derivation begins from the analytical solution for transient radial flow in a homogeneous medium:

$$p(r) = p_i - \frac{q\mu}{4\pi kh} Ei\left(\frac{\phi\mu c_t r^2}{4kt}\right) \tag{B.1}$$

Denote r_o as the radius at which the block pressure matches the pressure predicted by Equation (B.1).

$$p(r_o) = p_i - \frac{q\mu}{4\pi kh} Ei\left(\frac{\phi\mu c_t r_o^2}{4kt}\right) \tag{B.2}$$

Now consider the material balance equation solved for the cell containing the well by the finite difference simulator:

$$q = \frac{kh}{\mu}\left[p_1 + p_2 + p_3 + p_4 - 4p_o\right] \tag{B.3}$$

The layout of the finite difference grid is shown in Figure B.1.

The block pressure in Equation (B.3) are given by:

$$p_j = p_i - \frac{q\mu}{4\pi kh} Ei\left(\frac{\phi\mu c a^2}{4kt}\right) \qquad j = 1, 4 \tag{B.4}$$

Subsituting Equations (B.2) and (B.4) into (B.3) gives:

$$q = 4\frac{kh}{\mu}\frac{q\mu}{4\pi kh}\left[Ei\left(\frac{\phi\mu c_t r_o^2}{4kt}\right) - Ei\left(\frac{\phi\mu c_t a^2}{4kt}\right)\right] \tag{B.5}$$

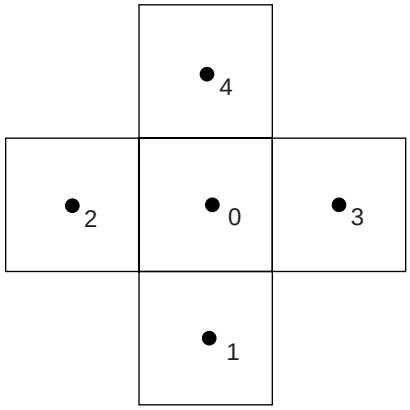

Figure B.1: Finite difference grid

The radius r_o can be derived in terms of a by numerically solving:

$$\left[Ei\left(\frac{\phi\mu c_t r_o^2}{4kt}\right) - Ei\left(\frac{\phi\mu c_t a^2}{4kt}\right)\right] = \pi \tag{B.6}$$

The well index can now be derived by considering the pressure at the well:

$$p_w = p_i - \frac{q\mu}{4\pi kh} Ei\left(\frac{\phi\mu c_t r_w^2}{4kt}\right) \tag{B.7}$$

Equation (B.7) can be rearranged for q:

$$q = \frac{4\pi kh}{\mu} \frac{(p_i - p_w)}{Ei\left(\frac{\phi\mu c_t r_w^2}{4kt}\right)} \tag{B.8}$$

The initial reservoir pressure p_i must be eliminated from Equation (B.8). This can be done by substituting Equation (B.2) into Equation (B.8) to give:

$$q = \frac{4\pi kh}{\mu} \frac{(p_o - p_w)}{Ei\left(\frac{\phi\mu c_t r_w^2}{4kt}\right)} + q\frac{Ei\left(\frac{\phi\mu c_t r_o^2}{4kt}\right))}{Ei\left(\frac{\phi\mu c_t r_w^2}{4kt}\right)} \tag{B.9}$$

Equation (B.9) can be simplified to give:

$$q = \frac{4\pi kh}{\mu}(p_o - p_w)\frac{1}{Ei\left(\frac{\phi\mu c_t r_w^2}{4kt}\right) - Ei\left(\frac{\phi\mu c_t r_o^2}{4kt}\right)} \tag{B.10}$$

Equation (B.10) suggests a well index of:

$$WI = \frac{4\pi kh}{\mu}\frac{1}{Ei\left(\frac{\phi\mu c_t r_w^2}{4kt}\right) - Ei\left(\frac{\phi\mu c_t r_o^2}{4kt}\right)} \tag{B.11}$$

Appendix C

Accuracy of DRBEM and GEM

This section presents numerical results studying the performance of DRBEM and the one and two-dimensional GEM formulations. Test problem A is a one-dimensional flow problem with an exponential variation in the permeability distribution on the domain $x[0, 1]$:

$$k = e^{\alpha x} \tag{C.1}$$

The boundary conditions are:

$$p(0) = 0 \tag{C.2}$$

$$p(1) = 1 \tag{C.3}$$

The analytical solution to this problem is:

$$p = \frac{1 - e^{-\alpha x}}{1 - e^{-\alpha}} \tag{C.4}$$

Table C.1 shows a comparison of DRBEM and two-dimensional GEM with a ten element grid and $\alpha = 1$. The results show that GEM reproduces the analytical solution more closely than DRBEM.

No theoretical discussion of the order of accuracy of GEM is available. For transient problems both methods used in this work use a finite difference approximation in time. Therefore the errors introduced by discretizing time domain are expected

Table C.1: Comparison of DRBEM and GEM for flow in heterogeneous media

x	p, DRBEM	p, GEM	p, exact	% error DRBEM	% error GEM
0	0	0	0	0	0
0.1	0.157506	0.146912	0.150545	4.62	-2.41
0.2	0.299697	0.282507	0.286764	4.51	-1.48
0.3	0.427817	0.405484	0.41002	4.34	-1.11
0.4	0.542913	0.517019	0.521546	4.10	-0.868
0.5	0.645888	0.618176	0.622459	3.76	-0.688
0.6	0.737495	0.70992	0.713769	3.32	-0.539
0.7	0.818326	0.793127	0.79639	2.75	-0.410
0.8	0.888838	0.868593	0.871149	2.03	-0.293
0.9	0.94932	0.937036	0.938793	1.12	-0.187
1	1	1	1	0	0

Table C.2: Grid refinement to assess spatial errors in GEM

x	p, $\Delta x = 0.1$	% error	p, $\Delta x = 0.05$	% error	p, $\Delta x = 0.025$	% error
0.0	0.0	0.0	0.0	0.0	0.0	0.0
0.1	0.146912	-2.41	0.148834	-1.14	0.14975	-0.528
0.2	0.282507	-1.48	0.284428	-0.815	0.285636	-0.393
0.3	0.405484	-1.11	0.407348	-0.652	0.408754	-0.309
0.4	0.517019	-0.868	0.518778	-0.531	0.520278	-0.243
0.5	0.618176	-0.688	0.619794	-0.428	0.621268	-0.191
0.6	0.70992	-0.539	0.71137	-0.336	0.712701	-0.150
0.7	0.793127	-0.410	0.794388	-0.251	0.795487	-0.113
0.8	0.868593	-0.293	0.86965	-0.172	0.870462	-0.0788
0.9	0.937036	-0.187	0.937879	-0.0974	0.938382	-0.0438
1.0	1.0	0.0	1.0	0.0	1.0	0.0

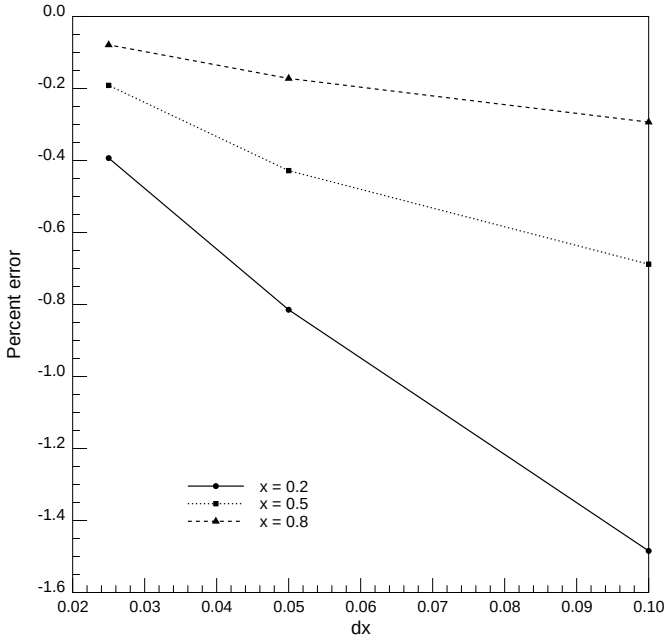

Figure C.1: Error behavior with grid refinement

to be of order Δt. To assess the spatial errors the test problem was solved on three grids with $\Delta x = 0.1, 0.05, 0.025$ and $\alpha = 1$. The results are presented in Table C.2.

The errors at three locations, x=0.2, 0.5 and 0.8, are shown in Figure C.1. The error at each location decreases linearly as the grid is refined. This behavior is believed to be related to the approximation of the pressure derivative at internal nodes. The matrix equation being solved is:

$$\sum_{e=1}^{M} \left(R_{ij}^{e} p_j + L_{ij}^{e} q_j - V_{ijl}^{e} ln k_j p_l \right) = 0 \tag{C.5}$$

The q_j terms are however treated as first order finite differences in terms of the nodal pressures so their accuracy is of order Δx.

The effect of heterogeneity was considered by using GEM to solve test problem A with $\Delta x = 0.05$ for $\alpha = 1, 3, 5$. The results are shown in Table C.3. These results show that the largest errors occur in areas where the permeability changes most rapidly.

To assess the difference in performance between the one- and two-dimensional

Table C.3: Errors with increasing heterogeneity

x	p, $\alpha = 1$	% error	p, $\alpha = 3$	% error	p, $\alpha = 5$	% error
0.0	0.0	0.0	0.0	0.0	0.0	0.0
0.1	0.148834	-1.14	0.266058	-2.48	0.384371	-2.97
0.2	0.284428	-0.815	0.467577	-1.53	0.626775	-1.51
0.3	0.407348	-0.652	0.617646	-1.10	0.774851	-0.932
0.4	0.518778	-0.531	0.729401	-0.818	0.865306	-0.600
0.5	0.619794	-0.428	0.812625	-0.605	0.920562	-0.387
0.6	0.71137	-0.336	0.874602	-0.436	0.954316	-0.245
0.7	0.794388	-0.251	0.920756	-0.300	0.974935	-0.148
0.8	0.86965	-0.172	0.955128	-0.188	0.987531	-0.0822
0.9	0.937879	-0.0974	0.980725	-0.096	0.995226	-0.0375
1.0	1.0	0.0	1.0	0.0	1.0	0.0

GEM formulations test problem B was introduced. It is also a one-dimensional flow problem. The permeability is given by:

$$k = \frac{1}{1+x} \tag{C.6}$$

The boundary conditions are:

$$p(0) = 0 \tag{C.7}$$

$$p(1) = 1.5 \tag{C.8}$$

The analytical solution to the problem is:

$$p = x + \frac{x^2}{2} \tag{C.9}$$

Tables C.4 and C.5 present results for test problem A with $\alpha = 3$ and test problem B for the one- and two-dimensional GEM schemes. These results show that the one-dimensional GEM formulation is significantly more accurate than its two-dimensional counterpart.

Table C.4: Comparison of one- and two-dimensional GEM, test problem A

x	p, 2D	% error	p, 1D	% error
0.0	0.0	0.0	0.0	0.0
0.1	0.266058	-2.48	0.27427	-0.552
0.2	0.467577	-1.53	0.476169	-0.282
0.3	0.617646	-1.10	0.625656	-0.181
0.4	0.729401	-0.818	0.736335	-0.124
0.5	0.812625	-0.605	0.818283	-0.0866
0.6	0.874602	-0.436	0.878956	-0.0593
0.7	0.920756	-0.300	0.923879	-0.0386
0.8	0.955128	-0.188	0.95714	-0.0225
0.9	0.980725	-0.096	0.981767	-0.00995
1.0	1.0	0.0	1.0	0.0

Table C.5: Comparison of one- and two-dimensional GEM, test problem B

x	p, 2D	% error	p, 1D	% error
0.0	0.0	0.0	0.0	0.0
0.1	0.106234	1.17524	0.105042	-0.0395762
0.2	0.221872	0.850909	0.220026	-0.0119711
0.3	0.34736	0.684058	0.345014	-0.00415591
0.4	0.482681	0.558542	0.480005	-0.0010909
0.5	0.627824	0.45184	0.624999	0.000195945
0.6	0.782776	0.355897	0.779995	0.000673287
0.7	0.947527	0.267407	0.944993	0.00074218
0.8	1.12207	0.184821	1.11999	0.000593794
0.9	1.30638	0.105747	1.305	0.0
1	1.5	0.0	1.5	0.0